

Murat KAAN

A Master's Thesis

AGU 2021

EVALUATION OF MATERIAL OPTIONS FOR ELECTRICAL POWER SUPPLYING AND PROTECTIVE WEARABLE EQUIPMENT

A THESIS

SUBMITTED TO THE DEPARTMENT OF ADVANCED MATERIALS
AND NANOTECHNOLOGY
AND THE GRADUATE SCHOOL OF ENGINEERING AND SCIENCE OF
ABDULLAH GUL UNIVERSITY
IN PARTIAL FULFILLMENT OF THE REQUIREMENTS
FOR THE DEGREE OF
MASTER OF SCIENCE

By

Murat KAAN
December 2020

EVALUATION OF MATERIAL OPTIONS FOR
ELECTRICAL POWER SUPPLYING AND
PROTECTIVE WEARABLE EQUIPMENT

A THESIS

SUBMITTED TO THE DEPARTMENT OF ADVANCED MATERIALS AND
NANOTECHNOLOGY

AND THE GRADUATE SCHOOL OF ENGINEERING AND SCIENCE OF
ABDULLAH GUL UNIVERSITY

IN PARTIAL FULFILLMENT OF THE REQUIREMENTS

FOR THE DEGREE OF

MASTER OF SCIENCE

By

Murat KAAN

December 2020

SCIENTIFIC ETHICS COMPLIANCE

I hereby declare that all information in this document has been obtained in accordance with academic rules and ethical conduct. I also declare that, as required by these rules and conduct, I have fully cited and referenced all materials and results that are not original to this work.

Name-Surname: Murat KAAN

Signature :

REGULATORY COMPLIANCE

M.Sc. thesis titled **Evaluation of Material Options for Electrical Power Supplying and Protective Wearable Equipment** has been prepared in accordance with the Thesis Writing Guidelines of the Abdullah Gül University, Graduate School of Engineering & Science.

Prepared By
Murat KAAN

Advisor
Assist. Prof. İlker ERDEM

Head of the Advanced Materials and Nanotechnology (AMN) Program
Prof. Dr. Murat DURANDURDU

ACCEPTANCE AND APPROVAL

M.Sc. thesis titled Evaluation of Material Options for Electrical Power Supplying and Protective Wearable Equipment and prepared by Murat KAAN has been accepted by the jury in the Advanced Materials & Nanotechnology (AMN) Graduate Program at Abdullah Gül University, Graduate School of Engineering & Science.

14/12/2020

JURY:

Advisor : Assist. Prof. İlker ERDEM.....

Member : Prof. Dr. Mustafa Serdar GENÇ.....

Member : Assist. Prof. Cihan ÇİFTÇİ.....

APPROVAL:

The acceptance of this M.Sc. thesis has been approved by the decision of the Abdullah Gül University, Graduate School of Engineering & Science, Executive Board dated /..... / and numbered.....

..... /..... /

Graduate School Dean

Prof. Dr. Hakan USTA

ABSTRACT

EVALUATION OF MATERIAL OPTIONS FOR ELECTRICAL POWER SUPPLYING AND PROTECTIVE WEARABLE EQUIPMENT

Murat KAAAN

M.Sc. in Advanced Materials & Nanotechnology (AMN)

Advisor: Assist. Prof. İlker ERDEM

December 2020

Ballistic vests used in military applications are usually made out of layers of various materials and then combined to form a solitary conservative vest. Contrasted with bygone eras, functionality and productivity of ballistic vests have improved to a critical sum. ANSYS was explicitly used to compute such *finite element analysis* and the initial segment of the postulation dealt with the determination of material used for the first/front layer of the vest. Since nowadays all ballistic vests almost use Kevlar and epoxy layers in the material formation of the vest, the similar material candidates were chosen for this research as well. Practically, the only choice of material that had to be decided is for the front layer of the vest since many different materials can be used in that regard. Silicon Carbide (SiC) was picked on the grounds that it demonstrated the least deformation and least stress compared to other materials that were tested in ANSYS. In total; three materials were tested and evaluated respectively were Silicon Carbide, Boron Carbide (BC) and Alumina (Al_2O_3). In order to prove the protection of the ballistic vest design and its reliability in the ballistic sense, 6 (six) flawless shots were fired at certain points on the vest, based on American NIJ standards. In short, the thesis examines the protection of ballistic protective vests from serious military injuries during combat and the development of a hybrid solution that will provide the vest with a new function to provide the power needs of the equipment the soldier will need during combat. In addition, a novel idea is proposed to the literature by adding the fourth layer into the FEA based examined ballistic vest.

Keywords: Ballistic Vest, Ballistic Resistance, Composite, Perforation, Lithium Battery

ÖZET

KORUYUCU VE ELEKTRİK GÜCÜ SAĞLAYICI ASKERİ KİYAFETLERE YÖNELİK MALZEME SEÇENEKLERİNİN DEĞERLENDİRİLMESİ

Murat KAAAN

İleri Malzemeler ve Nanoteknoloji Bölümü Yüksek Lisans

Tez Yöneticisi: Dr. Öğr. Üyesi İlker ERDEM

Aralık-2020

Askeri uygulamalarda kullanılan balistik yelekler, genellikle farklı malzeme katmanlarından oluşturulur ve sonrasında birleştirilerek son ürün haline getirilir. Geçmişe kıyasla günümüzde, balistik yeleklerin işlevselliği ve üretkenliğinin kritik bir öneme ulaştığı gözlemlenmektedir. ANSYS, FEA analizini hesaplamak için gerekli program olarak kullanılmış ve postülasyonun ilk bölümünde yeleğin ön katmanı için kullanılacak malzemenin tespiti sağlanmıştır. Günümüzde, neredeyse tüm balistik yeleklerin malzeme oluşumunda kevlar ve epoksi katmanları kullandığı için, bu araştırmada da benzer malzeme adayları önceliklendirilmiştir. Balistik yelek tasarımında en önemli hususlardan olan malzeme seçiminde ise yeleğin ön tabakasının doğru tespiti en kritik husustur, çünkü bu noktada birçok farklı malzeme alternatifi mevcut olup doğrudan yeleğin güvenilirliğini etkilemektedir. Bu kapsamda, Silisyum Karbür, Bor Karbür (BC) ve Alümina (Al_2O_3) olmak üzere üç malzeme test edilmiş ve değerlendirilmiştir. Aday malzemelerden olan Silikon Karbür (SiC), diğer malzemelere kıyasla düşük deformasyon, gerilme, gerinim ve kayma gerilmesi sergileyerek yeleğin ön katman malzemesi olarak seçilmiştir. Tasarımın balistik anlamda güvenilir olduğunu kanıtlamak için NIJ standartları baz alınarak yeleğe belirli noktalardan, sırasıyla ve 6 (altı) adet kusursuz atış tabirinde atışlar yapılmıştır. Kısacası bu tez, balistik koruyucu yeleklerin muharebe sırasında ciddi yaralanmalardan korunma ve askerin taşıdığı ekipmanın güç ihtiyacını sağlayacak yeni bir işlev sağlayacak hibrit bir çözümü kapsamlı bir şekilde incelemektedir. Ayrıca, balistik yeleğe bir batarya katmanı eklenerek sağlanan avantaj literatüre yeni ve kullanışlı bir fikir olarak sunulmaktadır.

Anahtar kelimeler: Balistik Yelek, Balistik Dayanım, Kompozit, Delinim, Lityum Batarya

Acknowledgements

The author is grateful to the Advisor and local defense industry authorities who supported the project by their great recommendations and wisdom.

I would like to acknowledge the support of the SSB (Presidency of Defense Industries) and the company I currently have been working - ASPILSAN Energy Inc., which is a leading battery manufacturer & defense contractor in Turkey.

Table of Contents

1. INTRODUCTION	1
1.1 BACKGROUND OF THE PROJECT.....	1
1.2 INTRODUCING THE RESEARCH TOPIC	3
1.3 SCOPE OF THE THESIS	5
1.4 THESIS ORGANIZATION AND RESEARCH QUESTIONS	6
2. LITERATURE REVIEW.....	8
2.1. BALLISTIC TESTING	8
2.2 INTRODUCTION TO ARMOR SYSTEM	9
2.3 FUNDAMENTAL PRINCIPLES	10
2.4 MATERIAL PROPERTIES.....	12
2.4.1 Core property requirements	13
2.4.2 Density, tenacity and elastic modulus.....	13
2.4.3 Compressive strength, shear strength and hardness	14
2.5 BALLISTIC EFFICIENCY	14
2.6 DEPTH OF PENETRATION (DOP) ANALYSIS.....	15
2.6.1 Penetration mechanics, modes and phenomena of effects	15
2.6.2 Depth of penetration observation	21
2.7 IMPACT LOADS	23
2.8 TEST PROTOCOL - STANDARDS AND REQUIREMENTS.....	24
2.9 BACK FACE SIGNATURE (BFS) AND BALLISTIC LIMIT (BL).....	25
3. MATERIALS AND METHODS.....	28
3.1 ARMOR STRUCTURE.....	28
3.2 TEST PROTOCOLS.....	29
3.3 MODELLING AND MATERIAL SELECTION	30
3.3.1 Modelling methodology.....	30
3.3.2 Bullet/projectile determination.....	31
3.3.3 Material modelling in ANSYS.....	32
3.3.4 Vest materials and its design.....	33
3.3.5 Front layer.....	34
3.3.6 Backing layer.....	34
3.3.7 Analysis method.....	35
3.4 MATERIAL CLASSIFICATION AND DETERMINATION	36
3.4.1 Material selection	36
3.4.2 Layer thickness determination.....	43
3.5 COMPUTATIONAL ANALYSIS	44
3.5.1 Specific criteria and test protocols	44
3.5.2 Design approach.....	49
4. RESULTS AND DISCUSSION.....	56
4.1 FEA RESULTS FOR TYPE III PROTOCOL	56
4.1.1 Total deformation results for 7.62 mm bullet.....	56
4.1.2 Equivalent stress results for 7.62 mm bullet	59
4.1.3 Shear stress results for 7.62 mm bullet	60
4.1.4 Directional deformation results for 7.62 mm bullet	62
4.2 FEA RESULTS FOR TYPE IIA PROTOCOL.....	63

4.2.1	<i>Total deformation results for 9 mm bullet</i>	63
4.2.2	<i>Equivalent stress results for 9 mm bullet</i>	66
4.2.3	<i>Shear stress results for 9 mm bullet</i>	69
4.2.4	<i>Directional deformation results for 9 mm bullet</i>	73
4.3	FEA RESULTS FOR TYPE II PROTOCOL	74
4.3.1	<i>Total deformation results for 9 mm bullet</i>	74
4.3.2	<i>Equivalent stress results for 9 mm bullet</i>	76
4.3.3	<i>Shear stress results for 9 mm bullet</i>	79
4.3.4	<i>Directional deformation results for 9 mm bullet</i>	83
4.4	BALLISTIC LIMIT	86
4.4.1	<i>Fundamental approach</i>	86
4.4.2	<i>Ballistic limit of bullets under NIJ protocols</i>	86
4.5	MESHING PARADIGM	88
4.5.1	<i>Meshing determination</i>	88
4.5.2	<i>Direct effects of meshing on deformation</i>	91
4.6	TABLE OF RESULTS	92
5.	CONCLUSIONS AND FUTURE PROSPECTS	95
5.1	CONCLUSIONS	95
5.2	SOCIETAL IMPACT AND CONTRIBUTION TO GLOBAL SUSTAINABILITY	97
5.3	FUTURE PROSPECTS	98

List of Figures

Figure 2.1 Small arms ammunition visual commonly used in the resistance studies of body armors [18]	11
Figure 2.2 The figure above shows various materials' relationship between specific tensile modulus and specific tensile strength for ballistic fibers [18]	14
Figure 2.3 Various visuals and definitions for ballistic limit [31]	16
Figure 2.4 Penetration probability curve based on striking velocity by Sedgwick [32] ..	16
Figure 2.5 Failure modes occur over plates, proposed by Sedgwick [32]	17
Figure 2.6 Typical penetration modes of impacted armor plates by C.J. Hu et al [33] ..	19
Figure 2.7 Phenomena caused by perforation effect on the target and projectile by Zukas [31].....	21
Figure 2.8 Range of physical parameters for target impact response suggested by Zukas [31].....	21
Figure 2.9 Depth of Penetration (DOP) testing visual of Kaufmann [26].....	22
Figure 2.10 Strike face of a polycarbonate cube is seen after a successful shot at around 800 m/s with a 7.62 mm APM2, whereas 37 mm of DOP value is seen clearly [40]	22
Figure 2.11 Armor panel acceptable shot / fair hit locations are shown. (Adapted from NIJ 01.01.006 standard document) [30]	25
Figure 2.12 BFS Measurement examples [30] [16]	26
Figure 2.13 Caliber Deformation Envelope, taken from Wound Ballistics [42]	26
Figure 3.1 Side view of vest composed of different materials/panels and the direction of fair-hit	30
Figure 3.2 The 7.62 mm projectile visual.....	31
Figure 3.3 Meshed visual of 7.62 mm projectile	31
Figure 3.4 Bullet material - Steel 4340 material properties [34]	32
Figure 3.5 Element/surface coordinate system visual [45].....	32
Figure 3.6 Vest materials and dimensions, perfectly bonded structure.....	33
Figure 3.7 Front Layer Material - SiC mechanical properties	34
Figure 3.8 Backing Layer Material - Kevlar properties	35
Figure 3.9 Visual showing plate and bullet placement	38
Figure 3.10 Visual showing the material properties are designated for materials	38
Figure 3.11 Visual showing the material properties are designated for materials	39
Figure 3.12 First analysis result providing total deformation with SiC material used is shown.....	39
Figure 3.13 Second analysis result providing total deformation with BC material used is shown.....	40
Figure 3.14 Third analysis result providing total deformation with alumina (Al_2O_3) material used is shown.....	40
Figure 3.15 Visual providing equivalent stress values and formation for Al_2O_3	41
Figure 3.16 Visual providing equivalent stress values and formation for SiC	41
Figure 3.17 Visual providing equivalent stress values and formation for BC.....	42
Figure 3.18 NIJ standard requirements for all possible alternatives including bullet types, impact angles, velocity, total number of shots etc. [30]	45
Figure 3.19 SiC geometry to be used within multi-layered structure in Explicit Dynamics analysis	45
Figure 3.20 Resin epoxy geometry and thickness being 10 mm	46

Figure 3.21 Kevlar geometry and thickness being 15 mm	46
Figure 3.22 Li-Ion layer infused in PVC material and having a thickness of 15 mm	46
Figure 3.23 Multi-layer vest structure visual composed of all layers provided above ...	47
Figure 3.24 7.62 mm and 847 m/s analysis for Type III Test.....	47
Figure 3.25 The structure and position of the six 7.62 mm bullet	48
Figure 3.26 NIJ fair hit requirements visuals in similar view	48
Figure 3.27 Fair hit targets on the multi-layered panel	49
Figure 3.28 Meshed panel front view.....	50
Figure 3.29 Meshed panel side view	50
Figure 3.30 Meshed panel other side view	51
Figure 3.31 Meshed panel outlook view	51
Figure 3.32 Meshed bullet view.....	52
Figure 3.33 Contact established in between SiC and Epoxy Contact	52
Figure 3.34 Contact established in between Epoxy and Kevlar	53
Figure 3.35 Contact established in between Kevlar and Li-Ion.....	53
Figure 3.36 Projectile velocity determination in ANSYS	54
Figure 3.37 Further analysis settings and commands in ANSYS	54
Figure 3.38 Further analysis settings and commands in ANSYS	54
Figure 3.39 Further analysis settings and commands in ANSYS	55
Figure 4.1 Total deformation results' visual.....	56
Figure 4.2 Total deformation results' side view visual	57
Figure 4.3 Fair hit locations visual.....	57
Figure 4.4 Maximum and average total deformation information vs. time results	58
Figure 4.5 Total deformation in time graph.....	58
Figure 4.6 Equivalent stress result front view associated with Type III armor conditions of 7.62 mm projectile.....	59
Figure 4.7 Equivalent stress result side view associated with Type III armor conditions of 7.62 mm projectile.....	59
Figure 4.8 Equivalent stress result top view associated with Type III armor conditions of 7.62 mm projectile.....	60
Figure 4.9 Maximum shear stress result front view associated with Type III armor conditions of 7.62 mm projectile.....	60
Figure 4.10 Maximum shear stress result side view associated with Type III armor conditions of 7.62 mm projectile.....	61
Figure 4.11 Maximum shear stress result top view associated with Type III armor conditions of 7.62 mm projectile.....	61
Figure 4.12 Directional deformation result front view associated with Type III armor conditions of 7.62 mm projectile.....	62
Figure 4.13 Directional deformation result side view associated with Type III armor conditions of 7.62 mm projectile.....	62
Figure 4.14 Directional deformation result top view associated with Type III armor conditions of 7.62 mm projectile.....	63
Figure 4.15 Total deformation result front view associated with Type IIA armor conditions of 9 mm projectile.....	64
Figure 4.16 Total deformation result alternative front view associated with Type IIA armor conditions of 9 mm projectile	64
Figure 4.17 Total deformation result side view associated with Type IIA armor conditions of 9 mm projectile.....	65
Figure 4.18 Total deformation result top view associated with Type IIA armor conditions of 9 mm projectile.....	65

Figure 4.19 Minimum, maximum and average deformation values	66
Figure 4.20 Equivalent stress result front view associated with Type IIA armor conditions of 9 mm projectile.....	67
Figure 4.21 Equivalent stress result side view associated with Type IIA armor conditions of 9 mm projectile.....	67
Figure 4.22 Equivalent stress result top view associated with Type IIA armor conditions of 9 mm projectile	68
Figure 4.23 Minimum, maximum and average stress values	68
Figure 4.24 Equivalent stress in time graph	69
Figure 4.25 Maximum shear stress result front view associated with Type IIA armor conditions of 9 mm projectile.....	70
Figure 4.26 Maximum shear stress result side view associated with Type IIA armor conditions of 9 mm projectile.....	70
Figure 4.27 Maximum shear stress result top view associated with Type IIA armor conditions of 9 mm projectile.....	71
Figure 4.28 Minimum, maximum and average stress values	72
Figure 4.29 Maximum shear stress in time graph.....	72
Figure 4.30 Directional deformation result front view associated with Type IIA armor conditions of 9 mm projectile.....	73
Figure 4.31 Directional deformation result top view associated with Type IIA armor conditions of 9 mm projectile.....	73
Figure 4.32 Total deformation result front view associated with Type II armor conditions of 9 mm projectile.....	74
Figure 4.33 Total deformation result side view associated with Type II armor conditions of 9 mm projectile	75
Figure 4.34 Total deformation result top view associated with Type II armor conditions of 9 mm projectile	75
Figure 4.35 Minimum, maximum and average total deformation values	76
Figure 4.36 Equivalent stress result front view associated with Type II armor conditions of 9 mm projectile	77
Figure 4.37 Equivalent stress result side view associated with Type II armor conditions of 9 mm projectile	77
Figure 4.38 Equivalent stress result top view associated with Type II armor conditions of 9 mm projectile	78
Figure 4.39 Minimum, maximum and average stress values	78
Figure 4.40 Equivalent stress variation in time graph.....	79
Figure 4.41 Maximum shear stress result top view associated with Type II armor conditions of 9 mm projectile.....	80
Figure 4.42 Maximum shear stress result front view associated with Type II armor conditions of 9 mm projectile.....	80
Figure 4.43 Maximum shear stress result side view associated with Type II armor conditions of 9 mm projectile.....	81
Figure 4.44 Minimum, maximum and average stress values	82
Figure 4.45 Maximum shear stress in time graph.....	82
Figure 4.46 Directional deformation result front view associated with Type II armor conditions of 9 mm projectile.....	83
Figure 4.47 Directional deformation result side view associated with Type II armor conditions of 9 mm projectile.....	84
Figure 4.48 Directional deformation result top view associated with Type II armor conditions of 9 mm projectile.....	84

Figure 4.49 Minimum, maximum and average directional deformation values	85
Figure 4.50 Directional deformation variation in time graph.....	85
Figure 4.51 FEA directional velocity result for Type II.....	87
Figure 4.52 FEA directional velocity result for Type IIA.....	87
Figure 4.53 FEA directional velocity result for Type III	88
Figure 4.54 Finer mesh front view of the multilayered panel	89
Figure 4.55 Finely meshed panel top view that is fairly hit	89
Figure 4.56 The Type III bullet of 7.62 mm with a speed of 847 m/s hitting the multilayered plate visual	90
Figure 4.57 The Type III bullet of 7.62 mm with a speed of 847 m/s hitting the multilayered plate visual	90
Figure 4.58 Comparison table on total deformation value between coarse mesh and fine mesh.....	91
Figure 4.59 Equivalent stress results table providing a specific comparison for all tested projectiles	93
Figure 4.60 Maximum shear stress results table providing a comparison for all tested projectiles	93
Figure 4.61 Directional deformation results table providing a comparison for all tested projectiles	94
Figure 4.62 Ballistic limit velocity (BLV) results table providing a comparison for all tested projectiles.	94

List of Tables

Table 3.1 Material properties of B ₄ C and SiC in various forms	37
Table 3.2 NIJ standard requirements for computational analysis [30].....	44
Table 4.1 An overall results' comparison for all FE analysis successfully computed	92

List of Abbreviations

FEA	Finite Element Analysis
BLV	Ballistic Limit Velocity
NIJ	National Institute of Justice
DOP	Depth of Penetration
P-BFS	Perforation Back Face Signature
POS	Point of Strike
BL	Ballistic Limit
ED	Explicit Dynamics
AP	Armor Piercing
LFP	Lithium Iron Phosphate
NMC	Lithium Manganese Cobalt Oxide
LTO	Lithium Titanate Oxide
PVC	Polyvinyl Chloride

Dedication

I would like to thank for their patience and love, so willing to dedicate this thesis to my wife Özge, one and only son Kemal Emir, and the newborn baby princess Alya, who brings joy to my family.

I also dedicate this and all future works to my wonderful parents Mukaddes & Kemal as well as my brother Levent who raised me under very tough circumstances to be someone.

Also, I do much appreciate my advisor Assist. Prof. İlker Erdem who gives full support to bring this work together in a legitimate way.

Chapter 1

Introduction

1.1 Background of the Project

The self-preservation instinct of human has led the emergence of various technologies such as body armors or, in today's world, ballistic vests, which is commonly used by law enforcements and armies all over the world. Body armors date back to ancient Greece and ages of Japanese samurai, and even about 2500 BC in Mesopotamia region. The first materials for the body armors were various layers of linen and silk as a protective clothing. Although the idea of the body armors has not been fully changed, the materials have highly progressed [1] [2]. During World War II, so called *flak jacket* were developed which was made of ballistic nylon, and it was not even strong enough to resist the bullet without any injury [1]. Body armors can be manufactured with variety of materials but mainly made out of woven fabric composites and mostly used by military personnel and other law enforcement agencies [3]. The most important part of a ballistic vest is, indeed, the protection/resistance capability to threats. Even though the purpose of body armor still stays same, the structure and the function has been changing constantly associated with the two main points: being light-weight and protective. However, it is not sufficient and comprehensive enough especially for military personnel because the vest also needs to allow user for critical movement tasks and also comply with other equipment, such as weapon, role-radio, helmet, night-vision goggles, assault pack and battery packs, etc. When all this equipment combined, it may be very tough for a soldier to carry such a heavy load and not to lose its maneuverability capability at the same time. Especially for military body armors, main goal is the protect soldier from injuries during combat but it is essential to take control its maneuverability and stand still during material handling. Material handling concept includes rifle loading/firing, grenade throwing, digging foxholes, as well as marching and moving tasks [4]. Hence, in the modern warfare, as methods and techniques of combat and usage area rapidly evolves, it is now essential to

make vests flexible, lightweight, compact, power supplying and highly-protective at the same [5]. For around 100 years, ceramic materials have been utilized as reinforcement in military equipment and vests. When ceramic materials are used with other materials alongside in ballistic vests, their material properties of high resistance to impact and low density compared to metals have made them an ideal material to be used in vests in military armor. Advancements in ballistic vests have been seen since the days of World War I. At first the armor was just mere metal plates enameled together but in modern times they have been reinforced by boron carbide (B_4C) to aluminum oxide (Al_2O_3) also known as alumina and also to silicon carbide (SiC) ballistic vest materials. Ceramic materials are anticipated to be at an improving side in the coming years to bring about huge abatement in their weight, their expense and their ballistic efficiency [6].

In 1965, Kevlar was invented by a company called DuPont, and it was described as extremely strong, lightweight and durable material. Mainly composite based materials such as Kevlar, Spectra, Twaron, Zylon etc. have been widely used nowadays to satisfy the core necessity of flexible movement and high resistance to threats [5]. Over the globe ballistic equipment and protection counts a lot towards countries military development and also a means of high investment by countries. In 2015, the market in the USA accounted for almost up to 3,9 billion US Dollars revenue for ballistic armors and vests including R&D expenses. In this scenario, ceramics accounted about %30 in revenue volume and it is foreseen that the armor market will be exceeding 5,7 billion US dollars by 2024. USA influences over the market share with an amount ranging up to 49.5 percent. Due to ascent of worldwide instability and altercations over the borders have given rise to the demand of modernized equipment for the military and the personnel all over South-East Asia and eastern side of Europe. Body armor Type 2A has the fastest monetary development intended to secure against bullets and projectiles and are considered perfect for policing, although in 2015 the interest in Type 4 body armor, which is heavier compared to Type 2A, gave rise to 24 percent of the market rate [7]. A short outline of meanings of various protective armor types is given in NIJ standards, and the appropriation of the market size is illustrated in Grand View Research, 2016 [7].

1.2 Introducing the Research Topic

All through history, lightweight and adaptable materials have been investigated for diminishing the weight of body armor frameworks to upgrade versatility, whereas giving assurance against specified dangers. Early materials such as calfskin and silk were utilized in conjunction with metal plates to supply the required assurance in making vests. These vests provided security against bomb and projectile parts, which accounted for the high majority of serious injuries and deaths among officers. In spite of the fact that nylon and e-glass filaments proceed to find a few uses nowadays due to their material characteristics, high performance fibers are presently considered as the standard for most fiber strengthened armor applications. High performance fibers are ordinarily utilized in the form of woven textures for vests and helmets.

The self-preservation instinct of humans has driven the development of different innovations such as body armors or, in today's world, ballistic vests, which are commonly utilized by law enforcement and armed forces' requirements all over the world.

The most critical portion of a ballistic vest is, undoubtedly, the protection/resistance capability to potential dangers. Indeed, in spite of the fact that the reason body armor still remains the same, the structure and the expectations from a conventional body armor has been changing, whereas main two primary expectations are: being light in weight and more comfortable. Be that as it may, it is not adequate and comprehensive enough particularly for military work force since the vest too should permit user for basic development assignments conjointly comply with other gear, such as weapon, role-radio, head protector, night-vision goggles, ambush pack and battery packs, etc. When all this hardware combined, it may be exceptionally intense for a warrior to carry such an overwhelming stack and not to lose its maneuverability capability at the same time. Particularly for military bodies, the primary objective is to safeguard troopers from wounds amid combat but it is basic to require control over its maneuverability and stand still amid fabric dealing. Fabric dealing with concept incorporates rifle loading/firing, projectile tossing, burrowing foxholes, as well as walking and moving tasks [4]. Thus, within the cutting edge fighting, as strategies and methods of combat and usage area quickly advances, it is presently basic to form vests adaptable, lightweight, compact, control providing and highly-protective at the same [5].

Since then, by the results of numerous numerical calculations, penetration simulations and actual field-tests; various body armor design alternatives are examined and many specific and important details are discovered on fabric microstructure, yarn-denier, end count, tow structures, filament spatial paths and fiber to fiber interaction [1]. Due to the technological advancements taking into account these parameters, to measure valid perforation resistance and characteristics, two approaches have become more valid [1]. One approach here is homogenous continuum and the other non-uniform approach focuses on a more detailed geometrical representation in tows/yarns [1]. Considering both approaches, especially the homogenous continuum; the main goal is to measure correctly how far the projectile perforates but also being able to measure the impact of the projectile inducing significant bulge at the back face of the armor even if the penetration is within the tolerated limits [3]. Materials used in armors having high tensile strength and failure strain are always considered for ideal candidates because they tend to absorb more energy per unit volume [3]. Even though strong and low density fibers are favored materials for ballistic protection purposes, the choice of the materials are still very limited for both providing the key essentials being lightweight and protective at the same time [8]. Hence, to examine a light-weight and protective enough ballistic vest materials composed with power-supplying battery panel, a Finite Element Modeling (FEA) is established in ANSYS software and optimum approach for a vest that is protective enough and lightweight is being computed. A three dimensional model of an armor, composed of various materials including an additional layer of a battery pack, has been created in the drawing tool of ANSYS and FEA analysis has been applied assuming the hit by a projectile at normal incidence as stated the National Institute of Justice (NIJ) standards.

In addition to the challenges of designing a ballistic vest which needs to be light-weight, protective-enough and having the capability of maneuverability at the same time; considering a compact solution is necessary. Achieving vest perforation results under different loads and materials applied by FEA analysis would be the fundamental and core part of this thesis. In other words, when designing a compact vest solution for a soldier, other belongings that a soldier must carry along with the vest, such as batteries, should also be taken into account. Hence, this study focuses to design and create a vest that is protective enough and lightweight but also composed of an additional layer that provides the energy/power requirement for soldier's equipment & belongings. To explain this necessity further in detail, it is reported that a modern soldier carry equipment up to 41

kg even under fully equipped and running conditions, almost 20% to 30% of this load comes from batteries [4]. In addition, these batteries are carried either in the back-pack or in the pockets located in various parts of the uniform and simply the weight is usually distributed non-uniformly which may significantly increase the cause of musculoskeletal injuries [9]. It was reported that for a 36-hour operation, depending on the battlefield role and the task, British infantrymen could carry up to a 12.3 kg of batteries [9]. It was studied that when wearing a body armor, the men soldiers completed 61% fewer pull-ups and women soldier's hang time were reduced by 63%, proving the direct negative effect of weight on performance [4]. It is clear that ballistic armors are designed to protect, when other belongings such as battery added to the vest - which has no specific placing on the vest, creates another problem of heating. Heat is a factor that negatively impacts individual soldier's ability and performance and must also be considered that both vest (causing heat by long-term wearing/usage) and batteries reveal heat to the user [4]. In conclusion, a protective body armor should be designed of multiple layers that are made out of high protective fibers, flexible and light in weight materials, as well as out of less heat-conductive material for the comfort of the user.

1.3 Scope of the Thesis

Earlier to advanced FEA programs, exploratory investigation was the instrument used to look at impacts that displayed any degree of complexity. Test investigation is expensive and requires numerous testing models, test gear, certain inventory, protocol necessities and test environment. In high-speed or affect testing, harm or pulverization of the model is required before meaningful quantitative data around the plan can be obtained. Moreover, effects and analysis such as crack initiation, propagation, bullet perforation, heat (conduction, convection and even radiation) transfer, fatigue etc. do require critical design requirements and real life experiments take very long time, extreme efforts and cannot be considered cost-effective in any means, FEA platform becomes very practical and easy to accomplish such analysis. Basically, the critical advantage of FEA over the exploratory strategy is the examination of a virtual model in a virtual environment. It is essential to define and determine parameters in FEA very carefully such as boundary conditions, loads and load types depending on the analysis and mesh fineness depending on the geometry and analysis type etc. Hence the commercial program ANSYS V19 and V2020 is being used to compute, whereas simulation results are compared to previous

analytical and experimental results from the literature. Since some built-in capabilities are found to be inadequate in all FEA analysis, a vest model/design is obtained in ANSYS by using basic elements and meshing is applied to drawing accordingly. This approach permits for a more concurrent investigation of the plan amid the designing process, in this way minimizing designing costs and testing whereas expanding item performance [10]. The understanding of material science included in impacts is fundamental to carry out great numerical analysis. The scope of this thesis incorporates the computational ponder of six various cylindrical bullets striking to a ballistic vest with high speed shot (effect) on lean plates of diverse materials using explicit finite element solver in ANSYS. The simulation outcomes are confirmed with three sorts of bullets whereas more detail given in the results and discussion part of the thesis. Ballistic constrain or most extreme speed of the shot that a target can stop with perforation was found. The fundamental center of the thesis is to supply a comprehensive, lightweight vest that underpins a lithium ion layer at the back conclusion and the points of interest on the detailing of affect analysis and parameters influencing the method.

1.4 Thesis Organization and Research Questions

This proposition endeavors to investigate by considering behavior of distinctive materials and impact introductions under comparable ballistic impact conditions. Ponders will incorporate stay time for the time period where the diverse geometries would stay intact earlier to breaking as well as the velocity, number of cycles connected by the distinctive material. The outcomes from each study are compared.

This proposal is organized into the following five chapters:

- Chapter I Introduction
- Chapter II Literature Review
- Chapter III Materials and Method
- Chapter IV Results and Discussions
- Chapter V Conclusion and Future Prospects

In Chapter I, a fundamental presentation to the beginning and objectives of this paper was displayed. The truths on the history of armor advancement in conjunction with a dialog on current armor frameworks, their inadequacies and proposed changes. Moreover, past research into composite ceramic-based armor frameworks were briefly

referenced. Chapter II deals with the literature survey of various articles and authors who have worked on similar research fields. The materials that have been used in the past and the future prospects of the studies are discussed. Chapter III describes the subtle elements the demonstrating strategies utilized to assess the ballistic vest affect conditions. It moreover depicts the computer reenactment that will be utilized to analyze and compare with three sorts of bullets. The theoretical conditions considered in this research will also be displayed. Chapter IV discusses the results obtained from ANSYS workbench - explicit dynamics - analysis. The outputs such as total deformation, the directional deformation and the maximum shear stress are found out from this workbench analysis. Also, the phenomenon of ballistic limit velocity is discussed by the results of ANSYS explicit dynamics values. Lastly, Chapter V presents conclusions and proposals for follow-on work. Note on units: the simulation program, ANSYS, is programmed to utilize SI units. For the purpose of consistency, all units, information and charts will be displayed in SI units alongside U.S. standard units when possible.

Chapter 2

Literature Review

2.1. Ballistic Testing

Whereas the analytical models are material science based, they utilize simplifying assumptions to diminish the administering conditions to one and two-dimensional conditions. These models moreover as it were seen at one angle of the issue, and are not able to look at each plausibility or viewpoint of a complex entrance issue [1]. Empirical conditions, too alluded to as entrance conditions, are greatly valuable because of their effortlessness and ease of utilization, but they too have deficiencies. To begin with, they are, in essence, curve-fits of exploratory information and are in this manner constrained to the extent of conditions and quality of the tests. Furthermore, as specified over, test results are not fundamentally exact, and it seems not feasible to conduct a real-world affect experiment for each possible scenario that can be experienced, hence restricting the databases from which these conditions are made.

With the ever expanding control and speed of computers, and the refinement of finite element (FE) codes and unequivocal energetic solvers, it is conceivable to utilize numerical examination and computer recreation to demonstrate ballistic effect occasions. Once a demonstration is made, simulation results can be compared with accessible exploratory test information, and the FE trusted results can be refined until the client is sure of the results produced by the reenactment. Certain FE modeling parameters, such as fabric properties at tall strain rates, depend on experimental data, but since the FE simulations are not based on curve-fits to affect test information, simulation results are not influenced by conceivable exploratory blunder in a few trials in a set of test data. Because of this, there can be more prominent certainty within the FE comes about, compared to penetration equations, in locales where test information is not accessible. FE simulations can be utilized to model impact tests instead of real-life experiments in arrange to diminish cost, overwhelming time and energy. They can moreover be utilized

to increase and refine the existing entrance equations, filling in holes where test information does not exist or inadequate.

2.2 Introduction to Armor System

Nowadays, defense industry officials and researchers are focusing to make faster, versatile and nimble military weapons to balance with the increasing warfare tensions [11]. In the past, gun shots on soldiers have cost many lives thus a critical need was seen for a bullet proof ballistic vest which could be used in warfare conditions. This all brought about the advancement of ballistic vests and their interest and demand progressively expanded around the world. The further consequence of increase demand prompted the exploration of new materials to be used in the vest to make it strong and also lightweight. Military companies over the globe have been utilizing various types of polymer matrix composites, ceramics and metal layers to strengthen the armor and increase its mobility [11]. Ongoing research foresees to remove even little amounts of metal from the armor and supplant it with composite materials which will offer brilliant solidarity to weight proportions [11].

The main goal of ballistic vest is to stop bullets from entering into the jacket (up to some point) so that the soldier remains safe and not injured. The vest in use should be durable and convenient for usage and should not be too heavy since the soldier at mission feel ease while wearing it. Nowadays, a multi-purpose armor systems are very desirable which is consisted of developed ceramic layers, fiber layers and metal layers. The basic function of the ceramic layer is to deflect the projectile and the artificial fibers that are used in the middle layers hold the bullet particles and prevent them from penetrating, or the Kevlar or metal layer completely stop the bullet without any perforation. When contrasted with steel layering utilized in medieval times, this multilayer framework is more proficient and gauges much less than the steel layering [12]. Boosting the resistance of bullet-proof ballistic vest by using various materials like ceramic and fibers is a common and generally used idea, hence results good durability for the armor [12]. In almost any structural ballistic vest, Kevlar and steel are seen as the most common materials that are preferably used in the back end layers [13] [14]. The design and the construction of the vest, which has maximum efficiency and contains multiple layers is usually done in two stages. In the first stage, the materials are chosen according to the desired characteristics and foreseeing the impact and threat situation is essential, whereas

the vest is designed regarding to these facts accordingly. In the second step, the vest is simulated and tested in which one gets to know the efficiency criteria and material's ballistic limits [15]. When designing a commercial ballistic vest, the three essential points that need to be counted for are: type of material (material characteristics), geometry and the application. Appropriate meshing and mechanical & physical properties also play a key role in the simulation procedure as the results are dependent on both the target and the projectile motion. It is stated by researchers that the isotropic properties of materials play an important role also like elasticity type, young modulus and the failure outcomes to model a noteworthy model in ballistic operations [16] [17].

2.3 Fundamental Principles

When designing a ballistic vest, there is a conventional balance between weight, comfort, protection and effectiveness. "Effectiveness" described here is the capability of having a power-providing solution that would create a more compact, protective and unique approach. [18]. The main principle is to maximize energy absorbing mechanisms when designing a protective body armor, whereas considering two major facts of formation of cruciform of stretched fibers and out-of-plane deformation around the Point-of-Strike (POS) which is related to the significant factor of Back Face Signature/Deformation, due to the z movement of the bullet [18]. In the very significant study on energy absorbing mechanism reported by Cunniff [19], the work done by the fibers due to the stretch is defined as Elastic Stored Energy, E_s which is calculated by equations [18] [19] [20]; where V is strain wave velocity in the fibers, E is the elastic modulus of fiber, and ρ is the density of fiber. Hence, the necessary related equations and relations of it are given below in Equation 2.1 and Equation 2.2:

$$V = \left(\frac{E}{\rho}\right)^{1/2} \quad (2.1)$$

$$E_s = \sigma\varepsilon/2\rho \quad (2.2)$$

Before creating a 3D model and computing finite element analysis, to see the perforation against the resistance of the composite laminated – battery powered module, the movement of the projectile and the structure of the loads need to be explained in detail. Thus, it needs to be clarified that laminated composite model should be composed of four

layers being front layer (SiC), Kevlar-Epoxy and the Battery Pack Layer with Silicon infused and the adhesive/epoxy (in between front layer and Kevlar). It must be thought that these four layers are assumed to be perfectly bonded together [3] [21]. On the other hand, there is a misconception of understanding on assuming every laminate is perfectly bonded in any design, so we still need to understand that composite laminates always brings certain difficulties to the analyst such as; based on transverse shear stresses that are undervalued and caused by the mismatch of material properties among layers, in-plane orthotropy in the principal material directions and bending-stretching coupling due to the asymmetry of module design [22] [23]. To prevent the possible issue of orthotropy, one may need to consider designing the fourth layer of the battery pack with such a material that is isotropic.


Ammunition	9mm FMJ remington	7.62mm M80 NATO bass	7.62×39mm AK47	US 30-06" [AP M2]	7.62mm× 51 [FFV]
Bullet and core					
Bullet weight/g	8.0	9.5	7.9	10.7	8.4
Core weight/g	~7.0	~7.0	3.6	5.2	5.9
Core dia/mm	8.0	~7.1	5.7	6.2	5.6
Core material	Lead-based	Lead-based	Mild steel	Hardened steel	Tungsten carbide
Hardness (Hv)	~30	~30	210	785	1 450

Figure 2.1 Small arms ammunition visual commonly used in the resistance studies of body armors [18]

Avoiding using an anisotropic material as for the casing of the battery may be beneficial to disregard transverse shear. In addition to analysis factors, various major parameters such as fiber density, fiber tenacity, elastic modulus, yarn friction, yarn twist, number of layers, mass/shape and velocity of projectile, shot distance/location and number of shots affect the results and accuracy [20].

2.4 Material Properties

It is common these days to build ballistic vest using composite metal-ceramic body or using monolithic ceramic [6]. This layer is covered with nylon which in turn is attached to fibers of high tensile strength or sometimes laminated with polyethylene such as Kevlar [6]. This polyethylene is attached at the back end of the vest for a last layer of protection. In some case soft metals are also used like aluminum as a backing layer [6] [24]. Sometimes a spall shield is used which is appended on the facade of the front-most layer. In some particular cases where the requirements of the ballistic armor are comparatively higher might require complicated framework of armor.

In ceramics and their composites with metals mostly alumina and alumina-mullite ceramics are used in ballistic vest. In some strength related cases Silicon carbide is also used and also some other non-oxide ceramics like borides, nitrides, carbides for both heterogeneous and homogeneous structures [6]. Ceramics ranging from 5 mm to 9 mm thicknesses are considered ideal for the first layer which are then attached to the epoxy and Kevlar layers. Although it is fact that the number of aramid fibers depends on the strength requirements and performances of the ceramic but even one or two layers of aramid fiber is considered good enough to stop several various projectiles. The number aramid fabric depends on the ceramic layer and are generally, inversely proportional as in the greater the aramid fibers will support the layer structure of ceramic.

Although alumina is having such a low density around 3.95 g/cm^3 , it is still commonly used and preferred for ballistic vest material and design [6]. This is due to the fact that alumina is very economical compared to alternatives and can be manufactured using various methods like pressing, slip casting and injection molding and the expense of the material is also very low like kilns. In addition, alumina has high performance to physical property ratio.

On the other hand, silicon carbide is studied extensively for the ballistic vest purpose and it is considered an excellent material for ballistic vest which can withstand high pressures and provide weight reduction also with good manufacturing conservation [25]. When the mechanical properties are compared with other non-oxide materials such as aluminum nitride (AlN), silicon carbide (SiC), boron carbide (B_4C), silicon nitride (Si_3N_4) etc. these materials have low densities ranging from 2.5 to 3.3 g/cm^3 which is an

important parameter in ballistic testing. All these composites also have high hardness rate and strength and young modulus.

2.4.1 Core Property Requirements

Choosing the right materials and material parameters are the most significant and challenging part of the analysis of a body armor. The influence and significance of main material properties on the determination of ballistic resistance has been investigated in detail and can be summarized as follows. These following six properties (density, tenacity, elastic modulus, compressive strength, shear strength and hardness) are the core properties to be considered for a perforation analysis on a laminated armor and shall be the basis for material consideration. However, it may not be sufficient and limited to these only six parameters to discover the full potential of the ceramic behavior and the penetration mechanism of the projectile. There are other properties of materials and formations to discuss and discover such as Hugoniot elastic limit, fracture toughness, crater size, etc. to contemplate the concept. On the other hand, it may be more logical to discuss the effects/response of these properties during or after the computational analysis.

2.4.2 Density, Tenacity and Elastic Modulus

Density is one of the major fiber property that has a direct relevance for resistance. It has been known that using a low density material for the targeted body armor has a significant advantage on ballistic resistance [26]. In addition, recent studies has shown that materials having high elastic modulus, high tenacity and low elongation at break shows better resistance to low to high velocity projectiles [20].

As Figure 2.2 below provides and substantiates, different fibers providing different resistance performance which is directly related to their modulus and tenacity values.

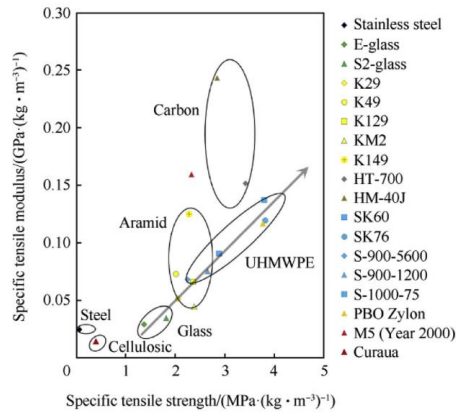


Figure 2.2 The figure above shows various materials' relationship between specific tensile modulus and specific tensile strength for ballistic fibers [18]

2.4.3 Compressive Strength, Shear Strength and Hardness

Compressive strength or tile thickness is another major resistance factor of the body armor that effects the initial resistance of the projectile for perforation [26]. More in detail, the projectile/bullet may suddenly be fractured, deformed or deflected depending on the compressive strength property of the armor material [1] [26]. High shear strength can also helpful for defeating/stopping a bullet however the armor material must be designed sufficient in thickness compared to the threat/bullet due to the large stress gradients may occur as a result of tension/compression effect around the projectile core and the contact area [26]. Woodward and Kaufmann stated that the hardness of composite material should be greater than the projectile aiming to penetrate because the movement of projectile may be decreased at the backing material effectively. However, further increase in hardness may be unnecessary or beneficial in any means [26] [27].

In addition, it must be noted that, in the vicinity of penetration, ductile and brittle materials may show very different behaviors. During or after the penetration in brittle materials or the impact response on brittle targets, it is noted that the fracture propagates much at very high speeds compared to ductile materials [28].

2.5 Ballistic Efficiency

The ballistic efficiency is simply defined by the Rozenberg as the average of static and dynamic compressive strengths divided by the density of the targeted backing material/ceramic, and can be mathematically expressed as follows [29]:

$$\eta = \frac{\rho_{Al} * P_{Al}^*}{\rho_c * h_c^*} \quad (2.3)$$

In this equation, ρ_{Al} and ρ_c are the densities of aluminum and ceramic respectively, h_c^* is the minimum tile thickness needed for prevention of perforation to backing material, P_{Al}^* is the penetration depth of the projectile to the target, whereas defining ballistic efficiency as the slope of the straight lines through the experimental points aimed to be calculated [26] [29]. In addition, determining ballistic efficiency may be helpful to compare different material structured/laminated vests' penetration resistance, only if tested against a same projectile under same threat conditions.

2.6 Depth of Penetration (DOP) Analysis

2.6.1 Penetration Mechanics, Modes and Phenomena of Effects

Penetration mechanics covers an assorted scope of issues and applications including perforation mechanisms. Penetration mechanics or analysis is used in studies to comprehend and underline the effects of a projectile hitting a plate or a substance. Penetration is basically an overall term defining the effect that alludes to the impact when a projectile penetrates the objective. Whereas *Perforation* alludes to a case which is similar to penetration but in which the bullet totally penetrates the objective. It is known that the term perforation is suggested to be used by NIJ instead of term of penetration for ballistic testing purposes [30]. There is another term which is often utilized in studies which is called *embedment*. A scenario where the shot stay appended to the objective and doesn't go through it at all even after the analysis is over is called Embedment [31]. To begin with, it is of utmost importance to affiliate oneself with the concepts of distinctive ballistic impacts. The ballistic limit velocity, V_{BL} , is that specify velocity at which it is definite that the projectile will penetrate the objective. When the velocity is lower than the ballistic limit velocity, the projectile basically would not be able to penetrate the given objective. Ballistic limit concepts are shown in the Figure 2.3 below [31].

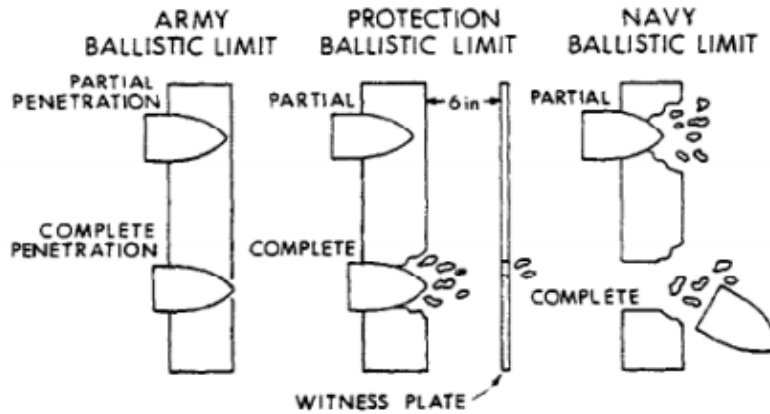


Figure 2.3 Various visuals and definitions for ballistic limit [31]

The above figure is fundamentally distinct with the perforation value and the rule applied to characterize any perforation. The real evaluation of ballistic limits is typically found on a factual distinction of several tests. In this scenario V_{50} speed is used with 50% likelihood that the bullet will penetrate the target. V_{50} data for a typical projectile is shown in the Figure 2.4:

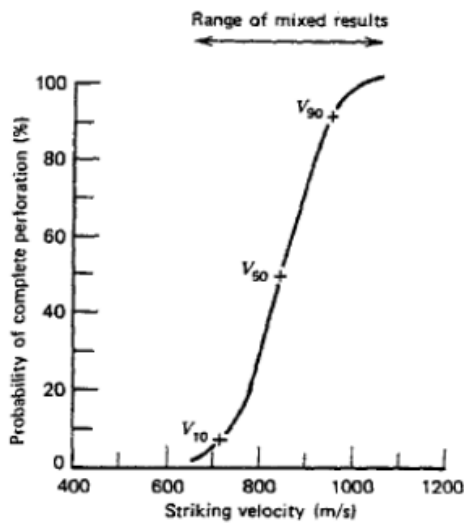


Figure 2.4 Penetration probability curve based on striking velocity by Sedgwick [32]

The failure modes are characterized by Sedgwick [32]. This identification was done post penetration into the objective mechanism. There are identified possible failure modes in a target plate after ballistic penetration. These failure modes provided by Sedgwick are given below:

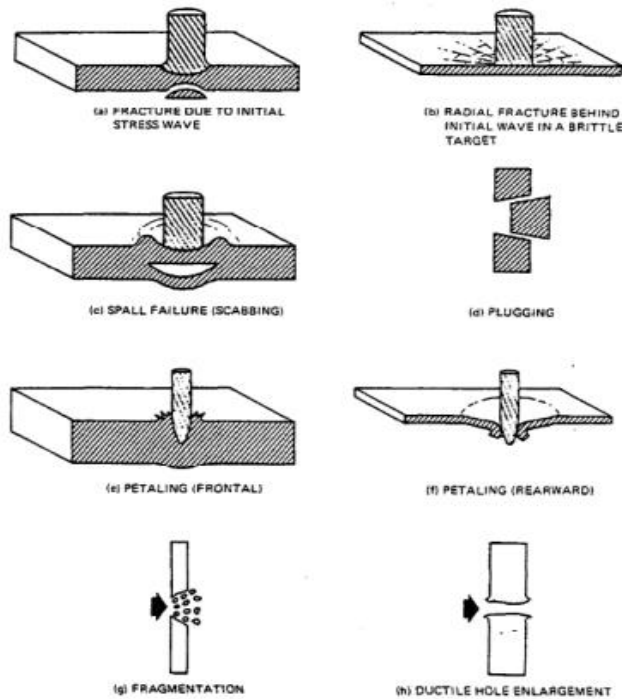


Figure 2.5 Failure modes occur over plates, proposed by Sedgwick [32]

According to his discussions these following definitions and conclusions can be interpreted:

a. Inertial stress resulting in Fracture

On impact, the compressive waves engender at the objective. On the off chance if the magnitude of the stress surpasses the dynamic yield strength of the objective, the unconfined area of the objective layer may result in fracture and failure. It is more likely that the back objective surface experiences and failure or fracture. If you increase the density of the objective layer or even its hardness or ultimate strength compressive yield strength it is expected that the likelihood of the fracture will decrease [32].

b. Initial wave front post Radial Fracture

As soon as the compressive wave engenders away from the impact position the tensile radial stresses start developing. On the off chance, if the magnitude of the stress surpasses the dynamic yield strength of the objective and the behavior of the material in discussion is tensile then, the probability of radial and circumferential arises.

Due to Poisson's ratio and its resulting effect, as the compressive wave spreads outward the circumferential stresses will become tensile. Circumferential tensile stress results in radial cracks.

c. Plugging

When a plate is pushed along the back surface by the projectile this type of failure occurs. The radius of the projectile and the plug is somewhat similar.

d. Spallation

Tensile waves are formed when compression waves are reflected from the back surface. Compressive waves are abandoned by the tensile waves. At the rear surface the compressive waves start spreading which results in their amplitude decay. The magnitude of the tensile stress surpasses the ultimate dynamic tensile strength of the objective resulting in tensile fracture.

Furthermore, the tendency of plugging is directly proportional to the hardness rate since if one is increased the other also increases. The logic behind this is that after some time it becomes difficult for the plate later to be pushed radially outward by the shot projectile. Therefore, in front of the shot a restricted shear develops in the outskirts area and the plastic stream is limited to this locale. The shape of the nose of the bullet and the layer thickness impact the development of plugging. Hence, thinner plate plugging is considered as relatively easy and effective with the end goal that significantly milder plates may result in failure in the event that the effective speed is not adequately near ballistic limit resulting in bending of plate. Along these lines, the possibility of failure also increases for projectiles which are blunt.

There are several penetration modes of impacted armor plates as most of them mentioned above are as follows:

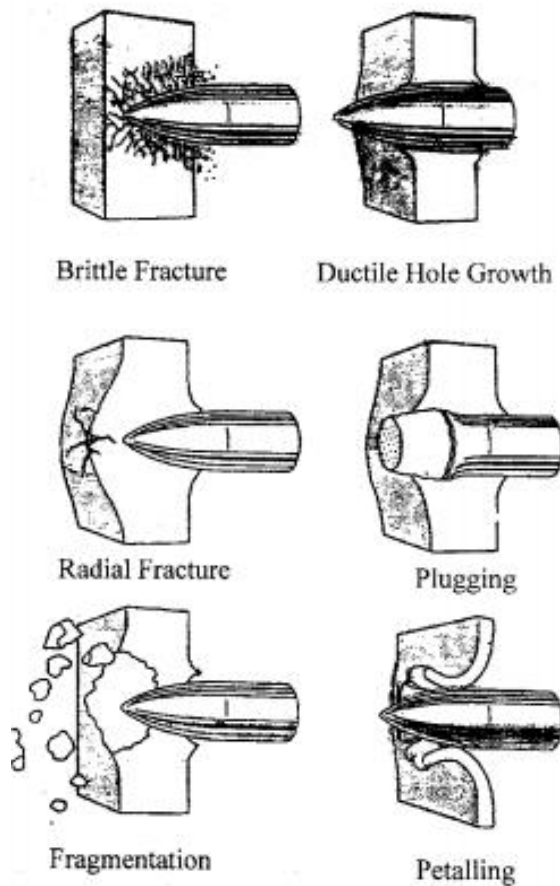


Figure 2.6 Typical penetration modes of impacted armor plates by C.J. Hu et al [33]

It is confirmed that a projectile that is barrel shaped would result in greater extents of shear stress than when it is compared to a conical or other shaped projectile. The failure caused by shear can be represented by the formation of a plug. Shearing becomes easier as shear is lowered by the plastic stream due to rise in temperature. Maximum shearing stress is the reliant factor in forming the shape of the plug.

In the event that there is unadulterated shear at the outskirts, the fitting will be barrel shaped. If there are tensile and compressive stresses near the surface of shear stress this will result in a shortened cone, altered shortened cone, barrel, transformed barrel just as tube shaped. Adiabatic shearing is a process in which extensive amounts of shear develops on the surface as narrow bands due to which the plug can be separated from the objective. The separation can also be seen due to shear growth and also due to the development of a void in the material caused by fracture.

It has been tested that the stress concentration sites are the main targets of instability of adiabatic shear. Heat is generated when plastic deformation takes place as confined deformation causes the generation of heat and well as flux. This heat stays for a while because it is unable to disperse from the high plastic deformation region Moss asserts in his research that the temperature of adiabatic shear can be foreseen to be 10^5 °C whereas the rate of shear strain can be seen to be around 10^7 s⁻¹ [34] [35]. As the temperature rises gradually this also gradually effects the local plastic flow which increases subsequently resulting in focusing local plastic strain. As a consequence of all this, a narrow band of intense plastic strain proceeds to the spreading throughout the material until the material fractures due to maximum shear stress forming at the surface.

Petalling

Petalling is a phenomenon which takes places in thin moderate plates [36]. As compressive waves engender in the outward direction enormous circumferential stresses start to develop throughout the length of the plate. The plates which are made of ductile substance are more prone to this kind of petalling failure when hit by solid conical projectiles. Petalling is more likely to occur when the projectile velocity is close to the ballistic limit as at this velocity the velocity is comparatively very low compared to usual scenarios so the momentum is not limited to only the district near projectile deformation [36]. Due to huge bending effects, thin plates behave like this because the stresses are at the free surface.

Fragmentation

A lot of energy is saved in a brief timeframe at higher impact speeds which brings about huge stress concentrations. In moderately thin plates, fragmentation of plate takes place due to the fracture of the bullet nose [37] [38] [39].

Ductile hole enlargement

In the case of ductile materials, the stresses are concentrated in the region close to the tip of the conical or give projectile which causes strong deformations in due path of the crater thereby resulting in axial fractures. The shot shapes a gap within the objective through the axis of the bullet and this gap is broadened as the aperture continues which is a property of high ductile objects. Zukas recorded a short rundown of the impacts watched

in shooter and objective both within the forms of penetration/perforation phenomena which are shown in following figures below respectively [31].

Phenomena Observed in the Target	Phenomena Observed in the Projectile
1. Wave propagation (elastic, plastic, hydrodynamic), normal, bending, shear stresses, hydrostatic pressure	1. Wave propagation
2. Plate deformation (elastic, plastic)	2. Permanent deformation
3. Cracks (initiation, propagation, arrest)	3. Fracturing
4. Petalling	4. Fragmentation
5. Plugging and spalling	5. Heating
6. Frictional effects	
7. Fragmentation, vaporization, phase changes	

Figure 2.7 Phenomena caused by perforation effect on the target and projectile by Zukas [31]

In addition, a few sign of the sizes of weight, strain, strain rate, and temperature experienced in numerous affect occasions is shown in following Figure 2.8 below:

Impact Event	Pressure (GPa)	Homologous Temperature	Strain	Strain Rate (s^{-1})
Gun launched, 0.5-1.5 km/s	Peak~20-40 Average~3-5	Peak~0.2-0.3 Average~0.1	Peak>1 Average~0.2-0.3	Peak~ $10^6 - 10^7$ Average~ $10^4 - 10^5$
Self-forged fragment, 1.5-3 km/s	Peak~70 Average~10	Peak~0.4-0.5 Average~0.2	Peak~1 Average~0.2-0.3	Peak~ 10^6 Average~ $10^4 - 10^5$
Shaped-charge jet, 3-10 km/s	Peak~100-200 Average~10-20	Peak>1 Average~0.2-0.5	Peak \gg 1 Average~0.1-0.5	Peak~ $10^6 - 10^7$ Average~ $10^4 - 10^5$

Figure 2.8 Range of physical parameters for target impact response suggested by Zukas [31]

2.6.2 Depth of Penetration Observation

Depth of penetration (DOP) is the crucial factor and may be called as the pure result to consider any study associated with ballistic armor resistance and its safety measurement level. To be able to create a solid model and analyze it computationally, the setup/test protocol must be within the given limits/standards and the impact loads must be understood and applied carefully. The DOP values is generally obtained by measuring

the depth of the impact crater in the backing material of the vest and by comparing the perforation of the threat/bullet into an armor [26].

Furthermore, to be more clear, the DOP of the projectile/bullet in the backing material should be determined for each shot and then to be compared to the penetration of depth of the projectile in the backing material without a ceramic strike face [40]. In Figure 2.7 and Figure 2.8., a schematic of a DOP test for a T6-6061 aluminum and for a polycarbonate (PC) cube used as a backing material after a successful shot is provided for a better visualization and understanding of the concept, respectively [26] [40].

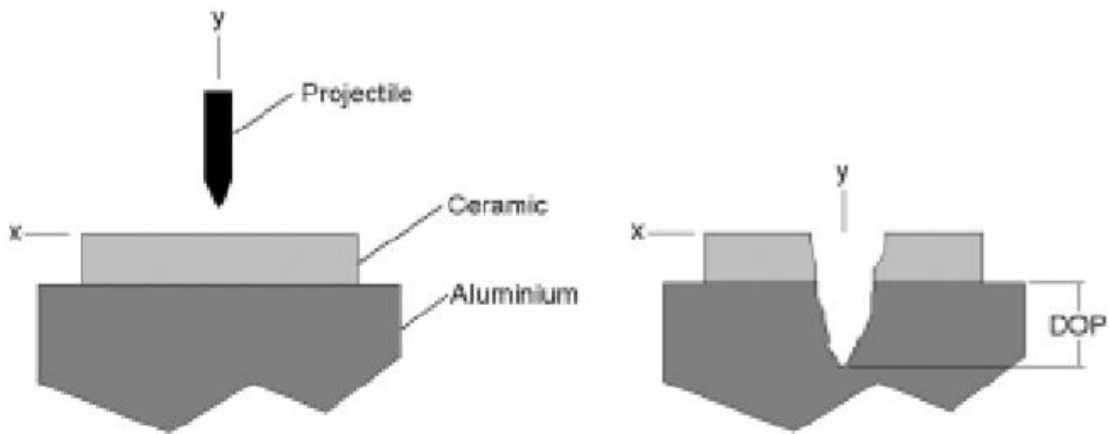


Figure 2.9 Depth of Penetration (DOP) testing visual of Kaufmann [26]

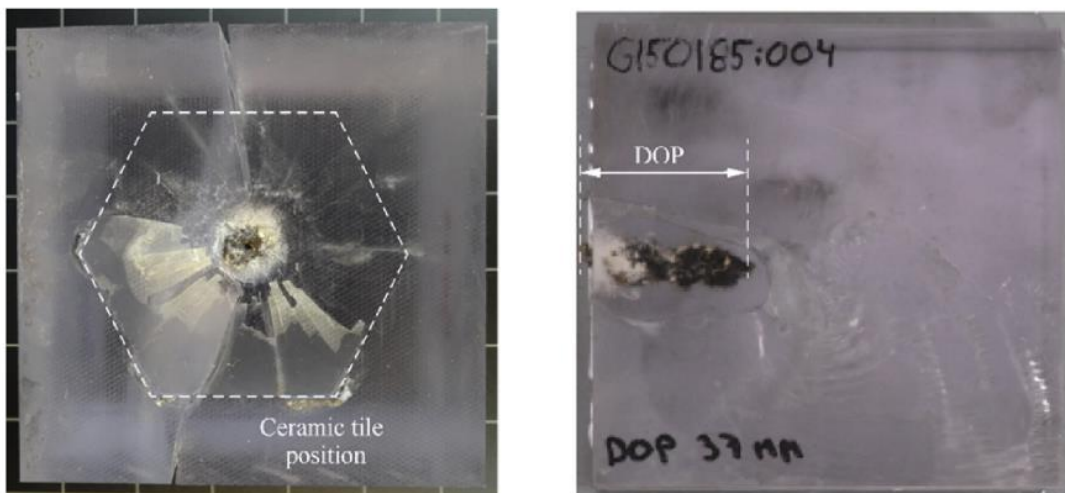


Figure 2.10 Strike face of a polycarbonate cube is seen after a successful shot at around 800 m/s with a 7.62 mm APM2, whereas 37 mm of DOP value is seen clearly [40]

In other words, by differentiating results of perforation between ceramic protected and ceramic-unprotected targets, one may have an idea of ballistic resistance of the targeted material of the armor [22] [26] [40]. In addition to these, a correlation in between ballistic efficiency and compressive strength is also reported by the use of thick-backing configuration, which may be helpful when determining the backing layer Kevlar's width in this study [29].

2.7 Impact Loads

There are many parameters and factors for determining an armor's protectiveness but defining the load and its impact on the target can be considered as highly critical. When a projectile hits the target, the dynamic response of a laminated armor is affected by many parameters such as impact velocity of the bullet, geometry and the material property of both of the bullet and the target, damage location and depth, size/pattern and the other boundary conditions defined by the test protocol [21]. To simplify the complexity and intricate structure of the analysis after a successful hit on the target, impact loads must be defined carefully. Within the given test protocol, there are different velocities of the projectile and these velocities usually defines the so called – impact load. Impact loads are usually defined in three categories as suggested by Naik and Shrirao; low velocity impact, high velocity impact and hyper velocity impact based on the energy transfer occurs between the projectile and the target [22] [41]. There is a fact that the projectile velocity cannot be underestimated because it has a direct relation with the dissipation of energy and with the perforation depth.

To be more specific, in low velocity impact regime, support conditions are important and fully vibrational response becomes the behavior of the target because the stress waves are generated outward from the impact point have satisfactory time to reach even the edges of the target [41]. In high velocity regime, the response behavior of the structural armor element is only governed by the local impacted zone; thus, making the impact response independent from the support conditions [41]. In the hyper velocity impact regime, projectile moves at extremely high speed so that the targeted material behaves and responds just like fluids and the occurring stress induced can be considered as only as the strength of the material [22] [41].

2.8 Test Protocol - Standards and Requirements

To determine the ballistic performance of a body armor, a multi-layered design must meet certain authority standards and regulations. There are different standards to follow up such as The National Institute of Justice of the USA, current one being *NIJ 0101.06 standard*, *NATO STANAG 4569*, *German SCHUTZKLASSE Standard*, *Ballistic Standards of European Union*, *Home of Scientific Development Branch Standard of United Kingdom* and etc. The NIJ standard, on the other hand is the most widely accepted standard all over the world for armor protectiveness evaluation and our study is based on this standard and its requirements. This public accessible standard is a technical document that specifies the minimum performance requirements that equipment must meet to satisfy the requirements of criminal justice agencies and the methods that shall be used to test this performance [30]. This could be more than enough to handle such body armor resistance study and related others (helmets etc.).

The NIJ standard can be classified into five different categories. Personal body armor covered by this standard can be classified by these five types (IIA, II, IIIA, III, IV) by level of ballistic performance whereas Type IIA, II and IIIA stay in the protection range of velocities for projectile in between 355 m/s and 448 m/s with ± 9 m/s and Type III and IV provide velocities 847 m/s and 878 m/s with ± 9 m/s [20] [30]. The number of shots per target is always determined and standardized as 6 (six) shots in any category. A shot must be considered valid if it is a *fair hit*, whereas a “fair hit” is defined by NIJ as a test shot shall be considered a fair hit if it impacts the armor panel at an angle of incidence no greater than $\pm 5^\circ$ from the intended angle of incidence, no closer to the edge of the ballistic panel than the minimum shot-to-edge distance, and no closer to a prior hit than the minimum shot-to-shot distance [30]. As mentioned above, an armor must receive 6 shots and must be considered as fair hits, the locations/acceptable zones of the shots over an armor must also be placed within the standard requirements, which is provided in Figure 2.9, taken from the original NIJ standard version of 0101.06:

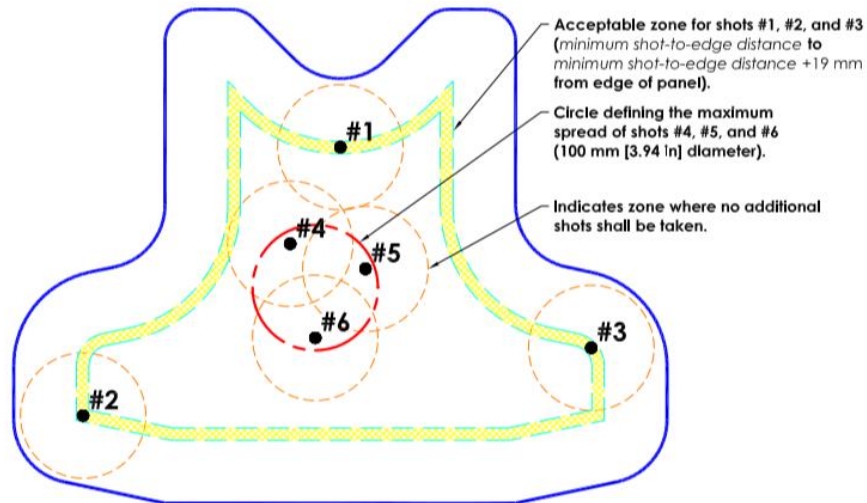


Figure 2.11 Armor panel acceptable shot / fair hit locations are shown. (Adapted from NIJ 01.01.006 standard document) [30]

The standard requires in detail that all flexible vests and jackets shall be tested with the mandated six shots but *specifically in the approximate pattern* as well which is shown in Figure 2.9. Shots 1, 2, and 3 shall meet the shot-to-edge distance requirements, but they shall not be located more than the minimum shot-to-edge distance plus 19 mm (0.75 in) from the edge of the panel. Shots 4, 5, and 6 shall meet the shot-to-shot distance requirements, but all three shots shall be located within a 100 mm (3.94 in) diameter circle [30].

2.9 Back Face Signature (BFS) and Ballistic Limit (BL)

The greatest extent of indentation in the backing material caused by a non-perforating impact on the armor. The BFS is the perpendicular distance between two planes, both of which are parallel to the front surface of the backing material fixture. One plane contains the reference point on the original (pretest) backing material surface that is collinear with the bullet line of flight (if armor were not present, the bullet would strike this point.). The other plane contains the point that represents the deepest indentation in the backing material. Depending on bullet–armor–backing material interactions, the two points that define the locations of the measurement planes may not be collinear with the bullet line of flight. Examples of how BFS is measured are shown in following visual.

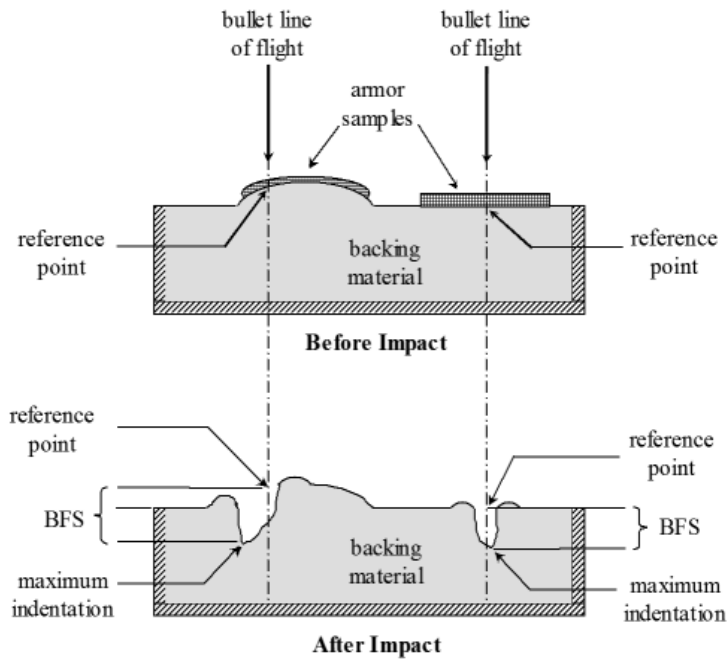


Figure 2.12 BFS Measurement examples [30] [16]

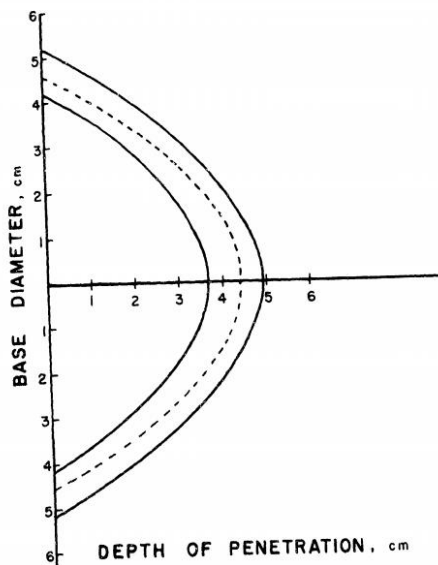


Figure 2.13 Caliber Deformation Envelope, taken from Wound Ballistics [42]

Regarding to NIJ Standard Ballistic Limit is defined as: “For a given bullet type, the velocity at which the bullet is expected to perforate the armor 50 % of the time. The ballistic limit is typically denoted as the V50 or V50 value.” [30]. In the related section of the NIJ standard, the methods and performance requirements for ballistic testing of body armor is explained in detail when formal test procedures with real shots are aimed to be applied to a new designed body armor to measure its ballistic resistance. This

protocol shall include the formal test procedures for the Perforation-Backface Signature (P- BFS) and baseline Ballistic Limit (BL) tests [30]. The first test series recommended by the standard is P-BFS testing and requires the armor to demonstrate consistent ballistic resistance to both perforation and excessive blunt force trauma [30]. The second test series is BL testing and is designed to statistically estimate perforation performance [30]. For a vest to be considered as safe and ballistic-resistive, receiving plate must satisfy some conditions. These conditions are directly related with the perforation of the projectile and the projectile's fair hit condition which is clearly specified in the standard. Hence, a random test panel to be tested must withstand the appropriate number of fair hits which is 6 (six) in our FE analysis and may not experience any complete perforations, whereas any complete perforation by a fair hit is considered to be a failure. NIJ standard has many limitations and protocol necessities but one of the most critical fact is that P-BFS cannot exceed 44 mm. In other words, all BFS depth measurements due to fair hits must be maximum 44 mm (1.73 in) or less [30].

Chapter 3

Materials and Methods

3.1 Armor Structure

The structure was made in a composite way which consisted of layers SiC of 5 mm, epoxy resin of 10 mm and of Kevlar of 15 mm. A fourth Li-Ion battery layer was also introduced in design but for Ansys analysis the material that was used was infused in PVC material since the bullet must not penetrate and pass through the Kevlar layer, so the Li-Ion material is of little use in this analysis. Since almost all ballistic vests are composed of Kevlar and epoxy layers in the material formation of vest, the same/similar materials were also used in this research, as recommended by the industry and academic literature data [11]. The only choice of material that had to be made was for the front layer of the vest since many different materials can be used in that regard. In total, three materials were tested namely as Alumina, Boron carbide and Silicon carbide. The layers of materials in the front, middle and back layer showed different stress and deformation levels which helped getting a clear idea of the material performances of the materials. The appropriate construction of the layers was found from researching different articles and it was found that a jacket/vest width of at least 20 mm is sufficient to stop a bullet impact [11] [43]. The dimensions of the layers are taken from NIJ standards choosing the smallest size of jacket which was 317.5 x 317.5 mm [30] [20]. This size was chosen to avoid exceeding time consume on meshing process of a vest and running the results in FEA. The vest was idealized as a square plate to minimize any functional errors. Three bullet testing was done to depict accuracy and the strength of the jacket. First testing was done with a single bullet to find the appropriate material for front layer and then the testing was done with six (6) bullets to exclude any errors and give a better image of the testing. This was done to optimize the hybridization and see actually how several bullets effect the ballistic performance.

Such findings contribute to the understanding of different ballistic responses in different positions of an armor panel under ballistic impact [16]. As indicated by above, hypothetical understandings of various ballistic attributes in various places of a defensive equipment, the layers were discreetly placed and no spacing was left between them to ensure compact bonding – so called and assumed as *perfectly bonded* [3] [21]. There are basically two types of contacts during impact, so called eroding and tied contacts which in our case defined as perfectly bonded and mostly used when contacts are in between ceramic and composite [43]. It is also recommended that when defining a tied contact between layers, the coarser mesh type should always be applied to the model in FEA [43].

Furthermore, three contacts were made in ANSYS workbench to make necessary contact bonds between the layers and form one single assembly with no spacing in between. The contacts were made between each residing layer to ensure a compact structure. The following contacts can be seen in the following figures below. The first contact is between the Silicon carbide and Epoxy layer. The second bond is between the Epoxy layer and Kevlar and the third bond is between the Kevlar and Li-Ion layer.

Contacts were used in ANSYS workbench to bond the materials assembly. Along these lines, tests with 317.5 x 317.5 mm layers were seen as adequate to test the ballistic conduct of the composite layered structure [30] [10]. The layers of different material were utilized to make the vest stronger in function and to add-on reinforced security. The basic function of the ceramic layer is to deflect the projectile and the artificial fibers that are used in the middle layers hold the bullet particles and prevent them from penetrating, the Kevlar or metal layer completely stops the bullet.

3.2 Test Protocols

9 mm and 7.62 mm round tip samples were tried and tested on the composite layered structure and analyzed with the ballistic performance. The bullets were shot at the front layer which is the silicon carbide layers and the deformation and other analysis were run. The bullets were shot at a distance of 30 mm and shot with the velocity as prescribed in the NIJ standards.

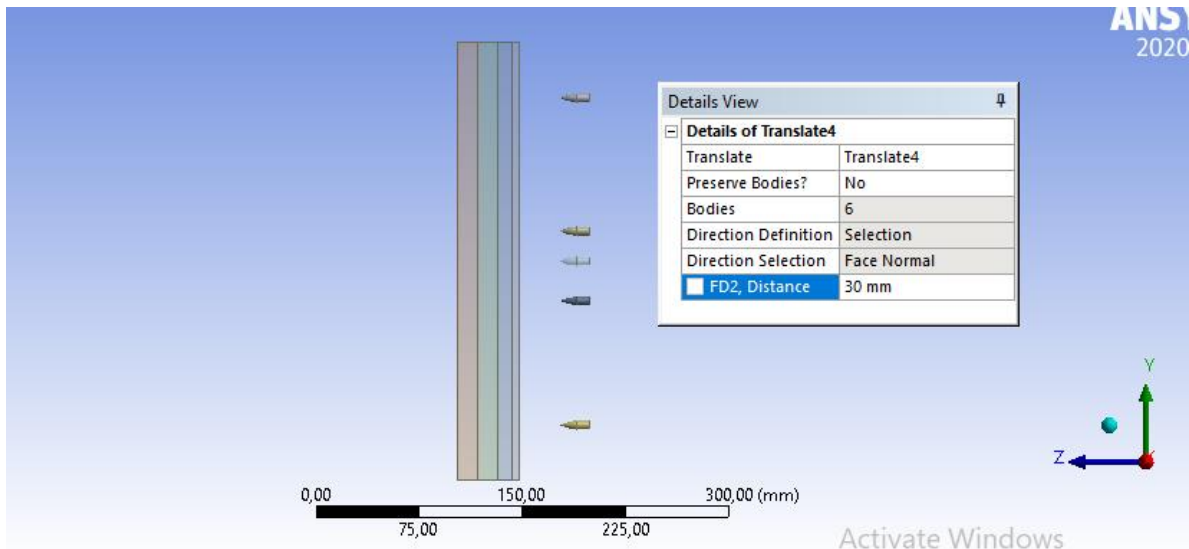


Figure 3.1 Side view of vest composed of different materials/panels and the direction of fair-hit

The composite structure was fixed at two ends on Ansys workbench explicit dynamics analysis with the help of fixed supports. The remaining sides are left as it is, as recommended in the according article and NIJ document [30] [12]. This should not be meant that the sides of the structure cannot be fixed in any means, it should only be comprehended in a way that the structure can be fixed depending on the analysis. Since a ballistic vest is not fixed at all in real life conditions by the user, only the ends are fixed design should be preferred to match the real life conditions. The sides are basically fixed in the first place because when the projectile hits the composite structure it stays intact and doesn't hinder from its prime position. It must be remembered that NIJ standard regulates that a bullet/projectile must hit the target in accordance with fair hits [30] [16].

3.3 Modelling and Material Selection

3.3.1 Modelling Methodology

The ballistic vest is modeled by using Ansys Workbench V19 and V2020 versions. In the first phase, the dimensions of both the bullets and composite structure were decided by keeping in mind the NIJ standards. The geometry is created in accordance to the standards with Ansys Design Modeler and then a separate simulation of the projectile against the front layer has been done to find out which material suits best according to

deformation and stress. In the final phase, a simulation of the composite layer structure along with six bullets was performed in Ansys Explicit Dynamics (ED). Ansys Explicit Dynamics was used to analyze the effects of the impact on the layered structure and thus all three models of the armor types were solved and evaluated in the model and the final stress/strain results were generated. Ansys engineering data is very rich and this library was used to determine the material properties to be able to evaluate and model the whole analysis accordingly. After modeling, the meshing is initiated and the structure was designed and the conditions of the contacts between layers were figured out respectively. In the last phase of the modeling part, the system statics were defined along with initial and boundary conditions to evaluate the desired output.

3.3.2 Bullet/Projectile Determination

The geometry of the projectiles was evaluated as it follows. Two bullets were made/drawn in ANSYS for these analysis. One of the bullet used has a diameter of 7.62 mm and the other having 9 mm, as also mandated in the NIJ standards [30] [2]. The allocated material for the bullet is Steel 4340 [34].

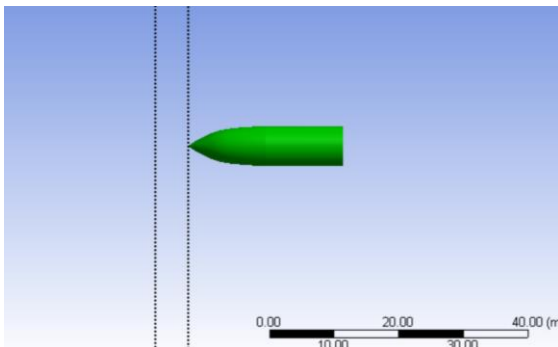


Figure 3.2 The 7.62 mm projectile visual



Figure 3.3 Meshed visual of 7.62 mm projectile

During the simulation the bullet was defined and set to material of Steel 4340 in Ansys explicit material repository. The figure above shows the structure and 3-dimensional mesh of the projectile generated through Ansys Explicit Dynamics mesh

modeler with element of hex-tetra to ensure rigorous results and also multizone size method was utilized for the bullet with center of medium relevance, center of coarse span angle and the default element size.

The projectile is considered an explicit material throughout the modeling [16]. In the following, Figure 3.4 the mechanical properties of steel 4340 are provided as well.

Steel 4340				
ρ_0 (kg/m ³)	Bulk modulus (kPa)	Shear modulus G (kPa)	Yield stress (kPa)	Hardening constant (kPa)
7830	1.59×10^8	7.7×10^7	7.92×10^5	5.1×10^5
Hardening exponent	Strain rate constant	Thermal softening exponent	Melting temperature (K)	Ref. strain rate
0.26	0.014	1.03	1.793×10^3	1

Figure 3.4 Bullet material - Steel 4340 material properties [34]

3.3.3 Material Modelling in ANSYS

The plates and the layers that were used as composite structure in the analysis were bonded to each other using SOLID185 also known as SOLID45 in Ansys. Layered SOLID185 is a solid structural element of eight-node layers with three degrees of freedom between each node [44]. By using this particular solid element (Solid185) obtained from the software element catalog, all aspects of the model were meshed. All layered solid sections can be modelled using this element. With the property of 8 nodes and three degrees of freedom of translation and they can use both reduced and complete methods of integration. In order to define the layers' thicknesses and orientations, a shell section was also associated with the solid element.

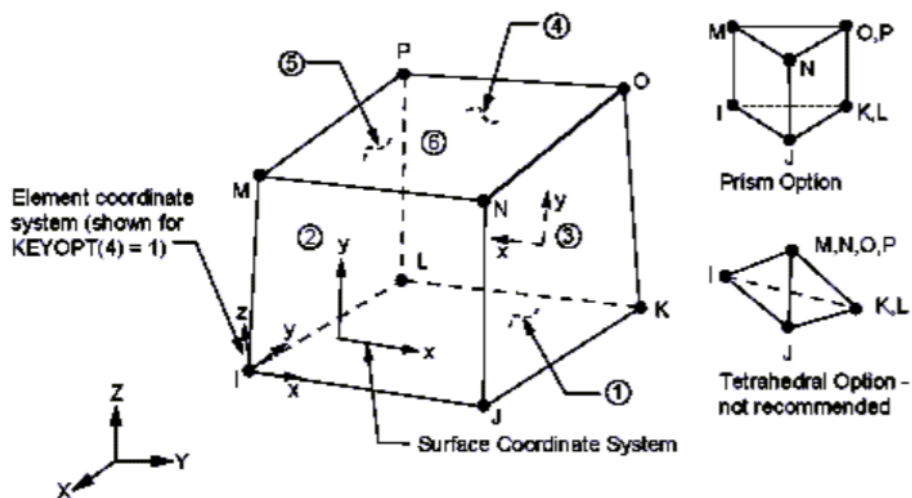


Figure 3.5 Element/surface coordinate system visual [45].

The composite layer was illustrated and modelled as volume knowing that SOLID185 is a rigid brick element and doesn't have shell elements in it [46]. Both SOLID185 and SOLID186 (solid46) could be used for the modeling of the layered structure of the composite as both are rigid elements. Firstly, the geometry was created for the composite and then the solid elements were enforced. SOLID185 and SOLID186 are used for thin layered composite layers and they can be generated using ANSYS which helps to create a layered solid mesh on a shell mesh based on the laminate concept [47]. The epoxy's elevated efficiency and the perfect bond concept was endorsed by being used to bind sheets to the experimental frames. For interference contacts, the interaction was modeled using 3-D surface-to-surface and surface-to-node contact components. The structure and node positions for this sort of feature can be seen in the diagram for SOLID185 [47].

3.3.4 Vest Materials and its Design

Ceramic composite armors had a use since Vietnam War due to their lightweight properties and the capability to defeat small caliber armor piercing (AP) projectiles during combat [48]. Hence, the ballistic vest is made up of three layers of assorted substances, ceramics, Kevlar synthetic fibers, and epoxy resin. Every component is individually constructed in Ansys material engineering records. The research work was carried out with various samples. The stack design has been designed as solid materials with a different thickness of each layer in Ansys Design Modeler. Tests had x, y specifications of 317.5 x 317.5 mm and the width differed as illustrated in: first sample had ceramic thicknesses of 5 mm, Kevlar material of 15 mm, and the thickness of epoxy resin was 10 mm.

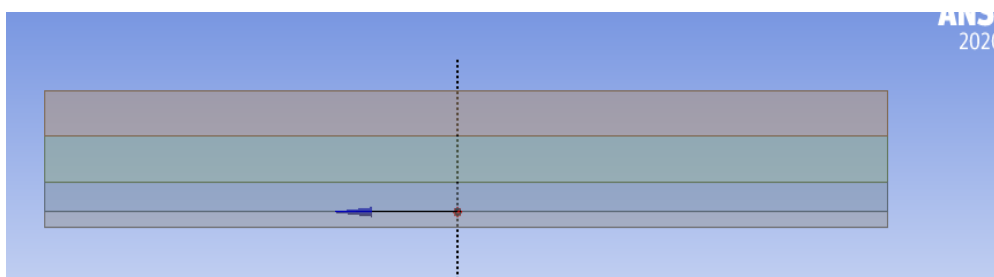


Figure 3.6 Vest materials and dimensions, perfectly bonded structure

The grey front layer represents SiC, the blue layer represents Epoxy resin, the green layers represents Kevlar and the red layer represents Li-Ion battery part. Kevlar fibers being based on a macro-homogeneous system which assumes the entire surfaces to be

homogeneous in configuration with mechanically orthotropic properties [49] [50] . Such a method is commonly used to identify material from Kevlar that provides adequate results with minimal resources [50]. Figure 3.5 demonstrates the structure on the Ansys workbench and the bullets as a pattern.

3.3.5 Front Layer

It is recommended by Heidenreich, Gahr and Medvedovski that reaction bonded silicon carbide (RBSC) ceramics and Biomorphic SiSiC ceramics under various conditions are considered as a promising front layer material due to their remarkable level of physical properties and have a significant cost benefit [25]. It was also found that three materials being aluminum oxide (Al₂O₃), silicon carbide (SiC) and boron carbide (B₄C) had the best combination of properties to meet the requirements for front layer applications when designing a vest [48]. Hence, for front layer application, by considering all other literature data as well, SiC is chosen. The SiC had the same thickness of 5 mm on all the tested samples and in all test protocols. It was modelled in this study as a composite material with linear isotropic elasticity and tensor isotropic stiffening. Mechanical material properties were obtained via Ansys engineering data and from the research paper [11] [14]. Figure 3.7 displays ceramic layer's (SiC) mechanical properties [48]. The mesh again for framework was generated as a body mesh with default element size and high blending using the Ansys Explicit dynamic mesh modeler. This method is applied and extended towards the other armor layers, as well.

SiC				
ρ_0 (kg/m ³)	Bulk modulus A1 (kPa)	A2 (kPa)	A3 (kPa)	B0 = B1
3215	2.2×10^8	3.61×10^8	0	0
G (kPa)	HEL (kPa)	S1 (kPa)	S2 (kPa)	P1 (kPa)
1.935×10^8	1.17×10^7	7.1×10^8	1.22×10^7	2.5×10^8
P2 (kPa)	C	SFMAX (kPa)	ALPHA	
1×10^7	9×10^{-3}	1.3×10^8	0.4	

Figure 3.7 Front Layer Material - SiC mechanical properties

3.3.6 Backing Layer

Kevlar is a certain type of material which mechanical and physical properties of it depends on yarn geometry and layer thickness [11] [45]. The Kevlar fabrics used in the ballistic applications can be categorized as knitted and woven fabrics. Despite their complex manufacturing methods and costs, the woven fabrics are usually preferred in

military areas [17] [20]. Specific simulations were conducted in order to conduct the Kevlar woven fabric modeling conditions. The literature suggest that Kevlar 29, Kevlar 149 and Kevlar 49 were the most useful elements evaluated in terms of ballistic testing and in addition to mechanical and ballistic properties [5] [12] [13]. Thus, Figure 3.8 displays the Kevlar 29's material characteristics specifically.

Temperature (°C)	Orthotropic elasticity						Shear modulus XY (Pa)	Shear modulus YZ (Pa)	Shear modulus XZ (Pa)
	Young's modulus X direction (Pa)	Young's modulus Y direction (Pa)	Young's modulus Z direction (Pa)	Poisson's ratio XY	Poisson's ratio YZ	Poisson's ratio XZ			
25	1.85e+010	1.85e+010	6e+009	0.25	0.33	0.33	7.7e+008	5.43e+009	5.43e+009
Density (kg.m ⁻³)			Constant and response			Specific heat constant pressure J.kg ⁻¹ .C ⁻¹			
1440						1420			
Compressive yield strength (Pa)						Yield strengths			Tensile yield strength (Pa)
1.85e+008									1.85e+009

Figure 3.8 Backing Layer Material - Kevlar properties

3.3.7 Analysis Method

The framework of the Explicit Dynamics was implemented in Ansys Workbench V19 and V2020 [43] [49] [51]. The boundary solution of the examination was modeled through specifying the initial component velocity to the components of the bullet according to that specified in NIJ standards along the Z direction. At the X and Y faces of the composite fixed supports were used as boundary conditions for an established analysis. The final analysis time was done at 7e – 004 seconds with a maximum number of cycles equivalent to 1e +07. In the Ansys model simulation settings, bonded connection was added between the ceramic layer and the epoxy layer and between the Kevlar layer and the epoxy layer to model the connection state between the sheets of the composite. There are many detailed reviews in the literature on the use of explicit dynamic problems [11] [51]. In short, the algorithm resolves the mass and momentum conservation of energy laws in the Eulerian or Lagrangian-form addressed as the preliminary boundary conditions. Even the algorithm has the capability to alleviate various forms of stress namely equivalent (von Mises) and shear stress. The solver function sets for measuring total and Z directional deformation of composite layers to predict the system's ballistic conduct. The material characteristics were demonstrated more in detail in the upcoming sections of this study. Furthermore, von Mises stress analysis were successfully completed to show the residual instability of the whole program.

3.4 Material Classification and Determination

3.4.1 Material Selection

As many various materials are being considered and tested for the front layer of the armors; it is assured that boron carbide and silicon carbide are highly-effective alternatives when vast majority of literature is considered. Specifically, considering studies made by Kaufmann, where depth of penetration tests have been conducted on four different ceramic materials including alumina, silicon carbide and boron carbide, silicon carbide had shown a significant resistance [26]. These experiments consisted of impacting ceramic tiles bonded to aluminum cylinders with 0.50 caliber armor piercing projectiles. The results are presented in terms of ballistic efficiency, and the validity of using ballistic efficiency as a measure of ceramic performance was examined. Hence, silicon carbide is announced as better at ballistic resistance results compared to boron carbide when Kaufmann and others' work included [26] [48]. Table 3.1 below provides material characteristics mainly for B₄C and SiC.

Table 3.1 Material properties of B₄C and SiC in various forms

	B₄C hot-pressed	B₄C pressureless sintered	SiC pressureless sintered	Reaction Bonded SiC (RBSC)	Reaction Bonded B₄C (RBBC)
Density (g/cm ³)	2.5	2.4 – 2.45	3.06 – 3.10	3.0 - 3.07	2.5 - 2.55
Rockwell hardness (HRA)	94 - 95	93 - 94	90 - 92	90 - 91	90 - 92
Knoop hardness <i>H_{KI}</i> (kg/mm ²)	2050 - 2250	1900 - 2100	1870 - 2020	200 - 2150	1550 - 1750
Vickers hardness <i>H_{VI}</i> (kg/mm ²)	2350 - 2450	2250 - 2400	2200 - 2300	2350 - 2450	1750 - 1900
Fracture Toughness <i>K_{IC}</i> (MPa · ml/2)	2.5 – 2.8	3.1 – 3.4	2.8 – 3.2	2.2 – 2.8	2.65
Flexural Strength (MPa)	400 - 430	380 - 400	350 - 400	190 - 250	180 - 200
Young's Modulus (GPa)	420 - 460	400 - 420	400 - 420	300 - 400	300 - 350
Sonic Velocity (km/s)	13.2 - 13.8	12.5 – 13.2	11.5 – 11.8	10.3 – 11.6	11.8
Brittleness <i>B</i> (10 ⁻⁶) /m	1230 - 1770	760 - 1030	840 - 1210		
Ballistic Energy Dissipation Criterion <i>D</i> (10 ² /s)	7.3	4.1	4.4		
Reference	<i>E. Medvedovski / Ceramics International 36 (2010) 2103–2115</i> [6]				

Moreover, for higher velocities, it is noted that boron carbide and silicon carbide provides much better performance compared to alumina and modified alumina based on ballistic resistance so that these two would be considered as ideal front layer candidates in this study [25] [26] [48]. Regarding with the facts and under the light of recent studies had been investigated, we have done our own testing also on the three materials mentioned above and also found out that silicon carbide is found to be the optimum material out of these three materials. The test was done on a 200x200 mm sheet of thickness 15 mm structure. All the conditions were kept the same for the tests and each

time only the material of the sheet has been changed. The geometry was drawn on design modular with a bullet of 9 mm where the bullet was placed at an initial distance of 5mm distance. The design was established through the modeling by designating appropriate properties of materials in the engineering data as seen below. For the bullet the meshing was designated with body sizing and making it course to 0.00001 m and for the plate sizing was defined 0.009 m.

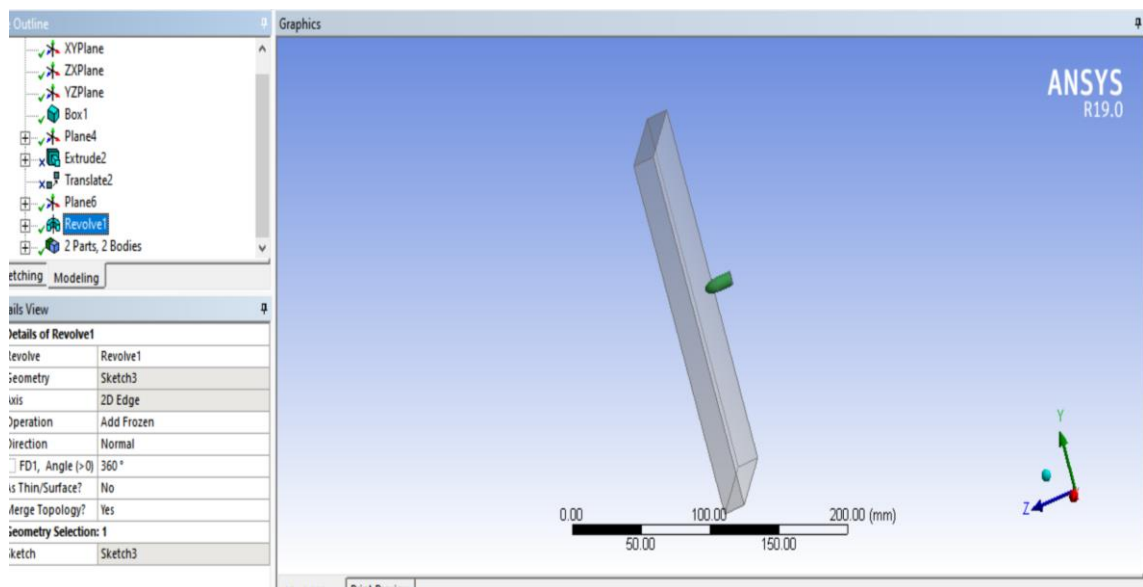


Figure 3.9 Visual showing plate and bullet placement

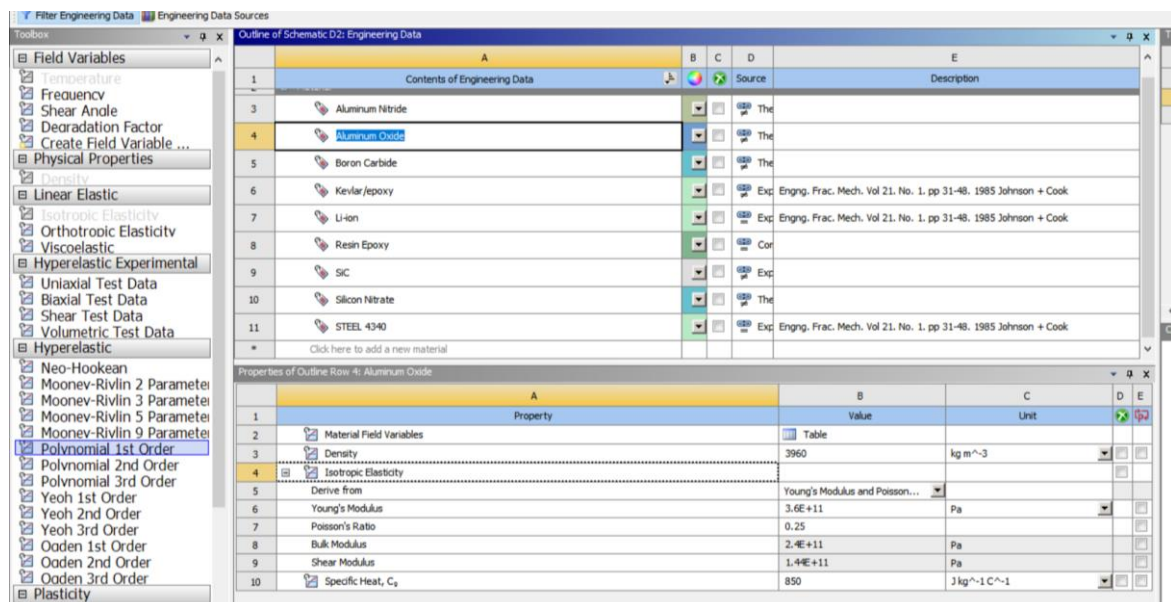


Figure 3.10 Visual showing the material properties are designated for materials

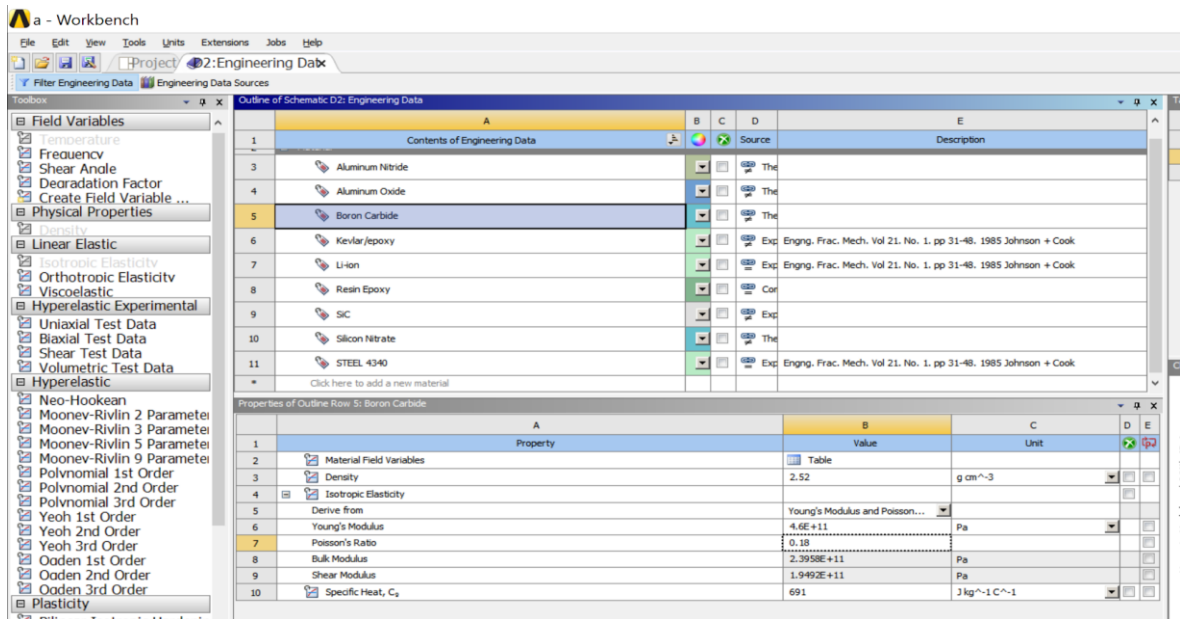


Figure 3.11 Visual showing the material properties are designated for materials

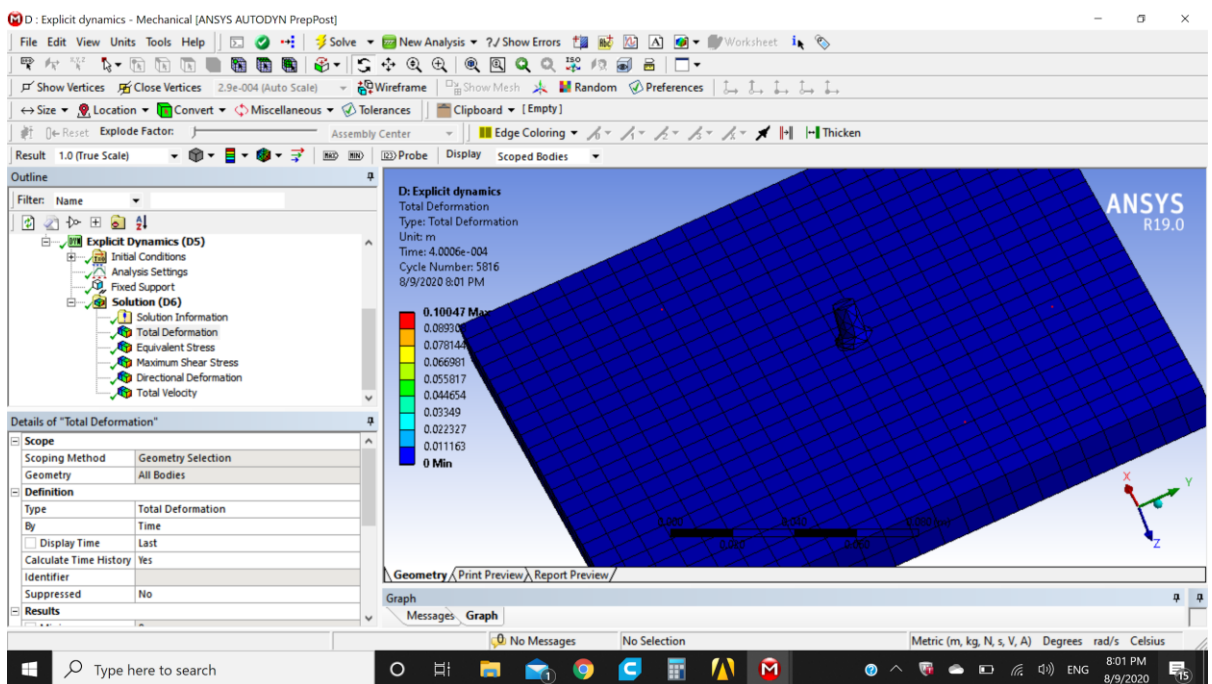


Figure 3.12 First analysis result providing total deformation with SiC material used is shown

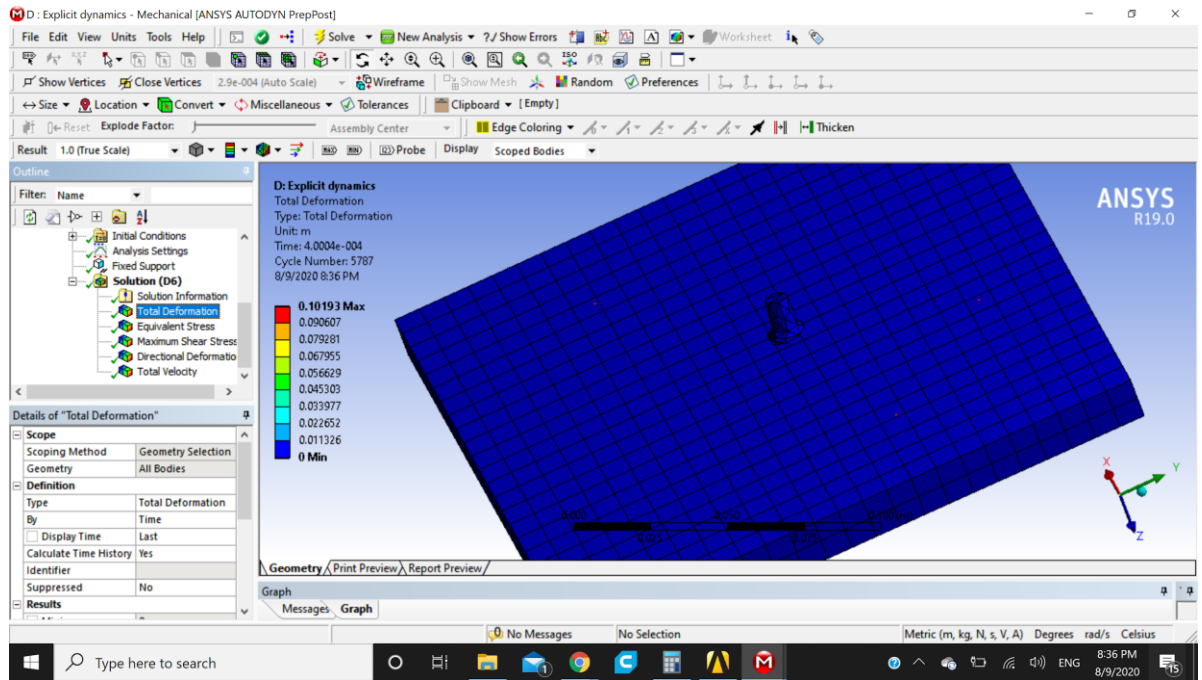


Figure 3.13 Second analysis result providing total deformation with BC material used is shown

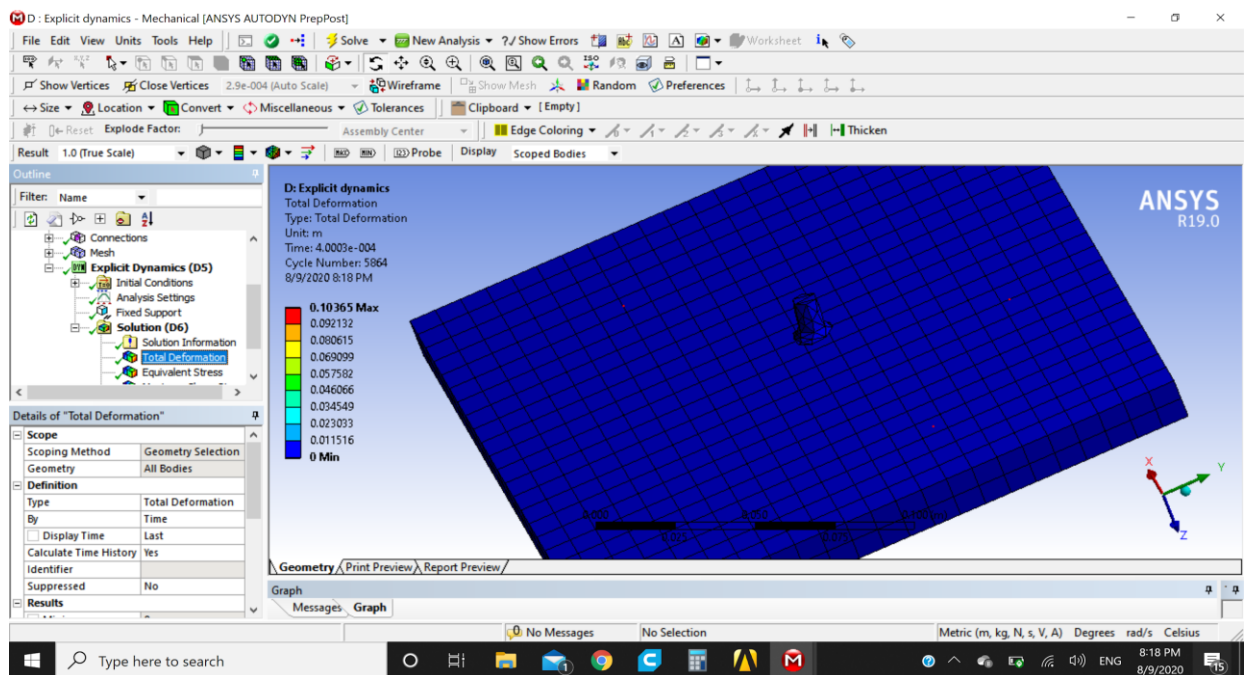


Figure 3.14 Third analysis result providing total deformation with alumina (Al_2O_3) material used is shown

As seen from the figures above, total deformation values of three different material used are evaluated. When explicit dynamics analysis results are compared, it can be

noticed that boron carbide has the least deformation from the impact which makes it the most suitable material for the ballistic testing.

The stress analysis was also completed in the same workbench and it also has been concluded that SiC had the least stress out of these three materials. The results are provided and could be seen in the following figures.

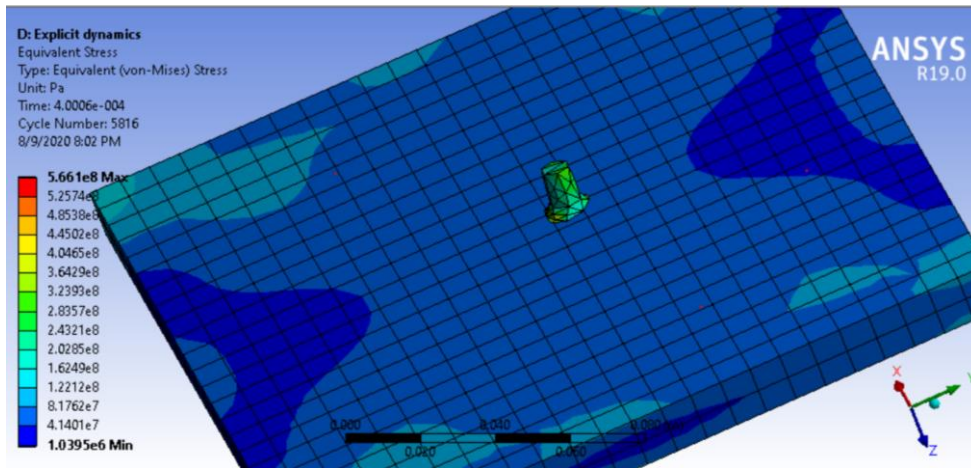


Figure 3.15 Visual providing equivalent stress values and formation for Al_2O_3

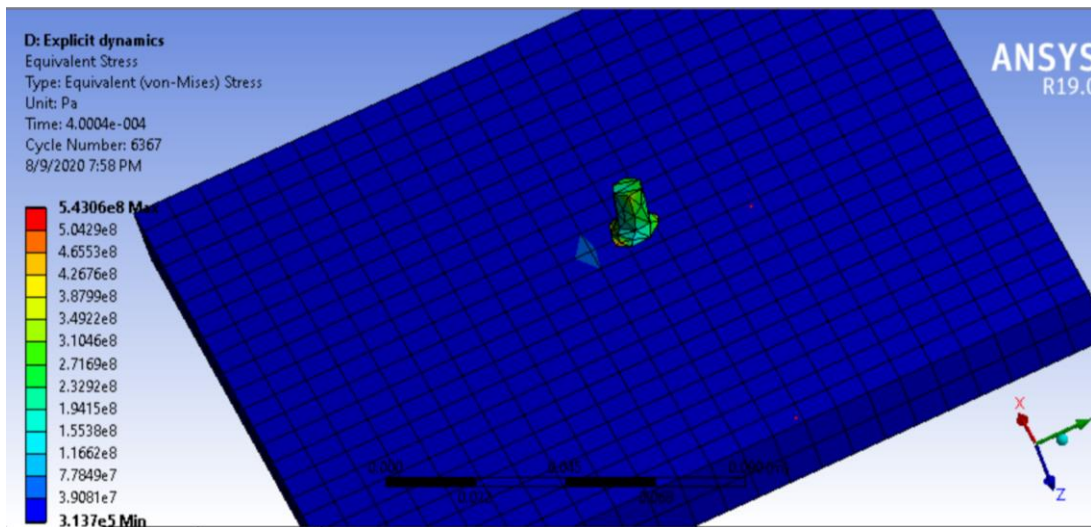


Figure 3.16 Visual providing equivalent stress values and formation for SiC

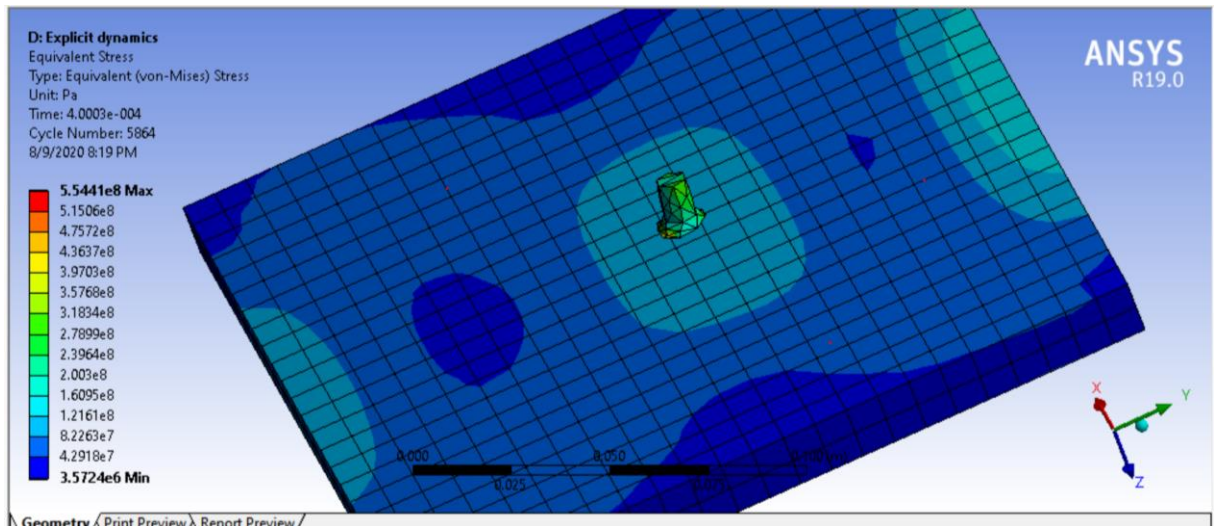


Figure 3.17 Visual providing equivalent stress values and formation for BC

Thus, seeing the stress and deformation values of all three materials it can be concluded that silicon carbide has the best performance (having a lower stress value of 5.43×10^8 Pa under same threat conditions) out of the three materials and could be a best fit for the targeted vest design front layer application and further analysis purposes. Even though the resistance of the ceramic material to deformation is significant to defend against a projectile, causing a lower stress under same threat conditions was a key for decision. This matter shows us the material durability and lower chances of destruction of the vest under same threat conditions which providing a preferable standard for the usage of the material.

Finally, by the literature recommendations and the ANSYS analysis completed; the following materials are decided to be used for further analysis. Hence, for the main/core layers of the body armor would be composed of the following material:

- Front Layer: SiC
- Middle Layer (usually adhesive): Epoxy resin
- Backing Layer: Kevlar/epoxy
- Fourth Battery Layer: Battery layer is embedded in PVC material

In rare cases; *a fourth layer is being used, so called an anti-trauma layer* which has the purpose of conforming the user. On the other hand, usually a clay witness is enough to measure penetration for such studies [30] [14] [52]. Traditionally, armor has been evaluated by the V50 (i.e. the velocity at which a projectile has a 50% probability of penetrating the armor) and maximum deformation.

For bullet/projectile; dimension is used usually 7.8mm and 20.4 mm respectively for diameter and length, respectively.

Hence, in our computational FEA analysis, SiC is being used as front layer material to validate and determine computationally whether the approach and choice is still valid for different tests and test protocols or not. On the other hand, we would use Kevlar which almost dominates the studies and frequently serves as a shield material for high safety required applications and sectors being helicopters, tanks, weapon systems, radar domes, body armors and etc. [13] [50] [53]. SiC and B₄C are mainly proposed materials in the literature and the reason that SiC is being chosen is that SiC shows a better performance under same conditions for small to medium range caliber shots [48]. In addition, SiC is considered to be more cost effective to the more expensive B₄C so that also was the reason to go further with it [48].

3.4.2 Layer Thickness Determination

Based on the simulation results and discussions provided in the specified article [54], it is concluded that 200 mm thickness of bullet proof vest approximately develops 138.77 J of energy which later on will be secure to utilize [54]. In accordance with the reports of Major General Julian S. Hatcher, a U.S. Army ordnance expert notes that the overall energy equal to 170.2 joules is competent of paralyzing the victim and causing serious harm [54]. In addition, based on the NIJ standard 0101.06, infiltration of the shot across a bulletproof vest may not surpass maximum limit of 44 mm, so the bulletproof vests with a thickness of 5, 10, 15, and 20 mm can be used safely [30]. Taking both the references (standard NIJ and Major Common Julian's) into consideration a bulletproof vest with a thickness of 20 mm is safe to be used.

In this study, a bulletproof vest that has thickness of 20 mm has the capability of absorbing the kinetic energy which is within the safe limit of 138.77 joules of energy. According to the principle of conservation of energy, the energy of the projectile is transferred into the kinetic and internal energy of the bulletproof vest.

3.5 Computational Analysis

3.5.1 Specific Criteria and Test Protocols

Computational analysis has been made via NIJ standard requirements and its regulations. Therefore, the projectile mass, velocity and test types are chosen according to those specifications as it follows in the Table 3.2 for the computational analysis made.

Table 3.2 NIJ standard requirements for computational analysis [30]

	Test Bullet	Bullet Mass (g)	Conditioned Velocity (m/s)	New Velocity (m/s)
Type IIA	9 mm FMJ RN	8.0	710	373
	.40 S&W	11.7	325	352
Type II	9 mm FMJ RN	8.0	379	398
	.357 Magnum JSP	10.2	408	436
Type III	7.62 mm NATO FMJ	9.6	847	
Reference	<i>NIJ Standard-0101.06</i>			

Definitions of different armor types according to USA National Institute of Justice (NIJ) and the threats they are designed to withstand (after NIJ, 2008) are given in the Table 3.2, above. Table 3.2 and Figure 3.18 provide designated information for testing types incorporating with the hard ceramic armor plates. Type I is no longer included in the standard and other test types are not intended to be executed in this work. Hence, Type IIA, Type II and Type III are found to be sufficient to determine the safety of the vest and further FE analysis are made within this scope.

Performance level	Test bullet	Bullet mass (gram)	Distance muzzle – target (m)	Velocity (m/s)	Performance requirements			
					Shots/panel 0° NATO impact angle	Shots/panel 30° NATO impact angle	Maximum Back Face Signature (mm)	Total shots per bullet threat
1	.22 caliber LR LRN	2.6	5	329 ± 9	4	2	44	24
	.380 ACP FMJ RN	6.2	5	322 ± 9	4	2	44	24
2A	9 mm FMJ RN	8.0	5	341 ± 9	4	2	44	24
	.40 S&W FMJ	11.7	5	322 ± 9	4	2	44	24
2	9 mm FMJ RN	8.0	5	367 ± 9	4	2	44	24
	.357 Magnum JSP	10.2	5	436 ± 9	4	2	44	24
3A	9 mm FMJ RN	8.0	5	436 ± 9	4	2	44	24
	.44 Magnum SJHP	15.6	5	436 ± 9	4	2	44	24
3*	7.62 mm NATO Ball	9.6	15	847 ± 9	6	0	44	12
4*	.30 caliber M2 AP	10.8	15	878 ± 9	1	0	44	2

Figure 3.18 NIJ standard requirements for all possible alternatives including bullet types, impact angles, velocity, total number of shots etc. [30]

Therefore, the final computational analysis was successfully completed with 6 (six) bullets/shots – so called fair hits and on the 3 (three) different test protocols Type IIA Type II and Type III. The geometry of each layer is shown separately below figures. In Figure 3.15, the front layer material is used is SiC and its geometry. The dimensions are kept the same as of the smallest armor available on NIJ Standards.

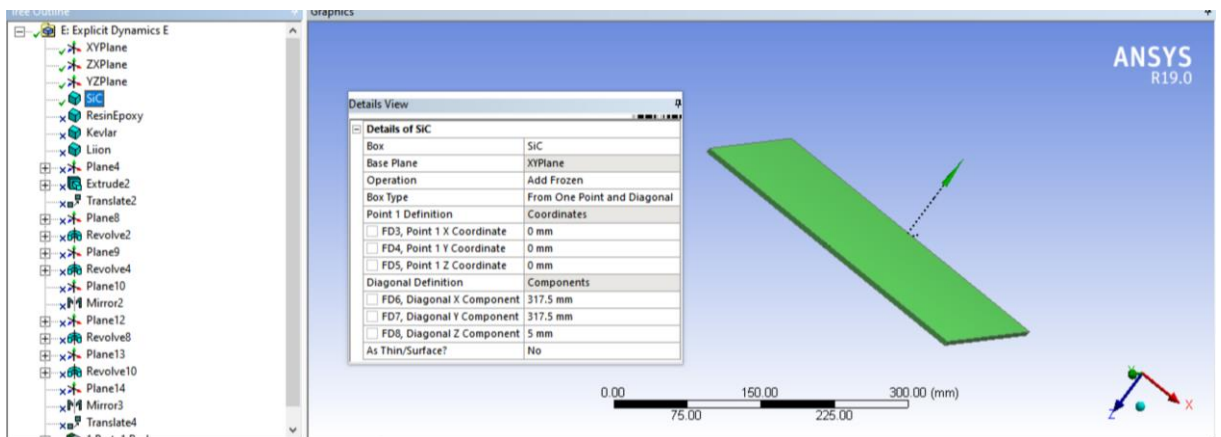


Figure 3.19 SiC geometry to be used within multi-layered structure in Explicit Dynamics analysis

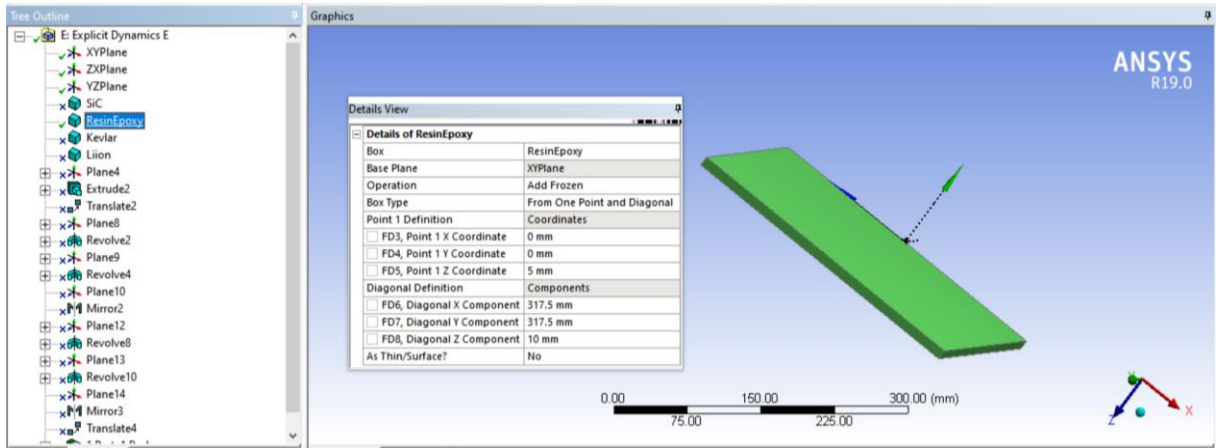


Figure 3.20 Resin epoxy geometry and thickness being 10 mm

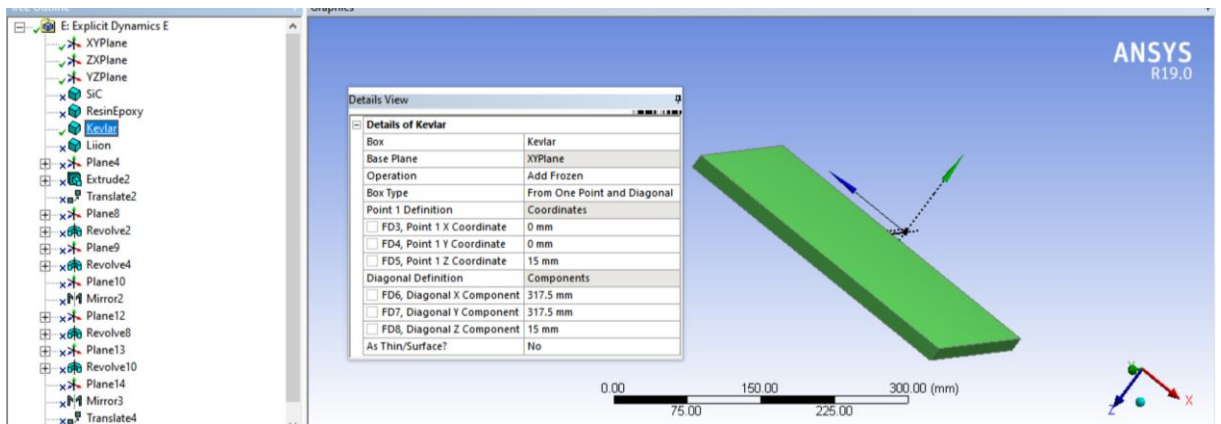


Figure 3.21 Kevlar geometry and thickness being 15 mm

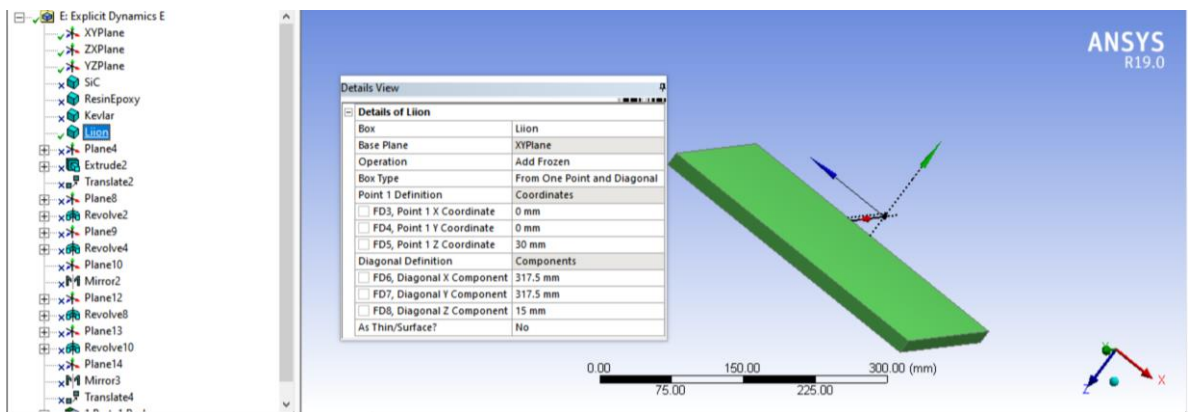


Figure 3.22 Li-Ion layer infused in PVC material and having a thickness of 15 mm

The total thickness of our multi-layered structure is 30 mm excluding the Li-Ion layer which has a very little purpose in the computational analysis as the bullet is not supposed to penetrate until the Li-Ion layer. The thickness of 15 mm only comes from the thickness of a Li-Ion battery itself with minimum dimensions. The figures below show the final multi-layer system geometry which has a thickness 45 mm in total and other analysis parameters.

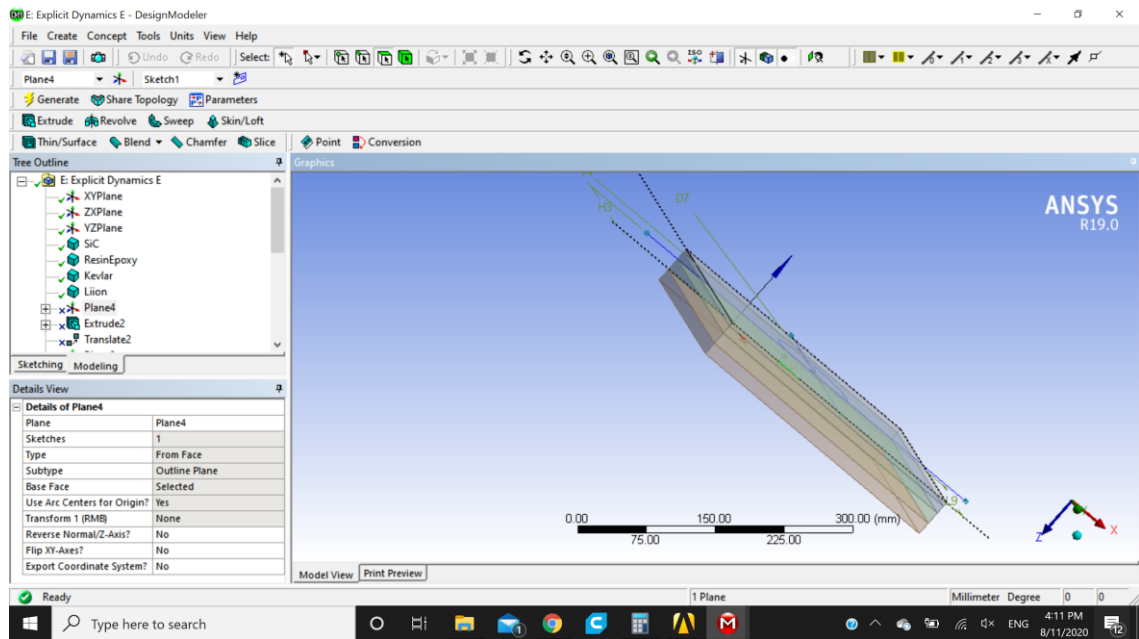


Figure 3.23 Multi-layer vest structure visual composed of all layers provided above

Now the first analysis is done on the 7.62 mm bullet under the Type III vest requirements.

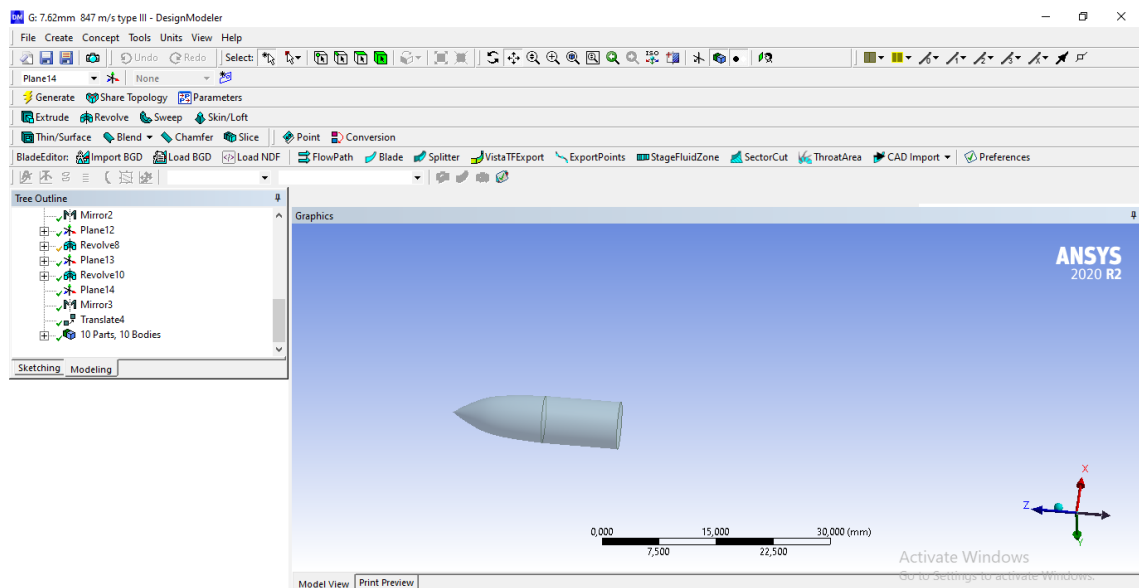


Figure 3.24 7.62 mm and 847 m/s analysis for Type III Test

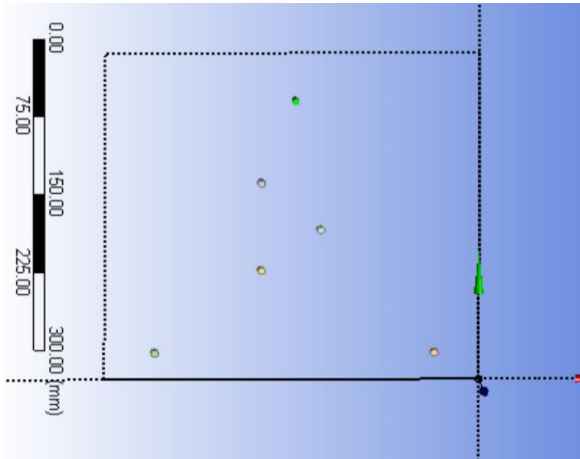


Figure 3.25 The structure and position of the six 7.62 mm bullet

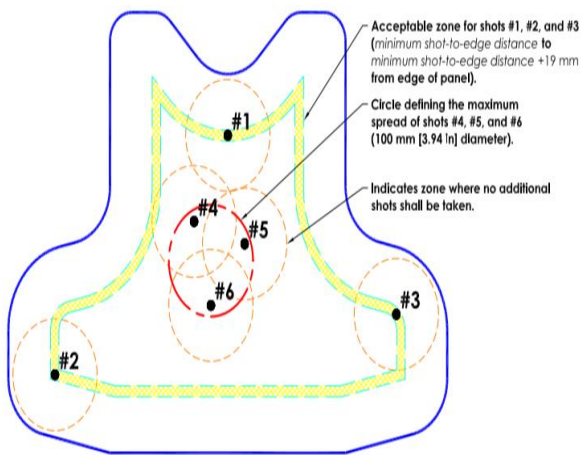
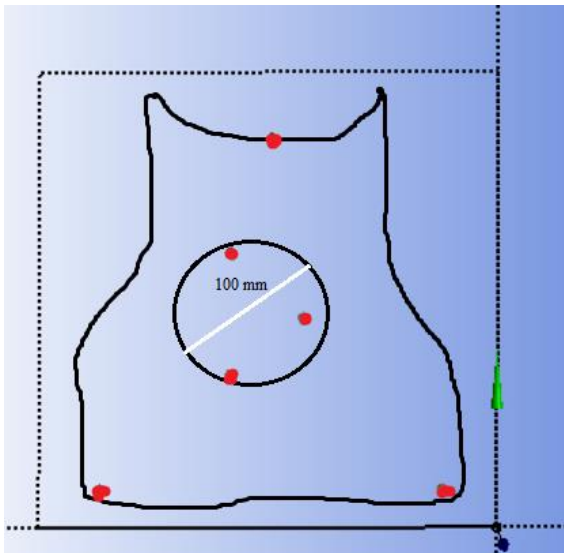


Figure 3.26 NIJ fair hit requirements visuals in similar view

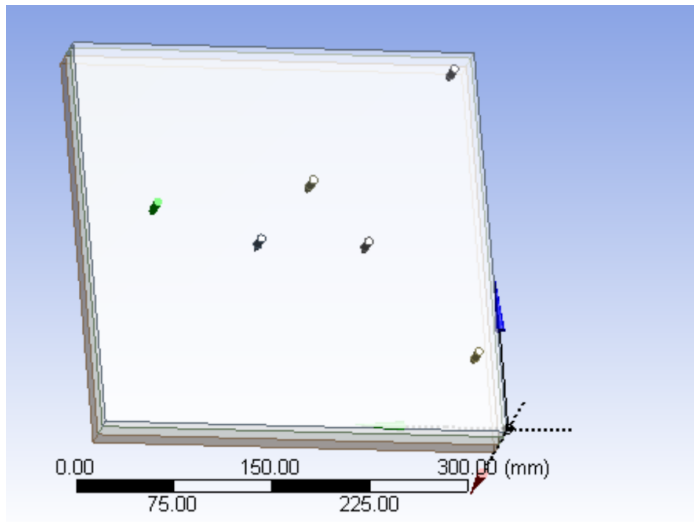


Figure 3.27 Fair hit targets on the multi-layered panel

3.5.2 Design Approach

After drawing the respective geometries of the bullets and the multi-layered composite structure, the material properties of each layer were outlined in the engineering data and the explicit dynamic analysis was then performed. It should be noted that material properties, dimension/thickness of material have a direct effect on the FEA results; used meshing type also has a direct effect on the result as well. Even though it is common sense using finer meshing always gives accurate results and of course there may be differences between the coarser and the finer meshes for the responsive behavior of the explicit dynamics of the software, it could be noticed by literature that a finer mesh generally results in a slightly lower load before the peak and a slightly higher load after the peak, but these differences never exceed 5% [10]. The choice of coarse meshing on a solid and straight block would also give accuracy and faster analysis results compared to finer meshing. Hence, for a multi-layered panel the meshing type was done by using coarse mesh of 0.002 for the composite structure as seen below in Figure 3.28.

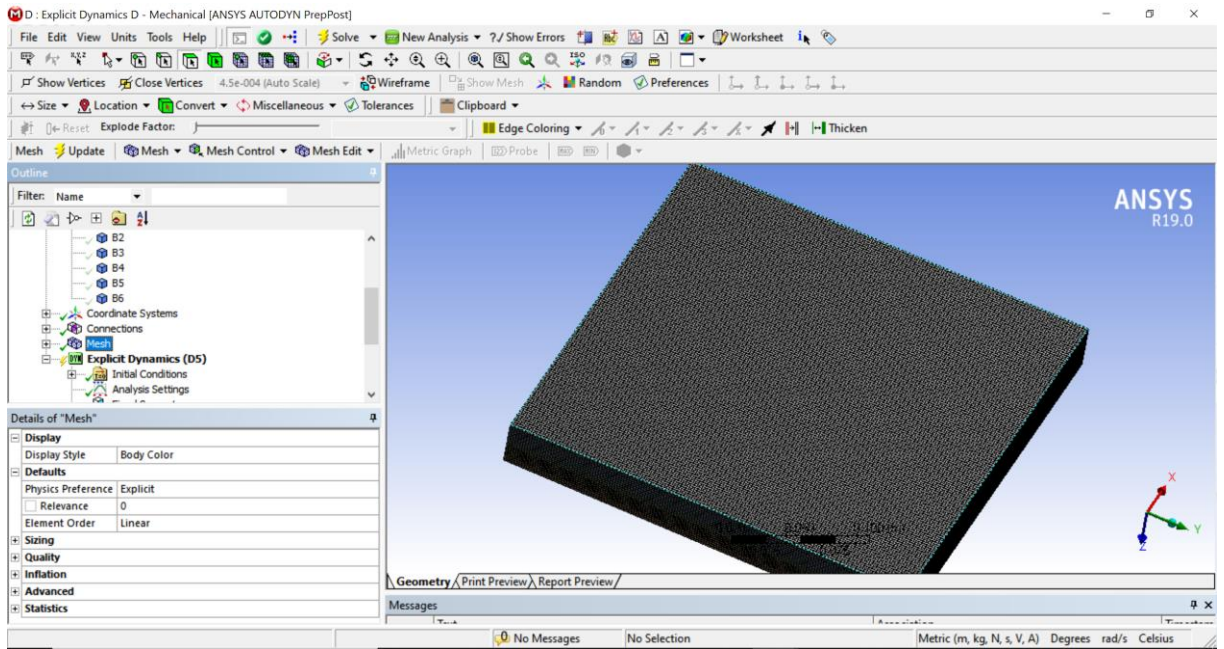


Figure 3.28 Meshed panel front view

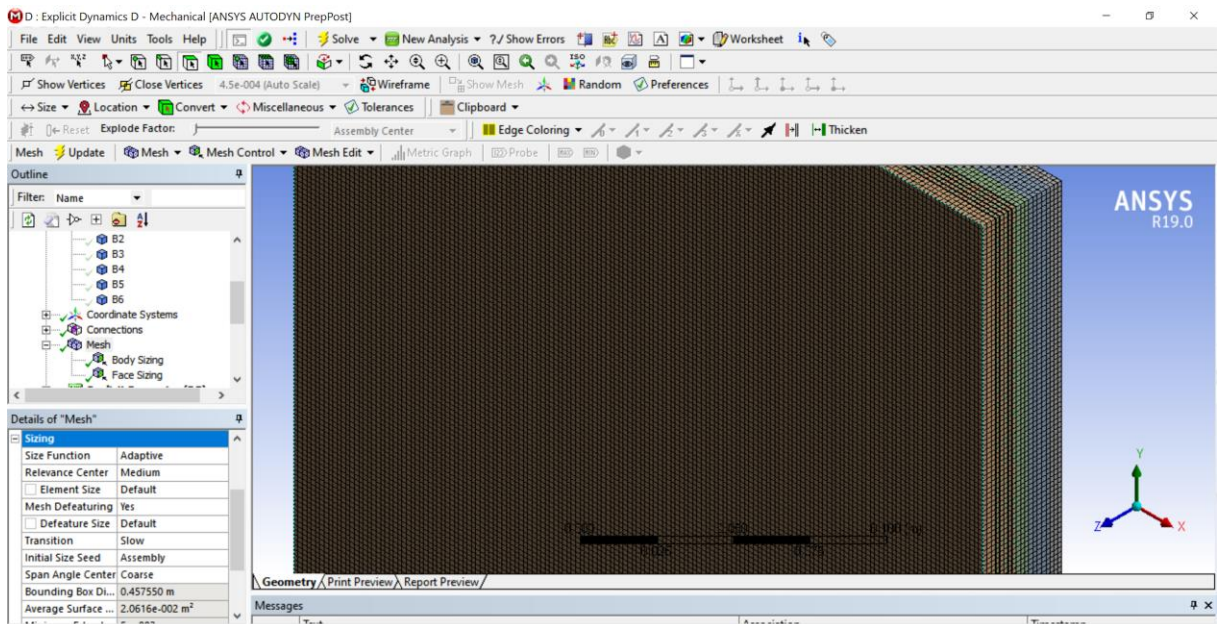


Figure 3.29 Meshed panel side view

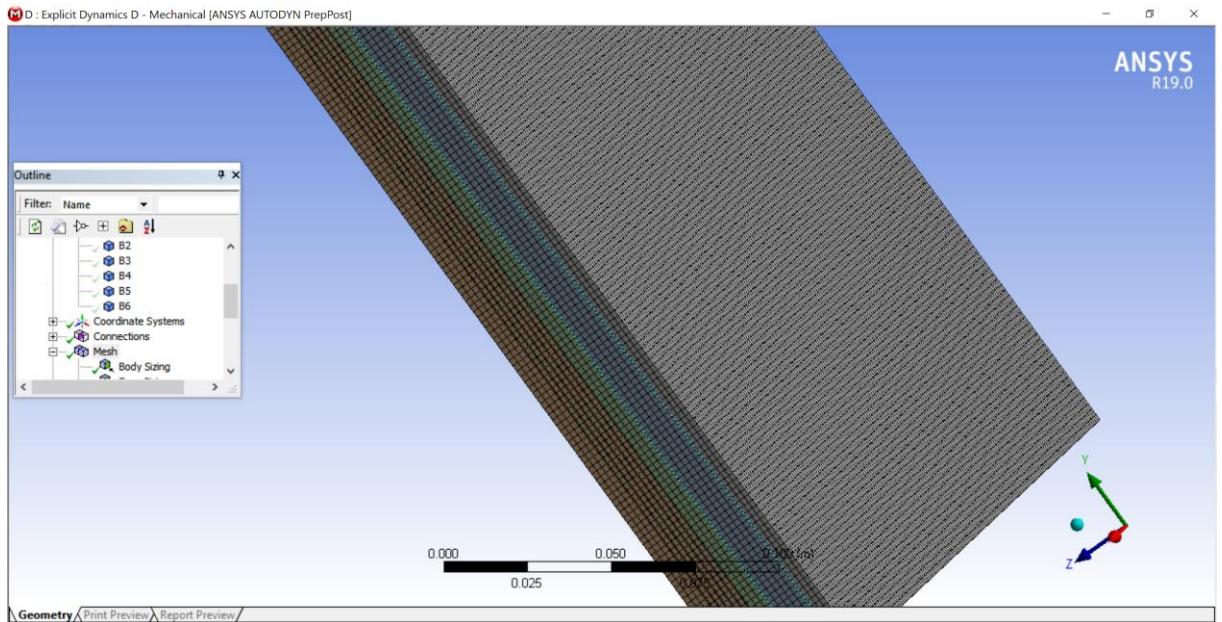


Figure 3.30 Meshed panel other side view

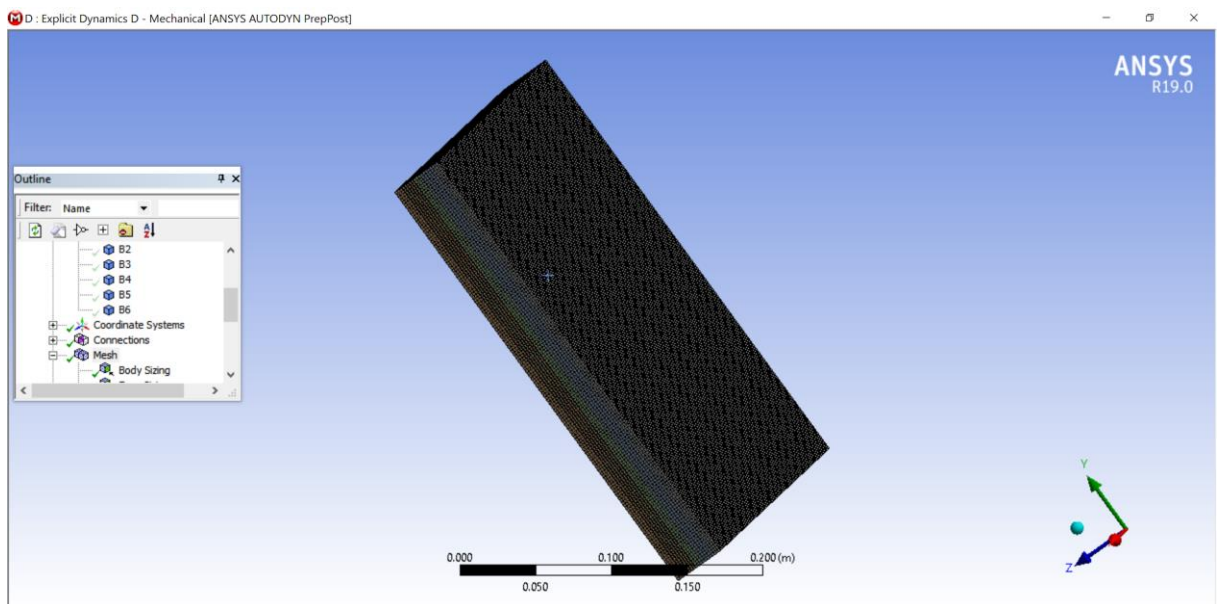


Figure 3.31 Meshed panel outlook view

The meshing on the bullets was done by using coarse type of meshing with of 0.0001 m as seen below.

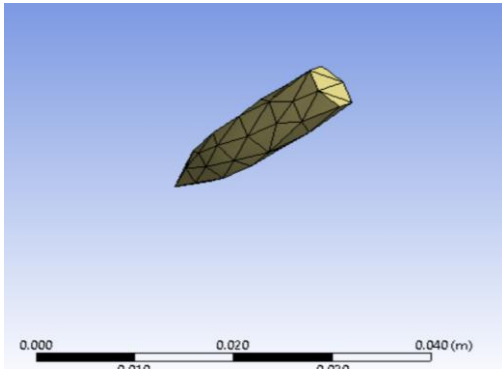


Figure 3.32 Meshed bullet view

Three contacts were made in ANSYS workbench to make necessary contact binds between the layers and to form one single assembly with no spacing in between is targeted. The contacts were made between each residing layer to ensure a compact and rigid structure. The following contacts can be seen in the figures provided below. The first contact established is applied in between the Silicon carbide and Epoxy layer. The second bond established was between the Epoxy layer and Kevlar and the third bond established was between the Kevlar and the Li-Ion battery layer. Contacts established and other necessary parameters are shown below:

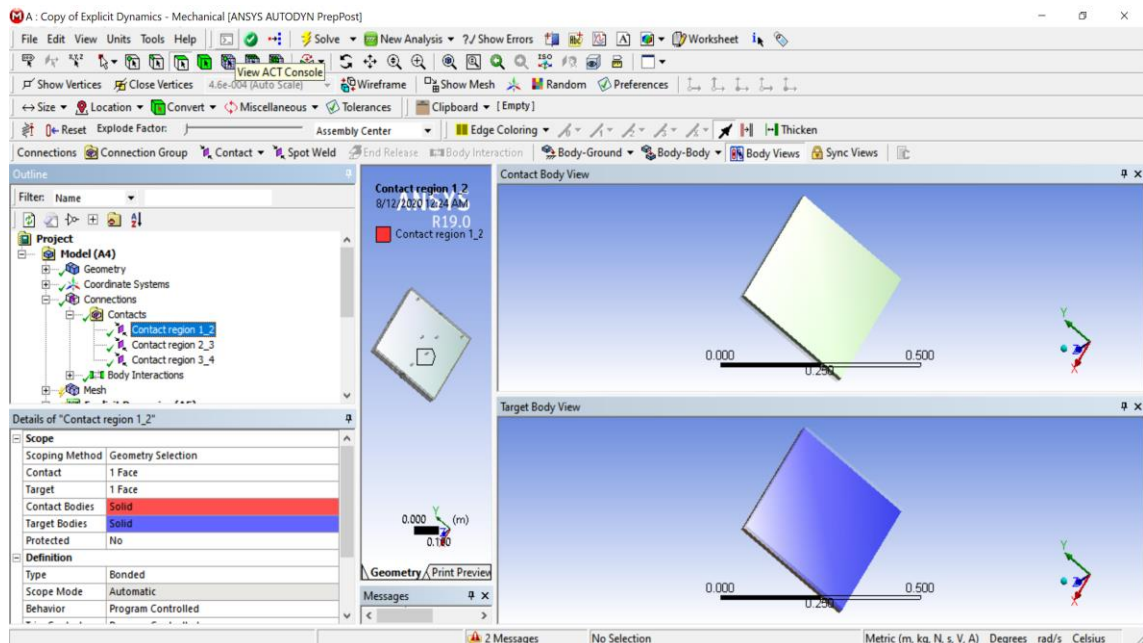


Figure 3.33 Contact established in between SiC and Epoxy Contact

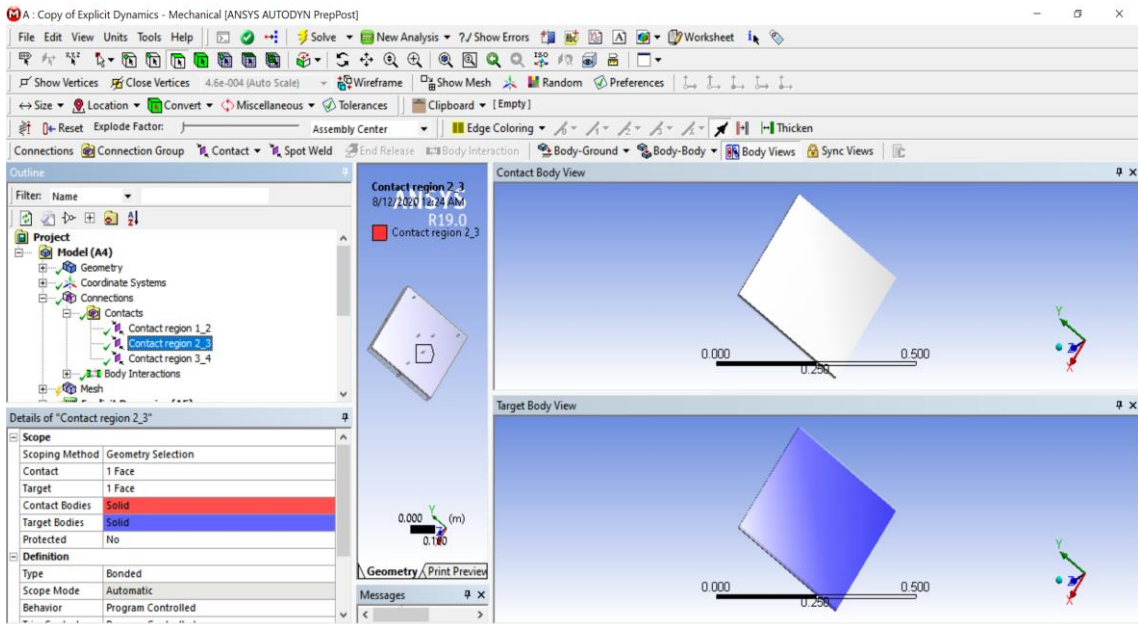


Figure 3.34 Contact established in between Epoxy and Kevlar

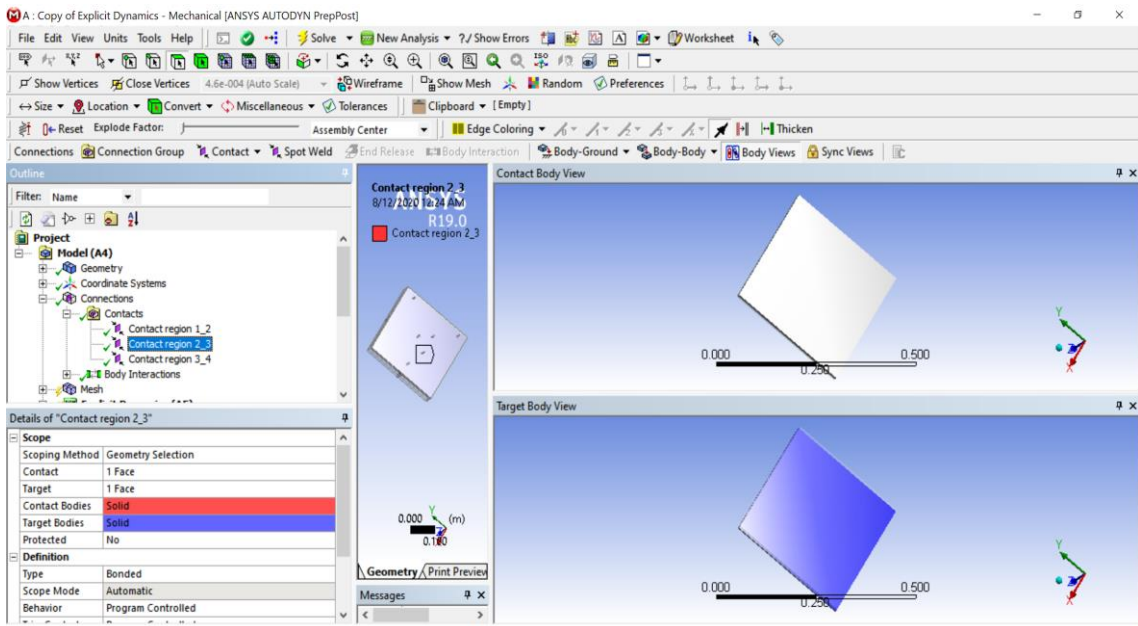


Figure 3.35 Contact established in between Kevlar and Li-Ion

The Velocity of bullets was set to 847 m/s in the Z direction as shown in Figure 3.36, below.

Details of "Velocity"	
Scope	
Scoping Method	Geometry Selection
Geometry	6 Bodies
Definition	
Input Type	Velocity
Define By	Components
Coordinate System	Global Coordinate System
<input type="checkbox"/> X Component	0. m/s
<input type="checkbox"/> Y Component	0. m/s
<input type="checkbox"/> Z Component	847. m/s
Suppressed	No

Figure 3.36 Projectile velocity determination in ANSYS

Further analysis settings defined are provided as follows:

Details of "Analysis Settings"	
Analysis Settings Preference	
Type	Program Controlled
Step Controls	
Resume From Cycle	0
Maximum Number of Cycles	1e+07
End Time	2.e-004 s
Maximum Energy Error	0.1
Reference Energy Cycle	0
Initial Time Step	Program Controlled
Minimum Time Step	Program Controlled
Maximum Time Step	Program Controlled
Time Step Safety Factor	0.9
Characteristic Dimension	Diagonals
Automatic Mass Scaling	No
Solver Controls	
Solve Units	mm, mg, ms
Beam Solution Type	Bending
Beam Time Step Safety Factor	0.5
Hex Integration Type	Exact
Shell Sublayers	3
Shell Shear Correction Factor	0.8333
Shell BWC Warp Correction	Yes
Shell Thickness Update	Nodal

Figure 3.37 Further analysis settings and commands in ANSYS

Details of "Analysis Settings"	
Shell Thickness Update	Nodal
Tet Integration	Average Nodal Pressure
Shell Inertia Update	Recompute
Density Update	Program Controlled
Minimum Velocity	1.e-006 m s ⁻¹
Maximum Velocity	1.e+010 m s ⁻¹
Radius Cutoff	1.e-003
Minimum Strain Rate Cutoff	1.e-010
Euler Domain Controls	
Domain Size Definition	Program Controlled
Display Euler Domain	Yes
Scope	All Bodies
X Scale factor	1.2
Y Scale factor	1.2
Z Scale factor	1.2
Domain Resolution Definition	Total Cells
Total Cells	2.5e+05
Lower X Face	Flow Out
Lower Y Face	Flow Out
Lower Z Face	Flow Out
Upper X Face	Flow Out
Upper Y Face	Flow Out
Upper Z Face	Flow Out

Figure 3.38 Further analysis settings and commands in ANSYS

Details of "Analysis Settings"	
Y Scale factor	1.2
Z Scale factor	1.2
Domain Resolution Definition	Total Cells
Total Cells	2.5e+05
Lower X Face	Flow Out
Lower Y Face	Flow Out
Lower Z Face	Flow Out
Upper X Face	Flow Out
Upper Y Face	Flow Out
Upper Z Face	Flow Out
Euler Tracking	By Body
+ Damping Controls	
- Erosion Controls	
On Geometric Strain Limit	Yes
Geometric Strain Limit	1.5
On Material Failure	No
On Minimum Element Time Step	No
Retain Inertia of Eroded Material	Yes
+ Output Controls	
- Analysis Data Management	
Solver Files Directory	C:\Users\fzali\OneDrive\De...
Scratch Solver Files Directory	C:\Users\fzali\OneDrive\De...

Figure 3.39 Further analysis settings and commands in ANSYS

Chapter 4

Results and Discussion

4.1 FEA Results for Type III Protocol

The framework and simulation in Ansys provide a sufficient shape and size approximation of the armor's impact conditions. Moreover, the simulation tool was able to foresee total and directional deformations and maximum shear stress also indicating the stress concentration of the projectile and aim that demonstrates whether or not the sample was able to stop the projectiles. The ballistic vest is modeled by using Ansys. Additionally, it could also be seen that the bullet goes through the layer and causes some deformation in the middle section of the layer of the sample. Recorded incident velocity of the projectile was 847 m/s for type III armor, 710 for type IIA armor and 379 m/s for Type II armor.

4.1.1 Total Deformation Results for 7.62 mm Bullet

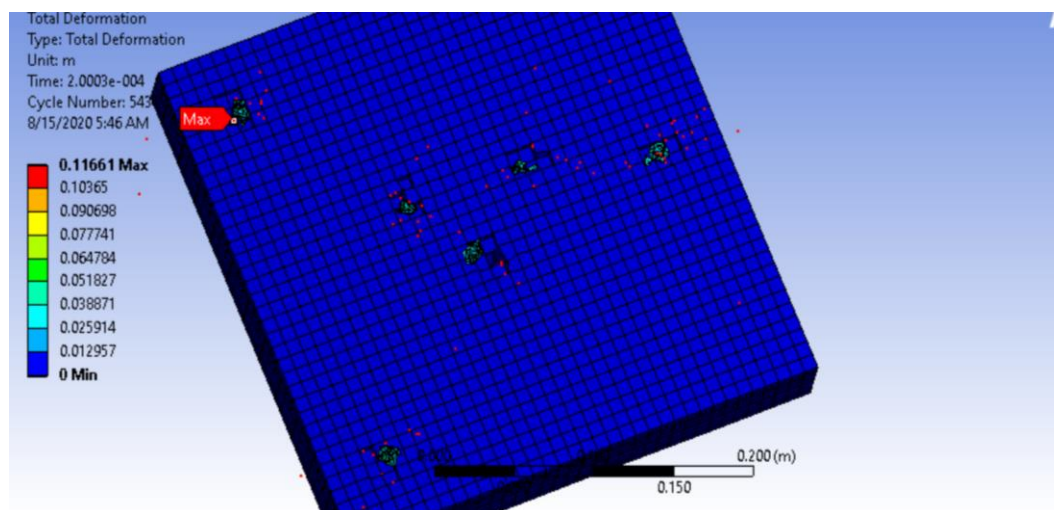


Figure 4.1 Total deformation results' visual

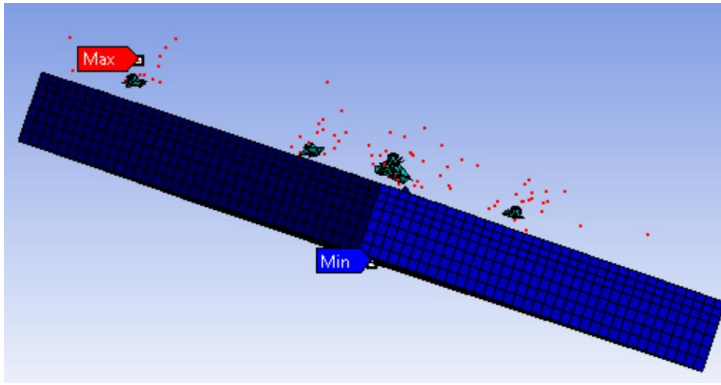


Figure 4.2 Total deformation results' side view visual

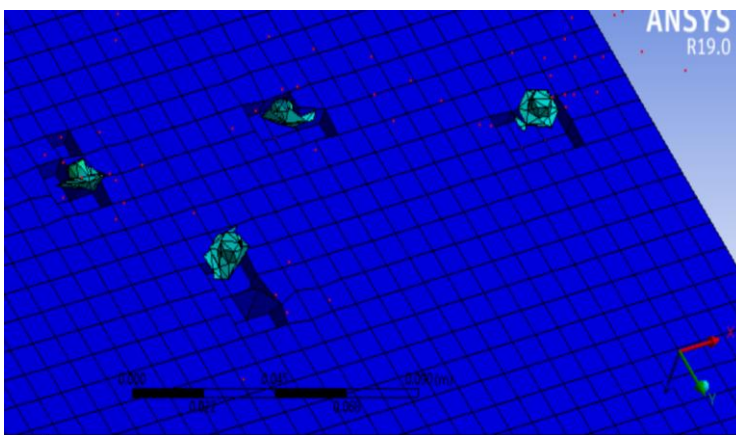


Figure 4.3 Fair hit locations visual

The 7.62 mm bullet of type III armor showed a total deformation of 0.11631 m which is not a bad value for a total of six separate bullets respectively hitting the multi-layered plate and causing deformation on the plate. In average of 6 shots, an average shot may cause around 1.93 cm or 19.3 mm directional deformation and showing that the design is resisting within the limits. Not any deformation is detected in the bottom layer, thus resulting in a successful experiment in terms of total deformation results. As it can be clearly identified in the Ansys results; the bullets break halfway through the 2nd layer (epoxy resin) so the penetration depth is within 5 to 20 mm and the Li-Ion layer stays safe as it is located at 30 mm away distance from the top.

Moreover, Explicit Dynamics provides an explanatory chart (Figure 4.4) that gives total deformation value which could be identified more in detail related with time as provided below.

Model (G4) > Explicit Dynamics (G5) > Solution (G6) > Total Deformation

Time [s]	Minimum [m]	Maximum [m]	Average [m]
1.1755e-038		0.	0.
1.007e-005		8.5295e-003	1.4258e-004
2.0046e-005		1.6979e-002	2.8382e-004
3.0023e-005		2.5429e-002	4.2506e-004
4.0036e-005		3.3946e-002	5.6447e-004
5.002e-005		4.2056e-002	6.8458e-004
6.0003e-005		4.882e-002	7.7995e-004
7.0022e-005		5.2729e-002	8.3999e-004
8.0011e-005		5.3399e-002	8.7264e-004
9.0009e-005		5.2861e-002	8.9293e-004
1.0001e-004	0.	5.8715e-002	9.0406e-004
1.1e-004		6.6192e-002	9.1405e-004
1.2004e-004		7.3959e-002	9.2821e-004
1.3004e-004		8.1886e-002	9.4814e-004
1.4003e-004		8.9938e-002	9.6879e-004
1.5003e-004		9.8099e-002	9.8302e-004
1.6002e-004		0.10633	9.928e-004
1.7002e-004		0.1139	1.0026e-003
1.8002e-004		0.11585	1.0135e-003
1.9001e-004		0.11604	1.0216e-003
2.0003e-004		0.11661	1.0253e-003

Figure 4.4 Maximum and average total deformation information vs. time results

In addition to that, for a clear comprehension, a graph below is plotted with the values shown, green line representing the maximum deformation, whereas red line representing minimum and the blue line representing the average total deformation.

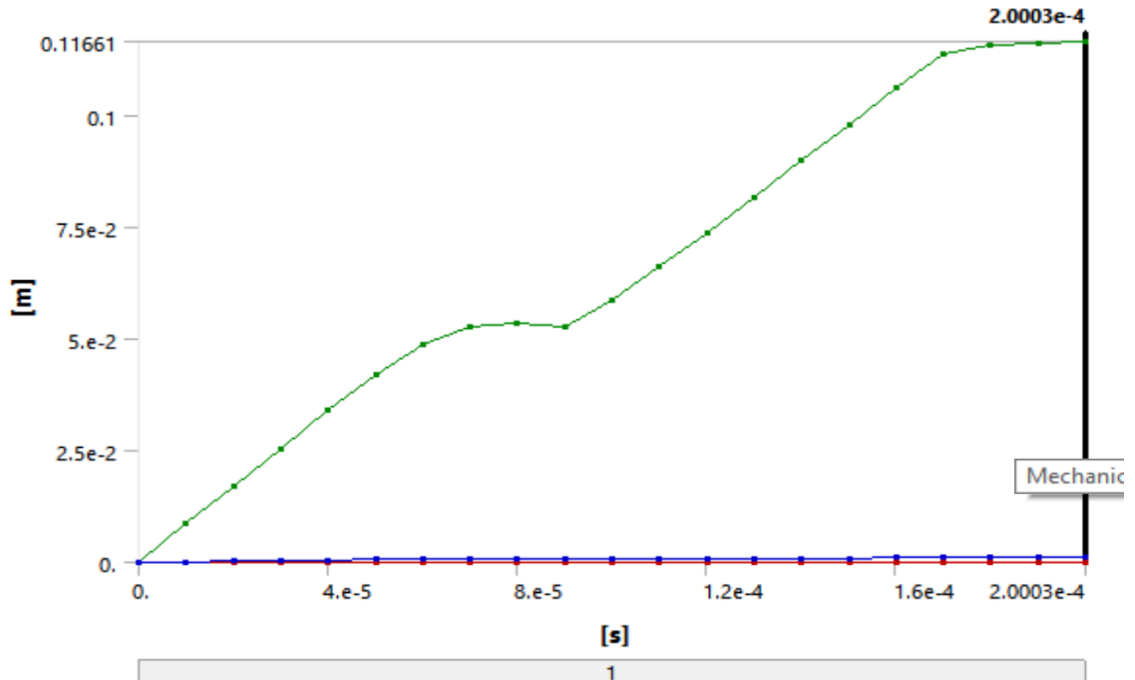


Figure 4.5 Total deformation in time graph

4.1.2 Equivalent Stress Results for 7.62 mm Bullet

The 7.62 mm bullet of type III armor showed a maximum equivalent stress of 5.3304×10^8 Pa. No stress is seen in the bottom most layer thus resulting in a successful experiment in terms of maximum equivalent stress also. Red dots seen indicate the pieces' thorn from the layer.

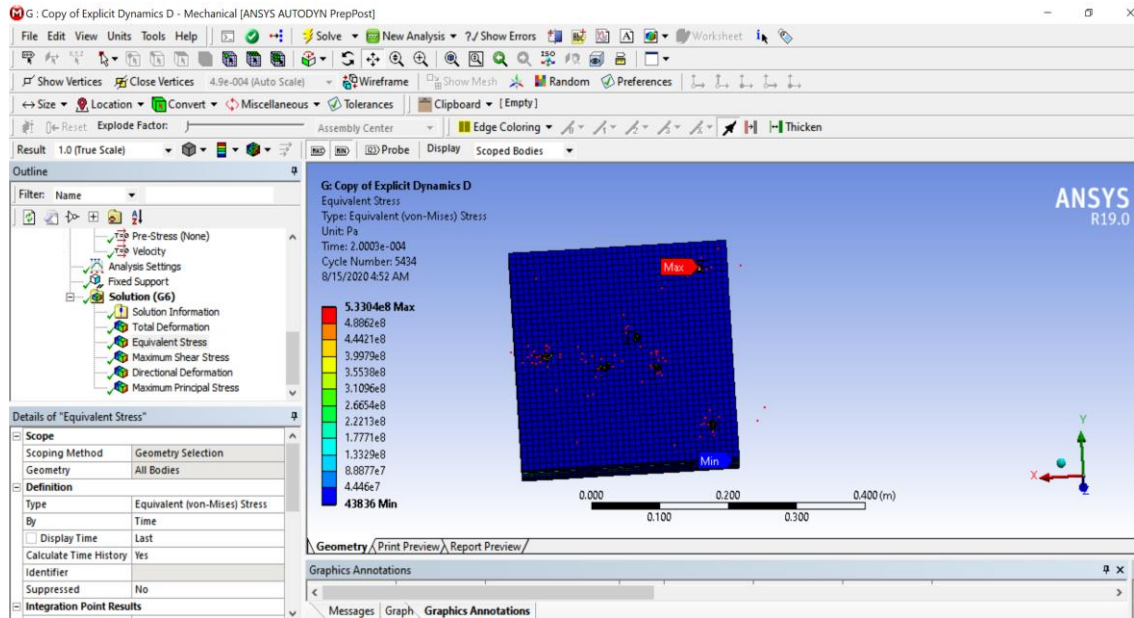


Figure 4.6 Equivalent stress result front view associated with Type III armor conditions of 7.62 mm projectile

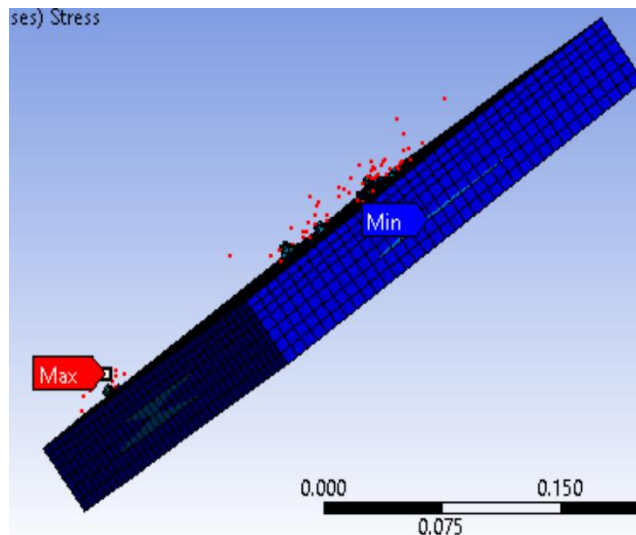


Figure 4.7 Equivalent stress result side view associated with Type III armor conditions of 7.62 mm projectile

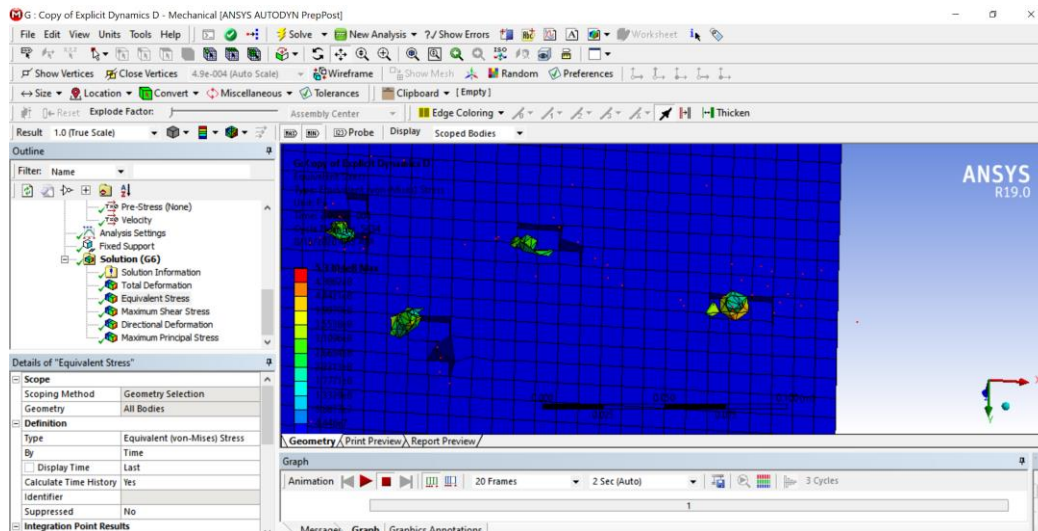


Figure 4.8 Equivalent stress result top view associated with Type III armor conditions of 7.62 mm projectile

As seen in the Ansys results; the bullets break halfway through the 2nd layer (epoxy resin) and no stress could be seen at the point where it penetrates the first layer on the plate. Hence, almost a very little or no stress effect could be noticed on the Li-Ion layer.

4.1.3 Shear Stress Results for 7.62 mm Bullet

The 7.62 mm bullet of type III armor showed a maximum shear stress of 2.9208×10^8 Pa. No stress is seen or detected in the bottom layer, thus resulting in a successful experiment in terms of maximum shear stress determination also for the whole multi-layer system.

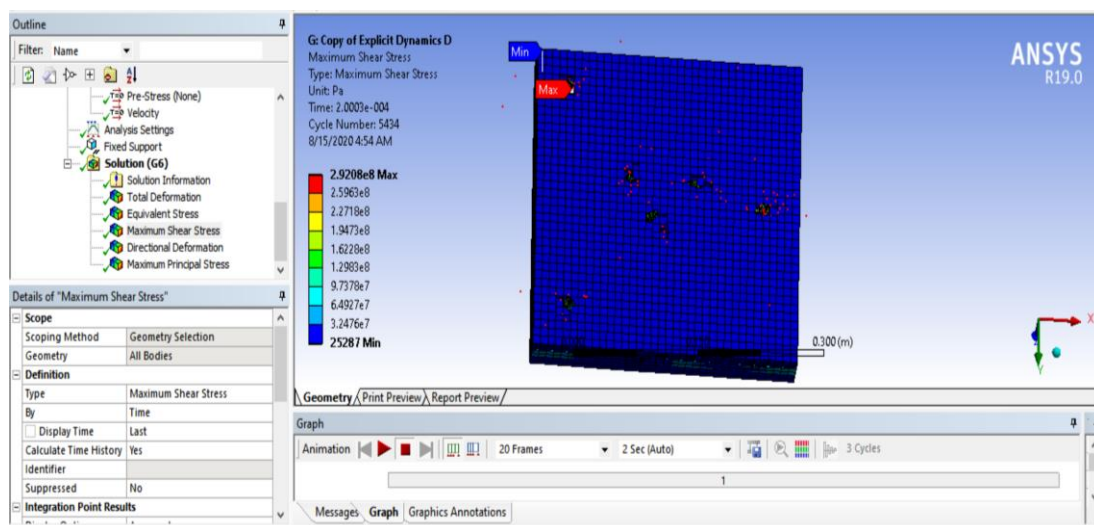


Figure 4.9 Maximum shear stress result front view associated with Type III armor conditions of 7.62 mm projectile

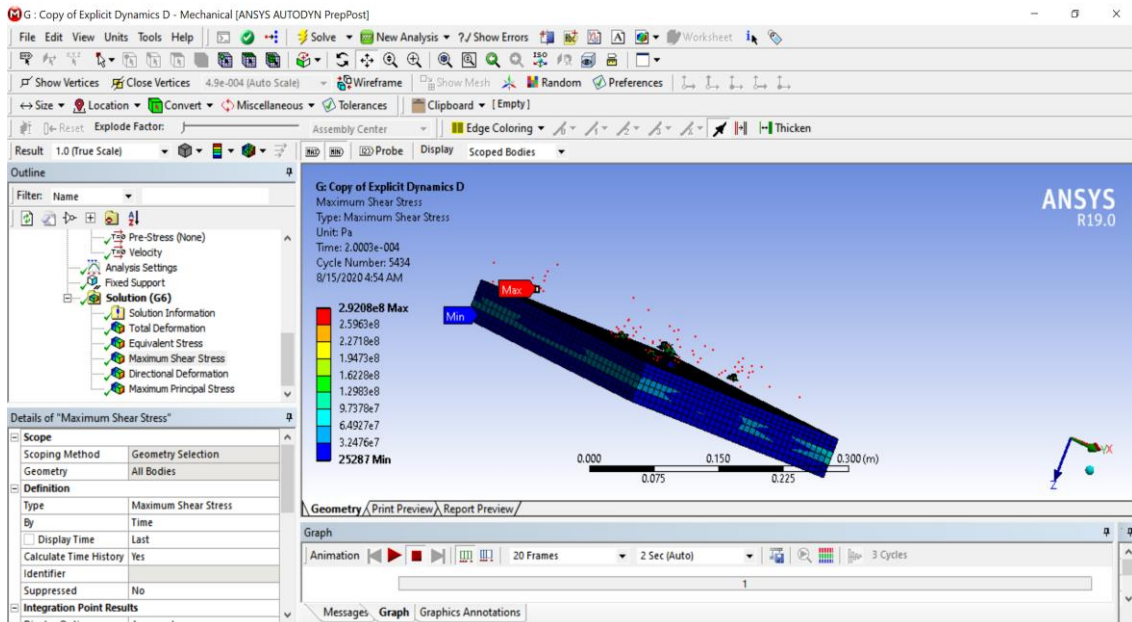


Figure 4.10 Maximum shear stress result side view associated with Type III armor conditions of 7.62 mm projectile

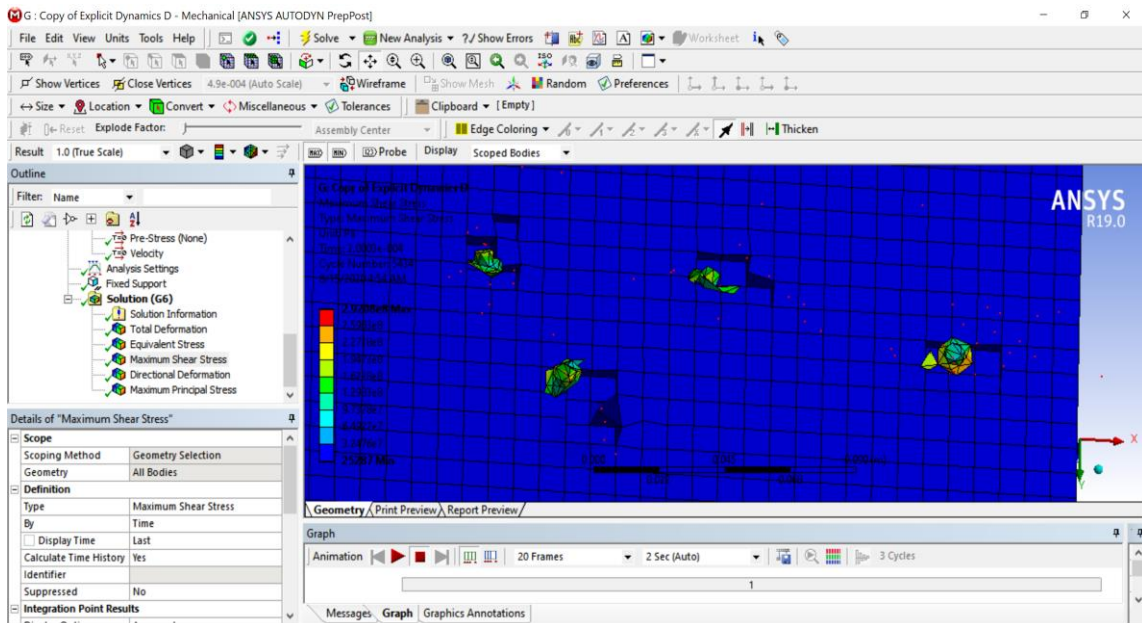


Figure 4.11 Maximum shear stress result top view associated with Type III armor conditions of 7.62 mm projectile

Consequently, as it could clearly be seen in the Ansys results; the bullets break halfway through the 2nd layer (epoxy resin) and no stress is seen at the point as the body stays blue where it penetrates the first layer on the multi-layered plate. Hence, exceptionally little or almost no stress effect could be seen or detected on the Li-Ion layer.

4.1.4 Directional Deformation Results for 7.62 mm Bullet

The 7.62 mm bullet of type III armor showed a total directional deformation of 0.044716 m, or 44,716 mm. As seen from the Figure 4.11 below, the lower layer does face some deformation which is around 0.002667 meters and equivalent to 2.6 mm; which is not that critical of a deformation thus resulting in a successful experiment in terms of directional deformation as well.

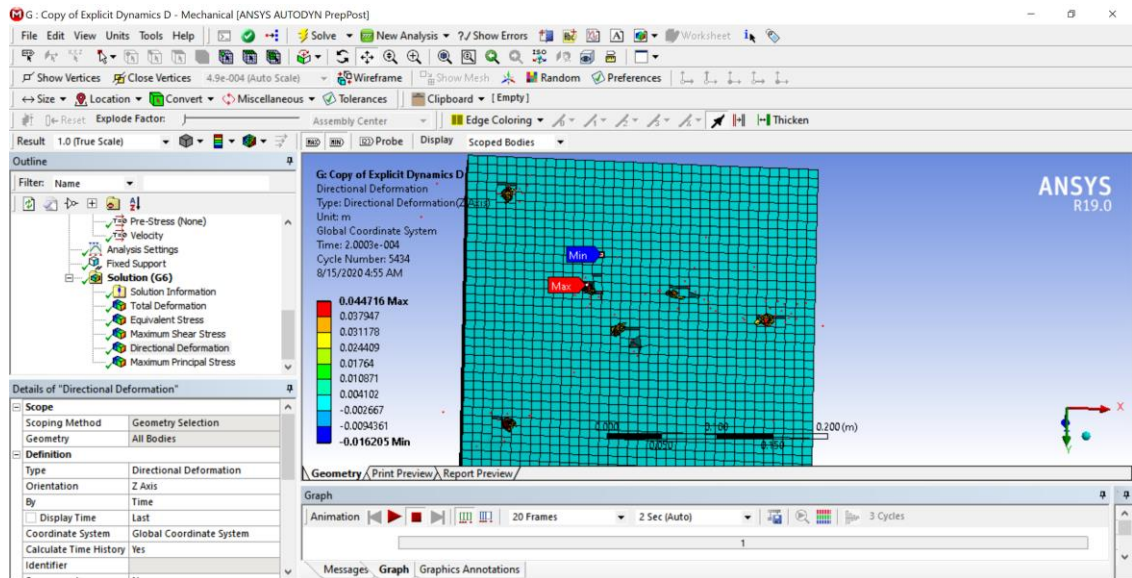


Figure 4.12 Directional deformation result front view associated with Type III armor conditions of 7.62 mm projectile

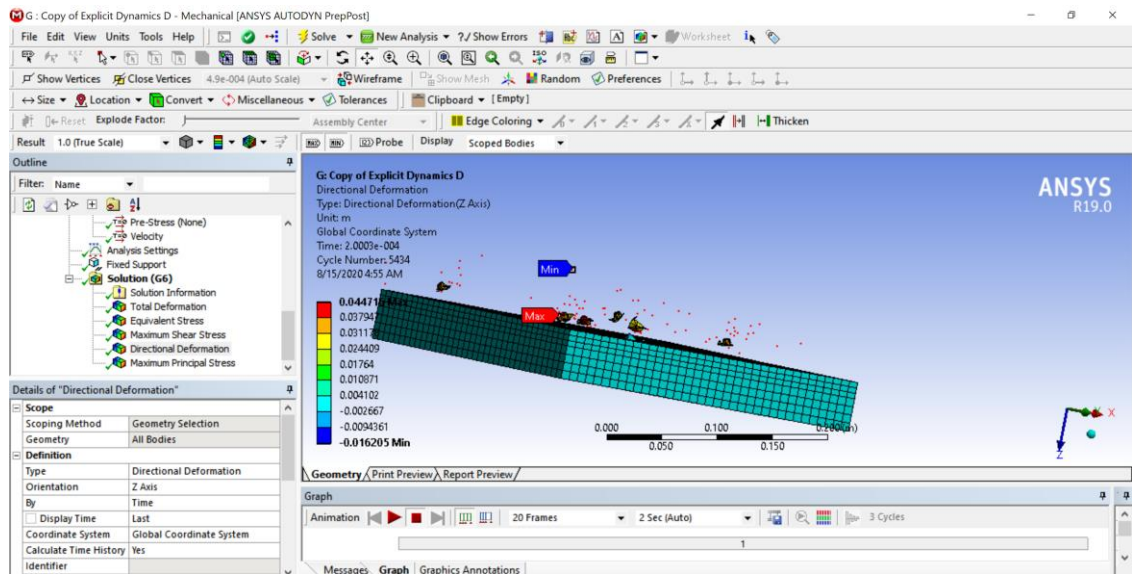


Figure 4.13 Directional deformation result side view associated with Type III armor conditions of 7.62 mm projectile

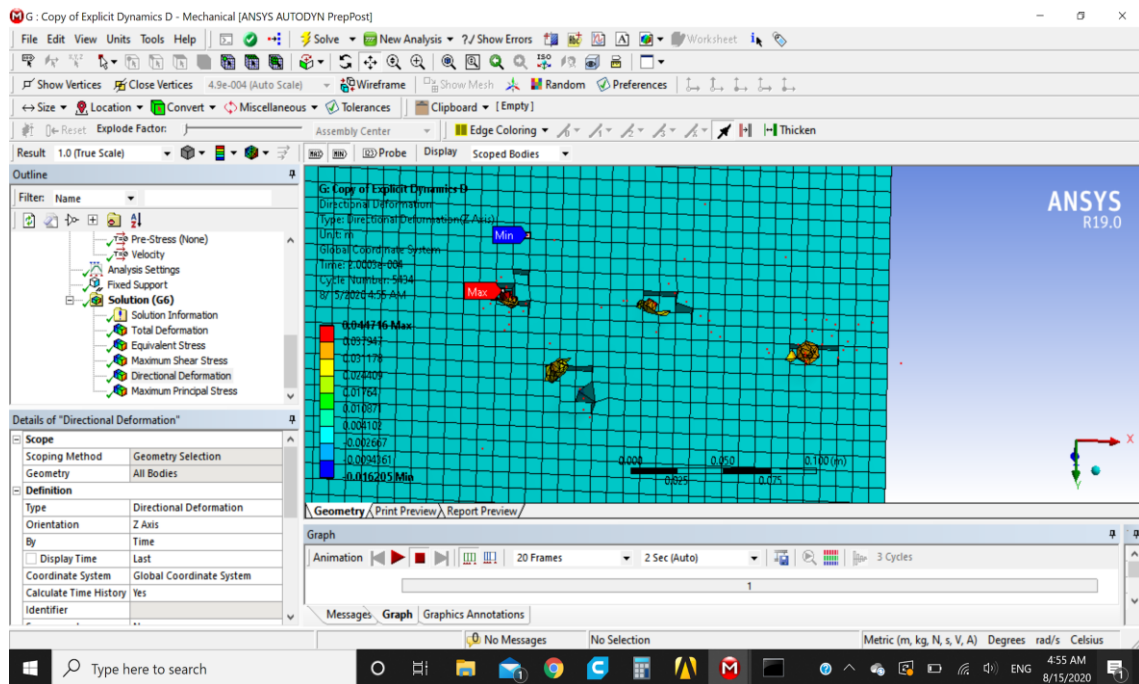


Figure 4.14 Directional deformation result top view associated with Type III armor conditions of 7.62 mm projectile

Consequently, and similarly, as it could clearly be seen in the Ansys results; the bullets break halfway through the 2nd layer (epoxy resin) and no deformation is seen at the point as the body stays blue where it penetrates the first layer on the multi-layered plate. Hence, exceptionally little or almost no stress effect could be seen or detected on the Li-Ion layer.

4.2 FEA Results for Type IIA Protocol

4.2.1 Total Deformation Results for 9 mm Bullet

The 9 mm bullet of type IIA armor showed a maximum total deformation of 17,349 mm which is lesser than that compared to a 7.62 mm. So it is seen that a bullet with greater diameter is less prone to deformation than a bullet which has a smaller diameter. The speed of this bullet is estimated as 710 m/s but no deformation could be detected in the bottom layer, thus resulting in a successful experiment in terms of total deformation.

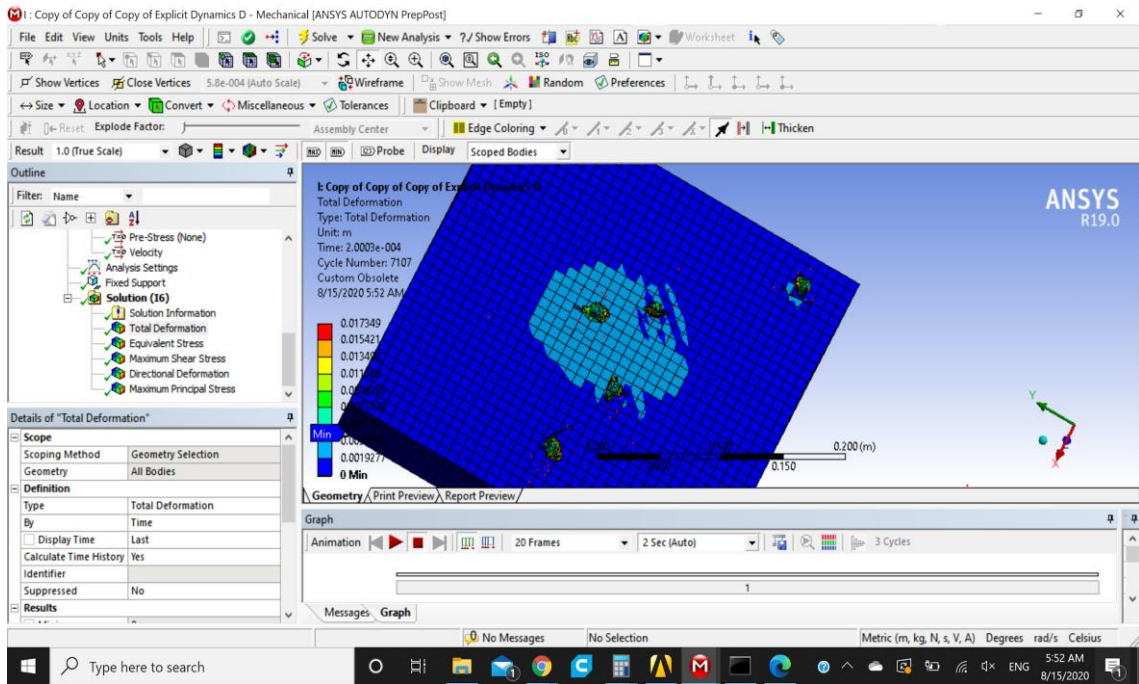


Figure 4.15 Total deformation result front view associated with Type IIA armor conditions of 9 mm projectile

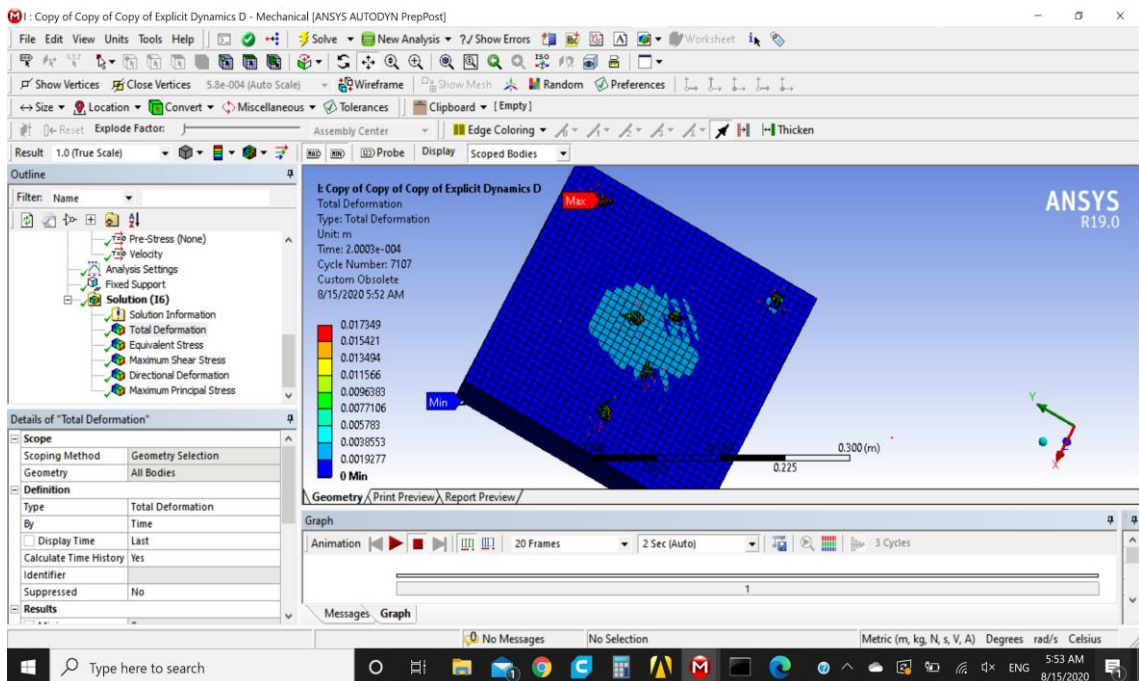


Figure 4.16 Total deformation result alternative front view associated with Type IIA armor conditions of 9 mm projectile

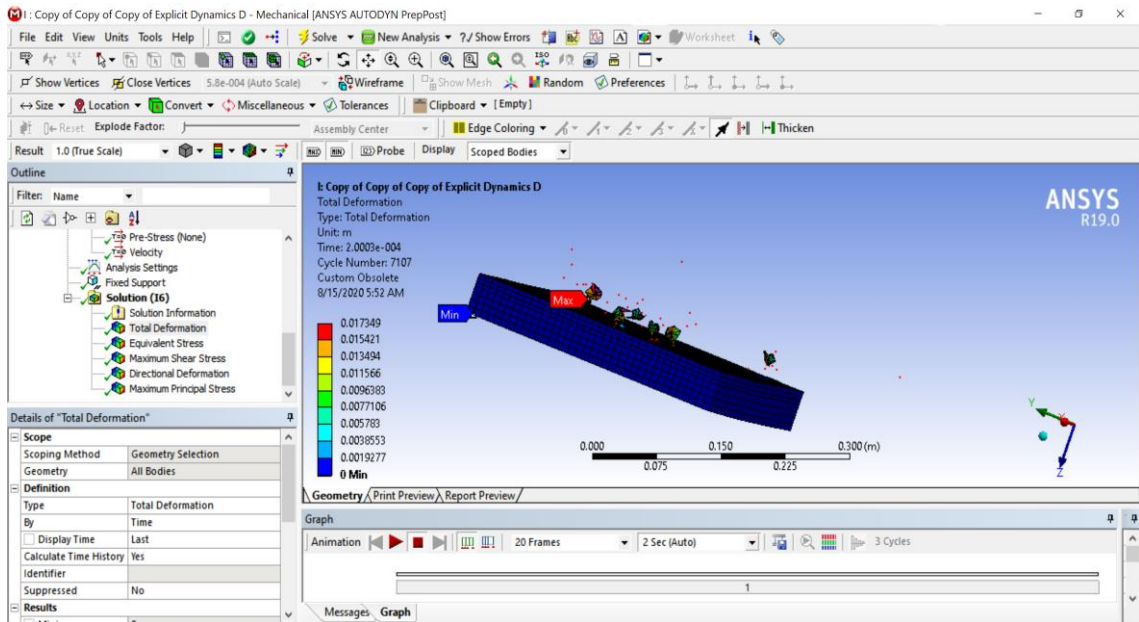


Figure 4.17 Total deformation result side view associated with Type IIA armor conditions of 9 mm projectile

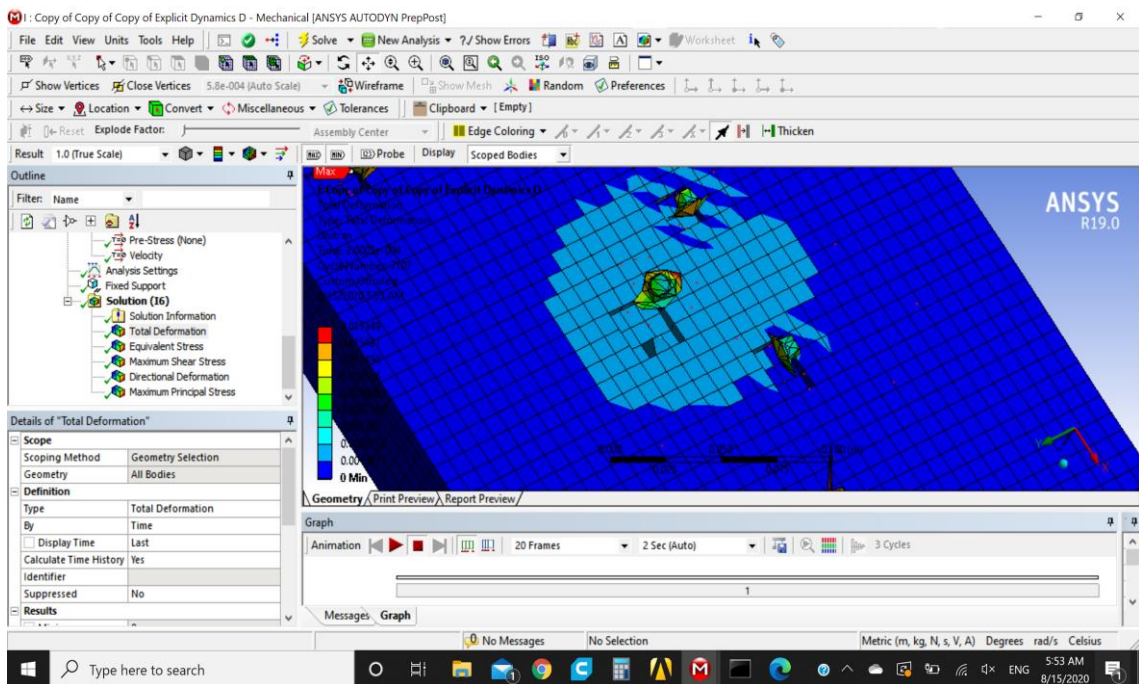


Figure 4.18 Total deformation result top view associated with Type IIA armor conditions of 9 mm projectile

Consequently, as it could clearly be seen in the Ansys results; the bullets break halfway through the 2nd layer (epoxy resin) so the penetration depth is within the limits of 5 to 10 mm and the Li-Ion layer remains safe. Moreover, Explicit Dynamics provides

an explanatory chart (Figure 4.19) that gives total deformation values which could be identified more in detail related with time as provided below.

Model (I4) > Explicit Dynamics (I5) > Solution (I6) > Total Deformation

Time [s]	Minimum [m]	Maximum [m]	Average [m]
1.1755e-038		0.	0.
1.004e-005		7.4915e-003	1.1258e-004
2.0028e-005		1.6771e-002	2.1979e-004
3.0015e-005		2.7583e-002	3.1717e-004
4.0004e-005		3.8795e-002	3.9782e-004
5.0003e-005		5.015e-002	4.7418e-004
6.0019e-005		6.1585e-002	5.399e-004
7.0013e-005		7.3026e-002	5.9233e-004
8.0008e-005		8.4485e-002	6.4456e-004
9.0006e-005		9.5962e-002	7.0586e-004
1.0002e-004	0.	0.10746	7.737e-004
1.1002e-004		0.11895	8.3693e-004
1.2001e-004		0.13044	8.9124e-004
1.3001e-004		0.14194	9.4191e-004
1.4e-004		0.15343	9.9277e-004
1.5002e-004		0.16496	1.0392e-003
1.6003e-004		0.17647	1.0757e-003
1.7e-004		0.18795	1.1082e-003
1.8001e-004		0.19947	1.1503e-003
1.9002e-004		0.21098	1.2079e-003
2.0003e-004		0.22251	1.2699e-003

Figure 4.19 Minimum, maximum and average deformation values

4.2.2 Equivalent Stress Results for 9 mm Bullet

The 9 mm bullet of type IIA armor showed a maximum equivalent stress of $8.3242e^{+8}$ Pa which is more than that of 7.62 mm bullet so it can be evaluated that the bullet with larger diameter has resulted greater stresses compared to the one with smaller diameter which was around $5.3304e^{+8}$ Pa. Some stress is seen half way through approximately 22.5 mm away from the top which is still considerably safe because the Li-Ion layer lies at 30 mm from the top surface. Thus, no stress is detected in the bottom layer thus resulting in a successful experiment in terms of maximum equivalent stress also.

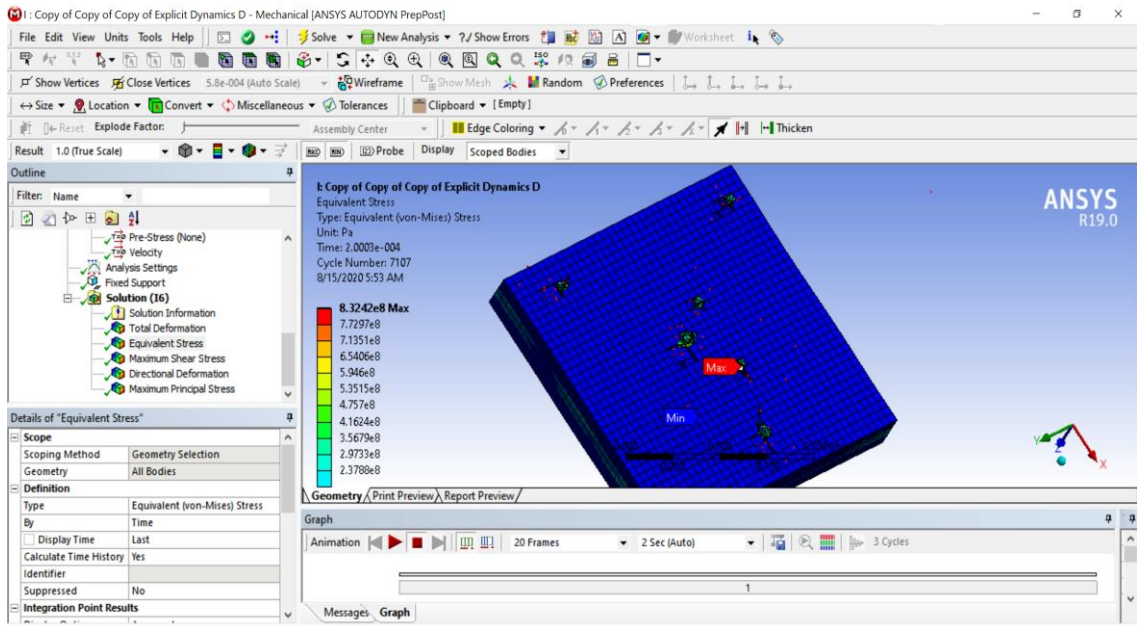


Figure 4.20 Equivalent stress result front view associated with Type IIA armor conditions of 9 mm projectile

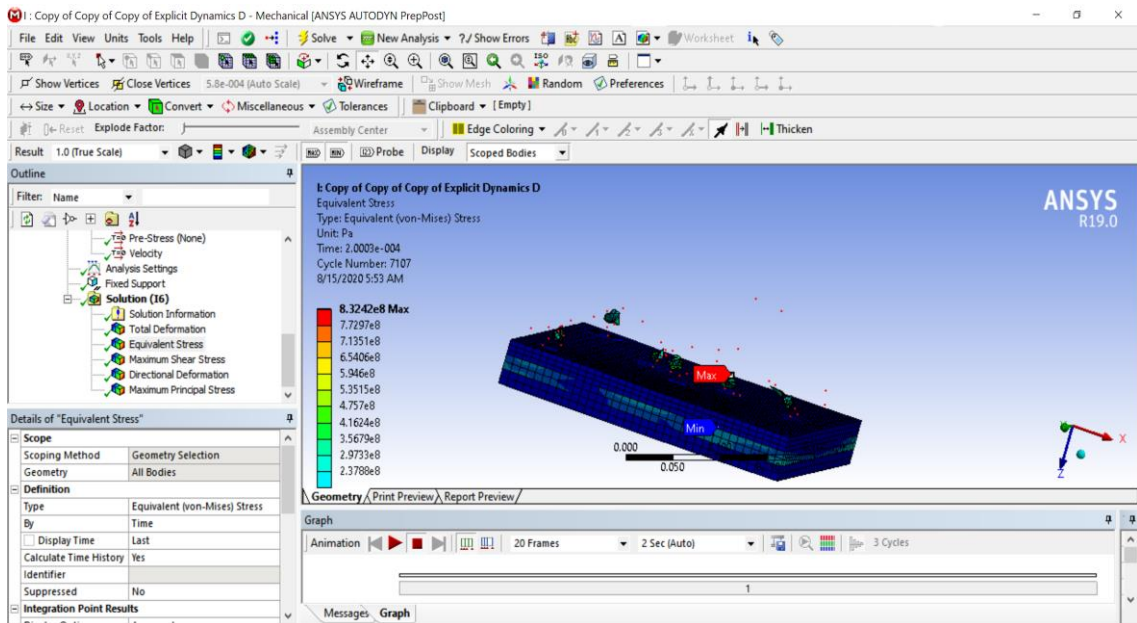


Figure 4.21 Equivalent stress result side view associated with Type IIA armor conditions of 9 mm projectile

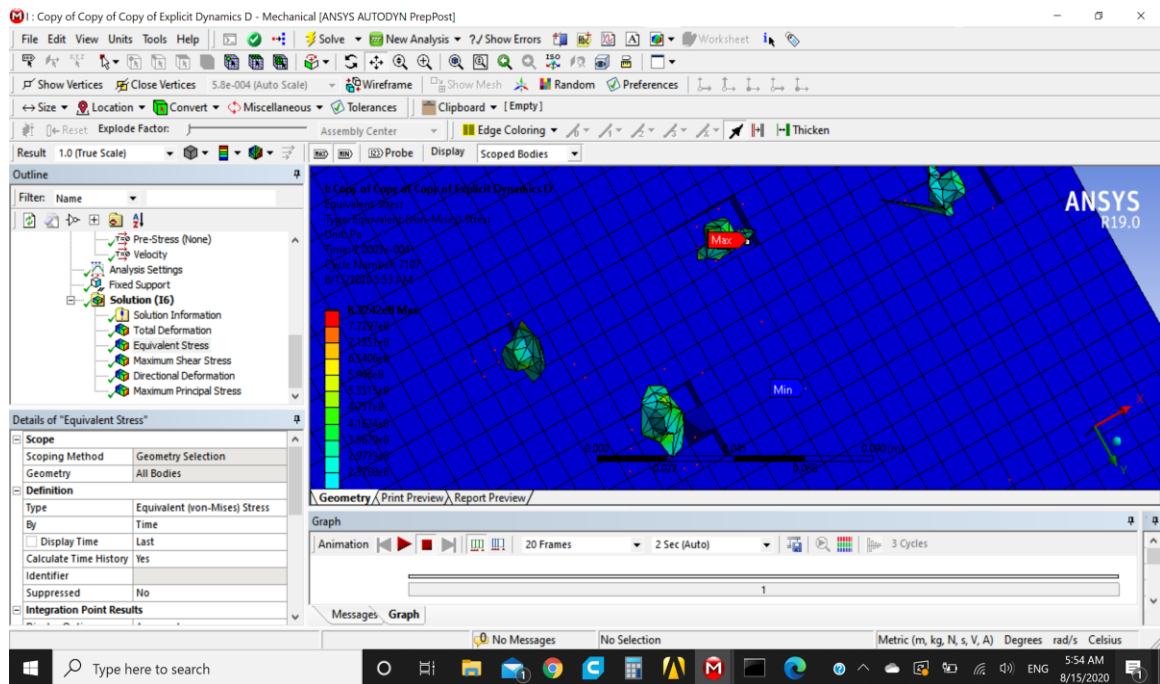


Figure 4.22 Equivalent stress result top view associated with Type IIA armor conditions of 9 mm projectile

As seen in the Ansys results; the bullets break halfway through the 2nd layer (epoxy resin) and no stress could be seen at the point where it penetrates the first layer on the plate. Hence, almost a very little or no stress effect could be noticed on the Li-Ion layer. Moreover, Explicit Dynamics provides a chart that gives total deformation value which could be identified more in detail related with time as provided below. Higher stress point may be noticed in the below Figure 4.23, however at the related time and point on layer (as seen on the ANSYS analysis visual), it is pointed out that the relevant stress value is as given. It is also provided at the last column of the below, Figure 4.23.

Model (I4) > Explicit Dynamics (I5) > Solution (I6) > Equivalent Stress

Time [s]	Minimum [Pa]	Maximum [Pa]	Average [Pa]
1.1755e-038		0	0
1.004e-005	0	1.2038e+009	1.2322e+007
2.0028e-005	0.45883	1.1338e+009	2.0952e+007
3.0015e-005	303.73	1.221e+009	4.3569e+007
4.0004e-005	2629.7	1.672e+009	5.1416e+007
5.0003e-005	6857.7	1.0477e+009	4.7342e+007
6.0019e-005	14344	1.0225e+009	4.451e+007
7.0013e-005	24689	8.7354e+008	4.1924e+007
8.0008e-005	39281	8.8395e+008	4.1538e+007
9.0006e-005	62076	8.936e+008	4.2309e+007
1.0002e-004	84149	9.3481e+008	4.3808e+007
1.1002e-004	49889	8.2863e+008	4.3536e+007
1.2001e-004	90022	7.4773e+008	4.5642e+007
1.3001e-004	68756	6.8432e+008	4.6733e+007
1.4e-004	1.0934e+005	8.3831e+008	4.6294e+007
1.5002e-004	56882	8.081e+008	4.4386e+007
1.6003e-004	73530	7.3584e+008	4.3137e+007
1.7e-004	81635	7.4531e+008	4.2074e+007
1.8001e-004	59769	7.0996e+008	4.0322e+007
1.9002e-004	1.0108e+005	8.5566e+008	3.9723e+007
2.0003e-004	60631	8.3242e+008	4.0381e+007

Figure 4.23 Minimum, maximum and average stress values

In addition to that, for a clear comprehension, the graph below is plotted with the values shown, whereas green line representing the equivalent stress, red line representing minimum and the blue line representing the average equivalent stress.

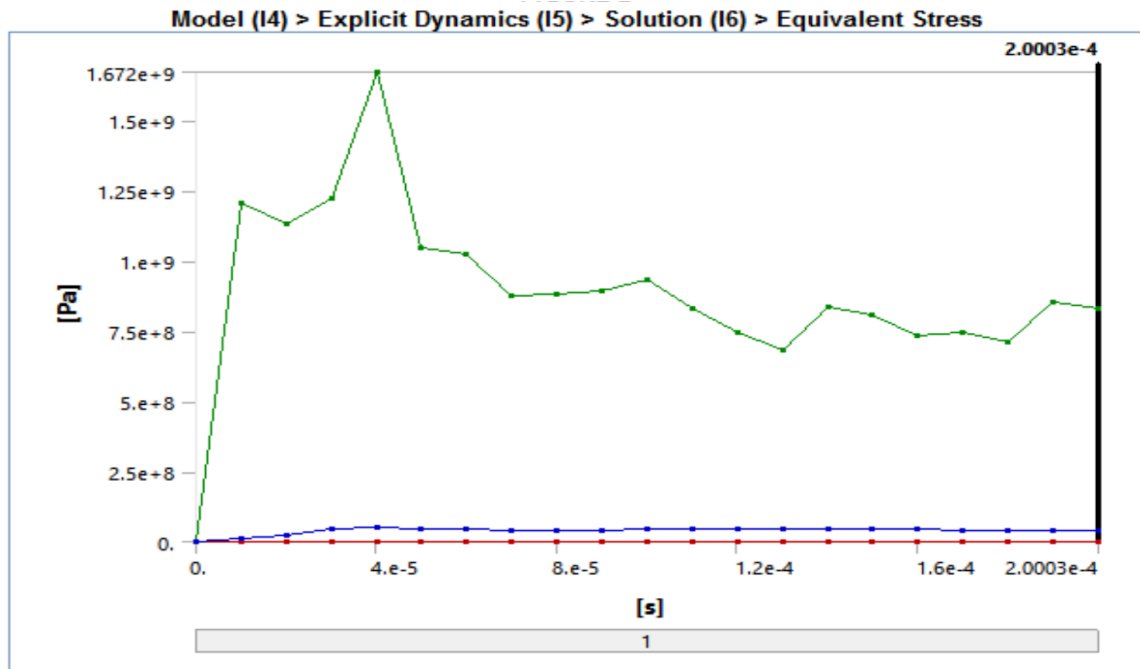


Figure 4.24 Equivalent stress in time graph

4.2.3 Shear Stress Results for 9 mm Bullet

The 9 mm bullet of type IIA armor showed a maximum shear stress of $4.6649e^{+8}$ Pa which is more than that of 7.62 mm bullet so it can be evaluated that the bullet with larger diameter has resulted greater maximum shear stress than the one with smaller diameter which was $2.9208e^{+8}$ Pa. Some stress is seen half way through from the side view approximately 22.5 mm from the top which is still considerably good because the Li-Ion layer lies at 30 mm from the top. Thus, no stress is detected in the bottom layer thus resulting in a successful experiment in terms of maximum equivalent stress also.

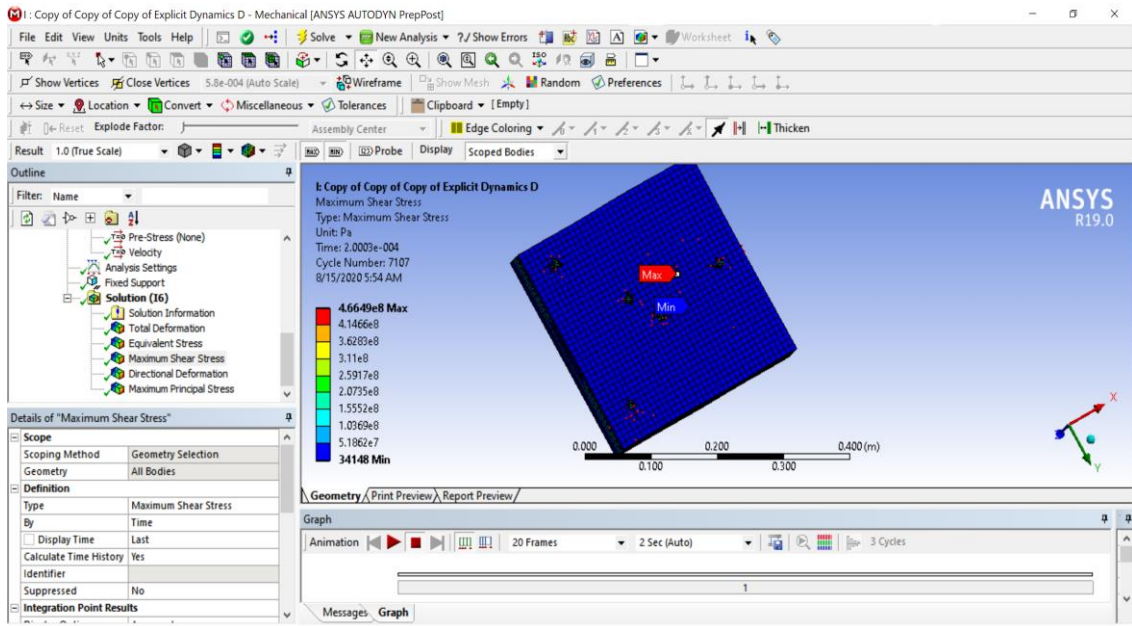


Figure 4.25 Maximum shear stress result front view associated with Type IIA armor conditions of 9 mm projectile

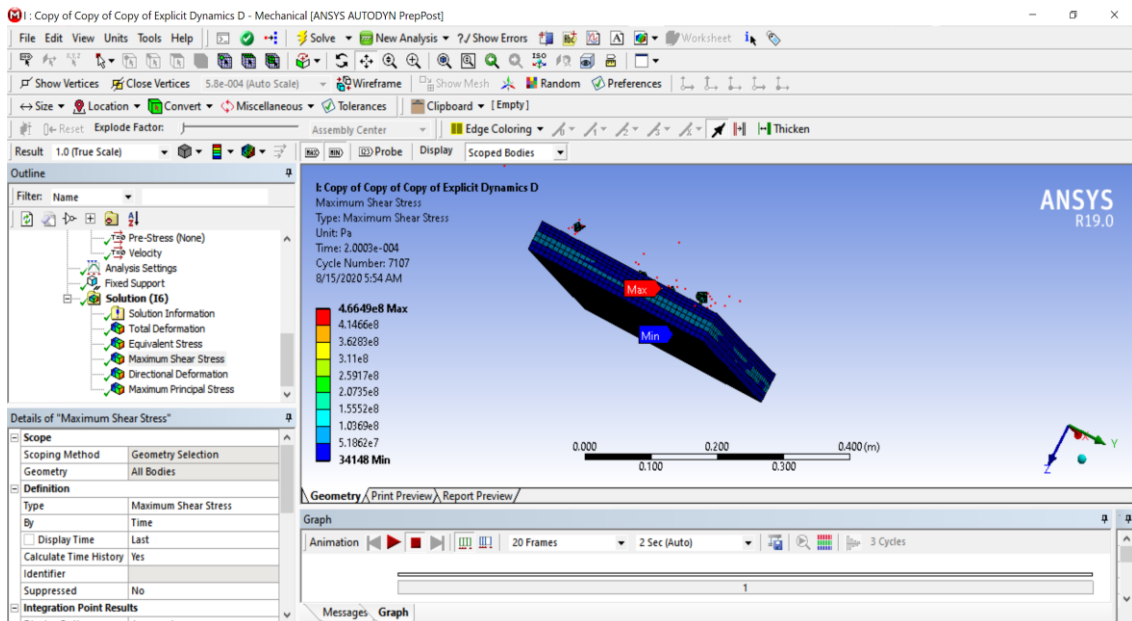


Figure 4.26 Maximum shear stress result side view associated with Type IIA armor conditions of 9 mm projectile

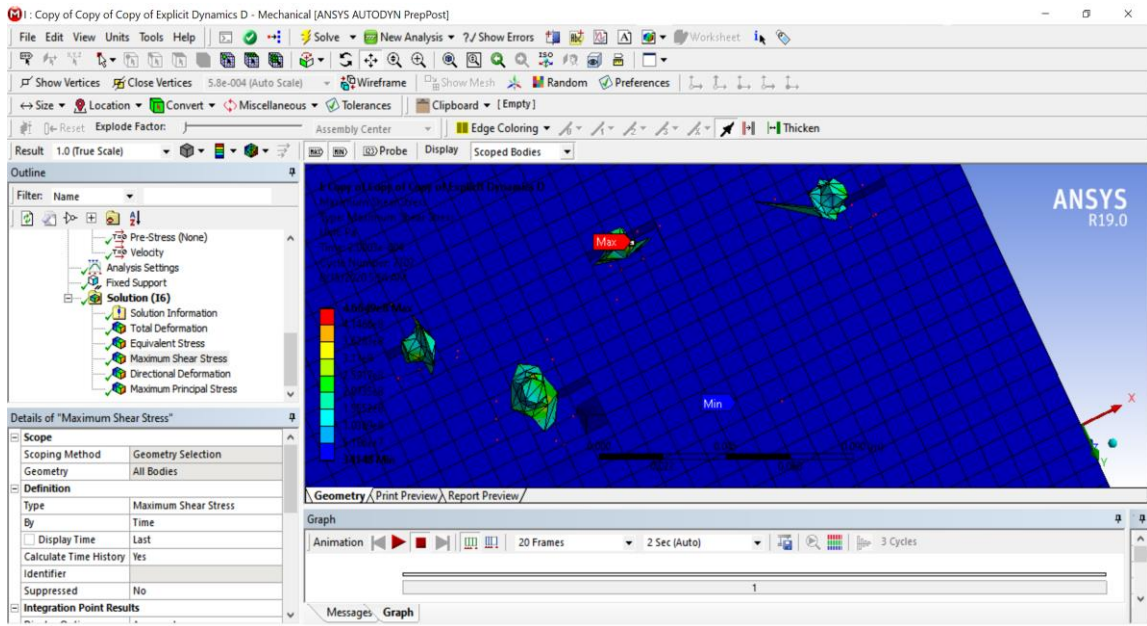


Figure 4.27 Maximum shear stress result top view associated with Type IIA armor conditions of 9 mm projectile

Consequently, as it could clearly be seen in the Ansys results; the bullets break halfway through the 2nd layer (epoxy resin) and no stress is seen at the point as the body stays blue where it penetrates the first layer on the multi-layered plate. Hence, exceptionally little or almost no stress effect could be seen or detected on the Li-Ion layer.

Moreover, Explicit Dynamics provides sufficient data that gives maximum shear values which could be identified more in detail related with time as provided below. Higher stress point may be noticed in the below Figure 4.28, however at the related time and point on layer (as seen on the ANSYS analysis visual), it is pointed out that the relevant stress value is as given. It is also provided at the last column of the below, Figure 4.28.

Model (I4) > Explicit Dynamics (I5) > Solution (I6) > Maximum Shear Stress

Time [s]	Minimum [Pa]	Maximum [Pa]	Average [Pa]
1.1755e-038		0.	0.
1.004e-005	0.	6.3177e+008	6.4797e+006
2.0028e-005	0.24281	6.2389e+008	1.1402e+007
3.0015e-005	170.34	6.8171e+008	2.3804e+007
4.0004e-005	1455.7	9.2103e+008	2.8488e+007
5.0003e-005	3747.2	5.9607e+008	2.6436e+007
6.0019e-005	8009.3	5.9033e+008	2.4801e+007
7.0013e-005	14019	4.9527e+008	2.3457e+007
8.0008e-005	22046	5.1034e+008	2.3219e+007
9.0006e-005	33114	4.8852e+008	2.358e+007
1.0002e-004	48348	5.0828e+008	2.4377e+007
1.1002e-004	27221	4.5313e+008	2.4308e+007
1.2001e-004	49016	4.2338e+008	2.5559e+007
1.3001e-004	39117	3.9079e+008	2.6251e+007
1.4e-004	62143	4.7583e+008	2.5918e+007
1.5002e-004	32181	4.6452e+008	2.4842e+007
1.6003e-004	40793	4.1036e+008	2.4151e+007
1.7e-004	46048	4.2016e+008	2.3509e+007
1.8001e-004	33908	4.0126e+008	2.2544e+007
1.9002e-004	58358	4.7728e+008	2.2143e+007
2.0003e-004	34148	4.6649e+008	2.2358e+007

Figure 4.28 Minimum, maximum and average stress values

In addition to that, for a clear comprehension, the graph below is plotted with the values shown, green line representing the maximum shear stress, red line representing minimum and blue line representing average shear stress.

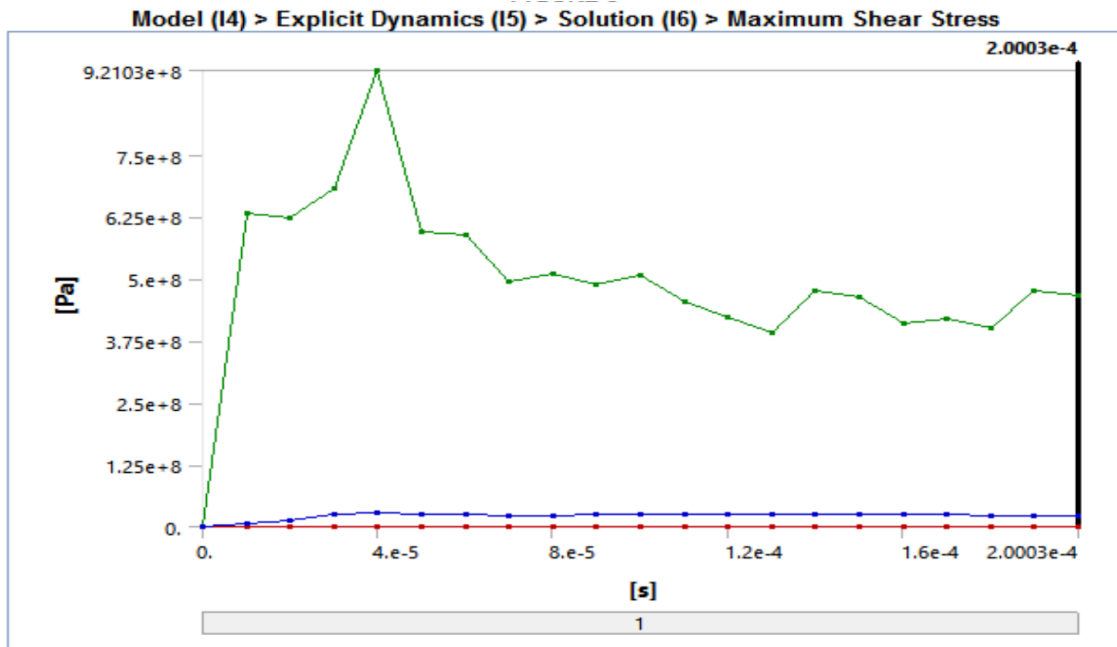


Figure 4.29 Maximum shear stress in time graph

4.2.4 Directional Deformation Results for 9 mm Bullet

The 9 mm bullet of type IIA armor showed a directional deformation of 0.017287 m which is less than that compared to a 7.62 mm bullet whose value was around 0.04716 m. So, it is seen that a bullet with greater diameter is less prone to directional deformation than a bullet which has smaller diameter. As seen from the Ansys results, the lower layer does face some deformation which is around 0.0056655 meters almost equivalent to 5,66 mm and greater than 7.62 mm bullet, however it still does not exceed the value thus the vest could be considered as safe for usage.

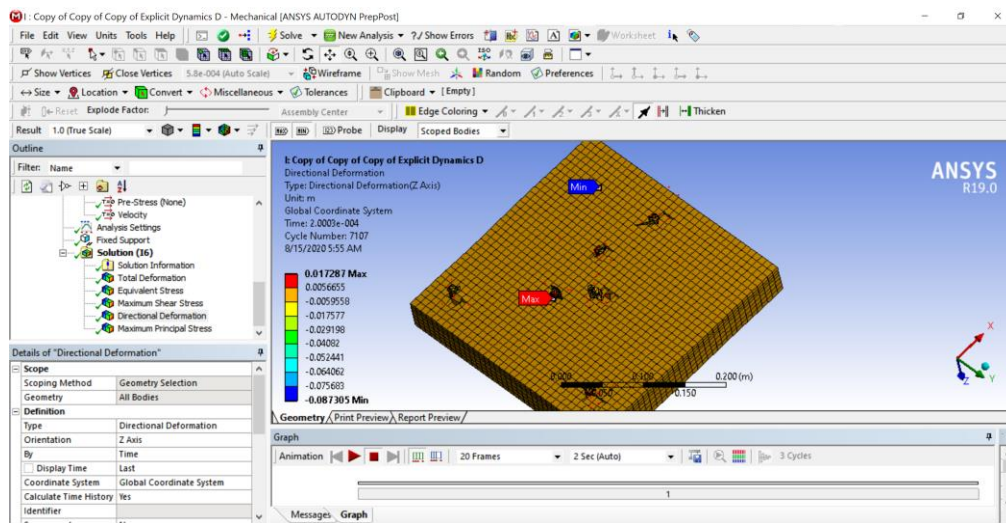


Figure 4.30 Directional deformation result front view associated with Type IIA armor conditions of 9 mm projectile

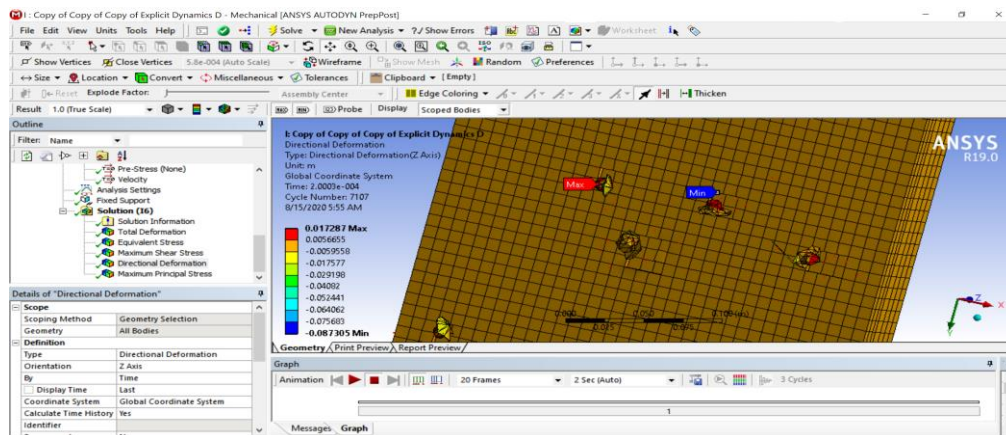


Figure 4.31 Directional deformation result top view associated with Type IIA armor conditions of 9 mm projectile

Consequently, and similarly, as it could clearly be seen in the Ansys results; the bullets break halfway through the 2nd layer (epoxy resin) and no directional deformation

is seen at the point as the body stays blue where it penetrates the first layer on the multi-layered plate. Hence, exceptionally little deformation effect could be seen or detected on the Li-Ion battery layer.

4.3 FEA Results for Type II Protocol

4.3.1 Total Deformation Results for 9 mm Bullet

The 9 mm bullet of type II armor showed a maximum total deformation of 0.017349 meters which is less than that compared to a 7.62 mm bullet but surprisingly equal to the 9mm type bullet for IIA protocol standards. However, there is a logical difference appears and it could be seen on the front surface when investigated. The only condition between type IIA and II is the difference that related with the velocity of the bullet. Type IIA uses 710 m/s velocity whereas type II uses 398 m/s velocity thus we can comprehend that no significant deformation could be seen on the surface of the bullet. Basically, the bullet barely penetrates the sheet. It is also seen that a bullet with greater diameter is less prone to deformation than a bullet which has smaller diameter in the case of 7.62 mm bullet. The speed of this bullet is 398 m/s but no deformation is detected and could be seen in the bottom layer or the sides thus resulting in a successful experiment in terms of total deformation.

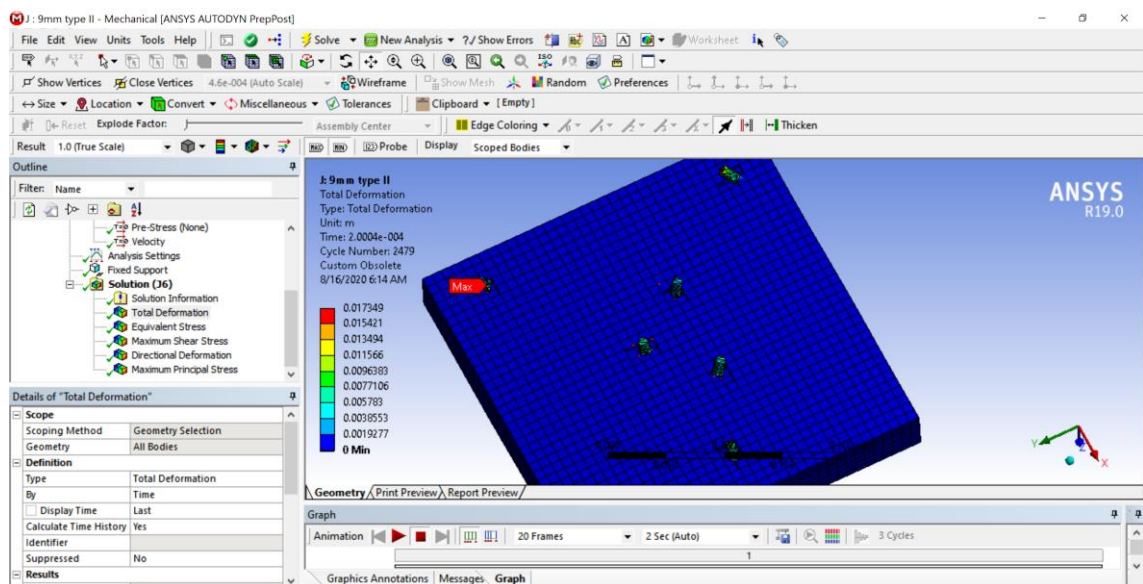


Figure 4.32 Total deformation result front view associated with Type II armor conditions of 9 mm projectile

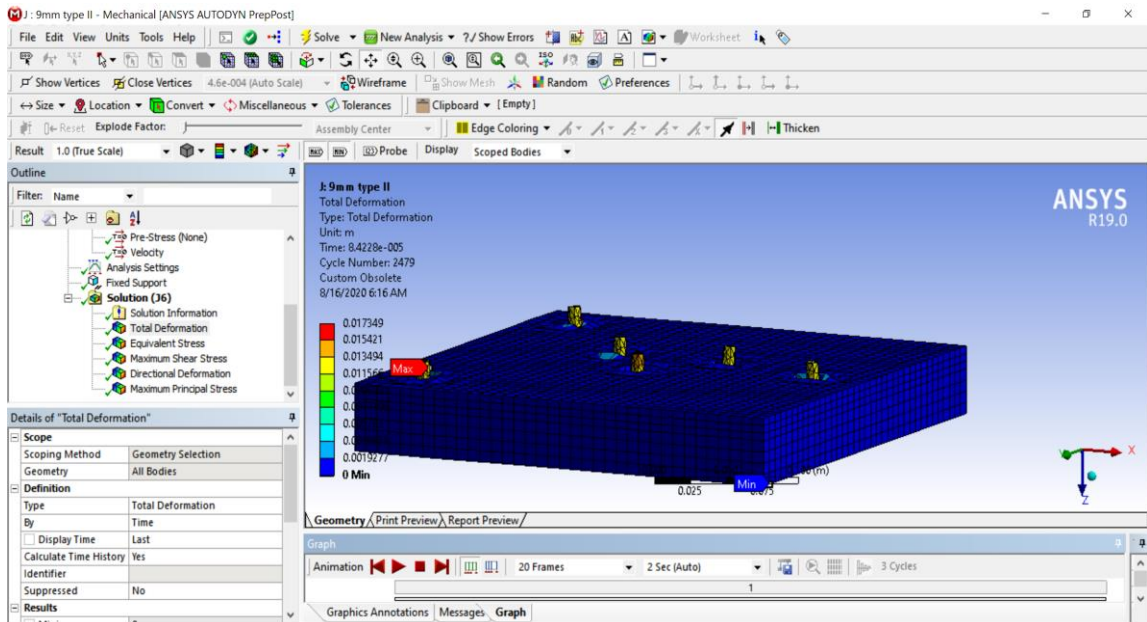


Figure 4.33 Total deformation result side view associated with Type II armor conditions of 9 mm projectile

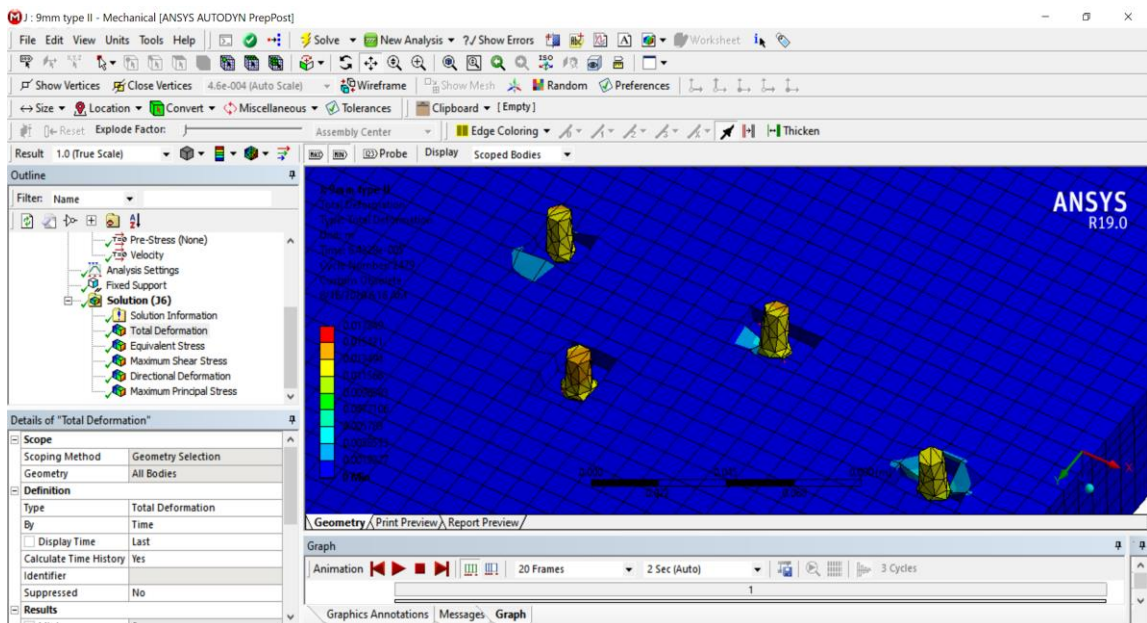


Figure 4.34 Total deformation result top view associated with Type II armor conditions of 9 mm projectile

Consequently, as it could clearly be seen in the Ansys results; the bullets penetrates/perforates few millimeters only through the SiC made front layer and Li-Ion layer still remains safe whereas the perforation depth is occurred around 5 mm.

Moreover, Explicit Dynamics provides sufficient data that gives total deformation values which could be identified more in detail related with time as provided below.

Model (J4) > Explicit Dynamics (J5) > Solution (J6) > Total Deformation

Time [s]	Minimum [m]	Maximum [m]	Average [m]
1.1755e-038		0.	0.
1.004e-005		3.9861e-003	6.3952e-005
2.0092e-005		7.7142e-003	1.2689e-004
3.0022e-005		1.0967e-002	1.8889e-004
4.0055e-005		1.3553e-002	2.4552e-004
5.0034e-005		1.5068e-002	2.9477e-004
6.0023e-005		1.5177e-002	3.3307e-004
7.0074e-005		1.468e-002	3.6352e-004
8.0048e-005		1.4172e-002	3.911e-004
9.0016e-005		1.364e-002	4.1918e-004
1.0008e-004	0.	1.3064e-002	4.4933e-004
1.1007e-004		1.3124e-002	4.7866e-004
1.2001e-004		1.2186e-002	5.06e-004
1.3002e-004		1.2505e-002	5.3086e-004
1.4004e-004		1.2953e-002	5.5286e-004
1.5006e-004		1.3608e-002	5.722e-004
1.6001e-004		1.4175e-002	5.8835e-004
1.7004e-004		1.5234e-002	6.0104e-004
1.8006e-004		1.6935e-002	6.1283e-004
1.9001e-004		1.8792e-002	6.2726e-004
2.0004e-004		2.0732e-002	6.476e-004

Figure 4.35 Minimum, maximum and average total deformation values

4.3.2 Equivalent Stress Results for 9 mm Bullet

The 9 mm bullet of type II armor showed a maximum equivalent stress of $7.9958e^{+8}$ Pa which is less than when compared with the results of 7.62 mm bullet whereas Type IIA vest result was around $8.3242e^{+8}$. Basically, in this case the bullet barely penetrates the sheet. It is also seen that a bullet with greater diameter is less prone to deformation than a bullet which has smaller diameter in the case of 7.62 mm bullet. The speed of this bullet is estimated as 398 m/s but no deformation is detected and seen in the bottom layer or on the sides, hence resulting in a successful experiment in terms of deformation.

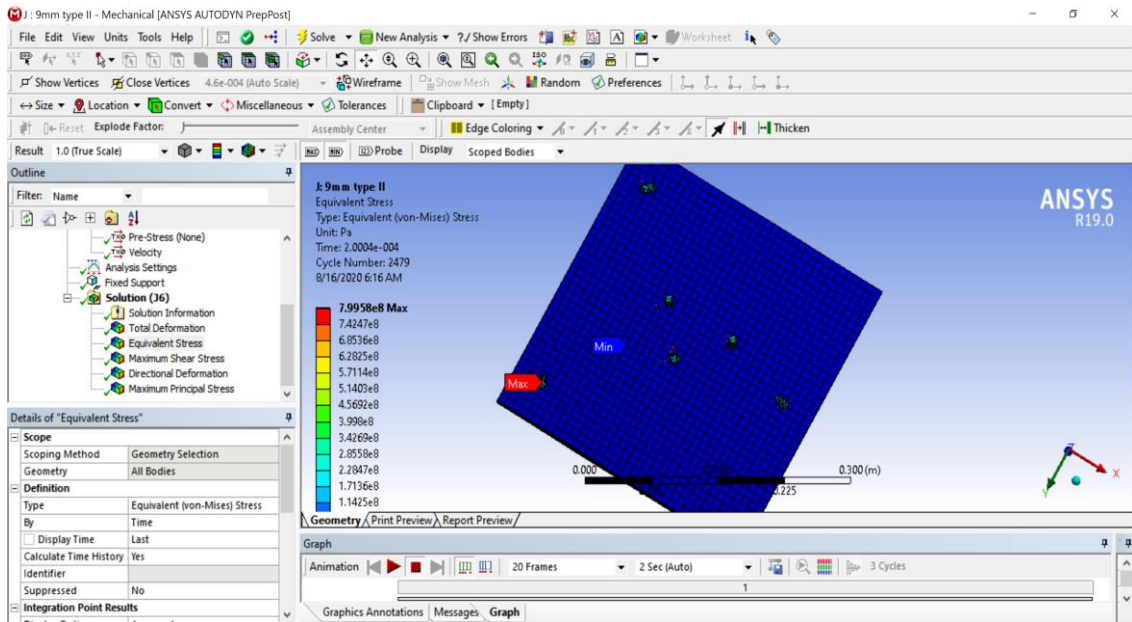


Figure 4.36 Equivalent stress result front view associated with Type II armor conditions of 9 mm projectile

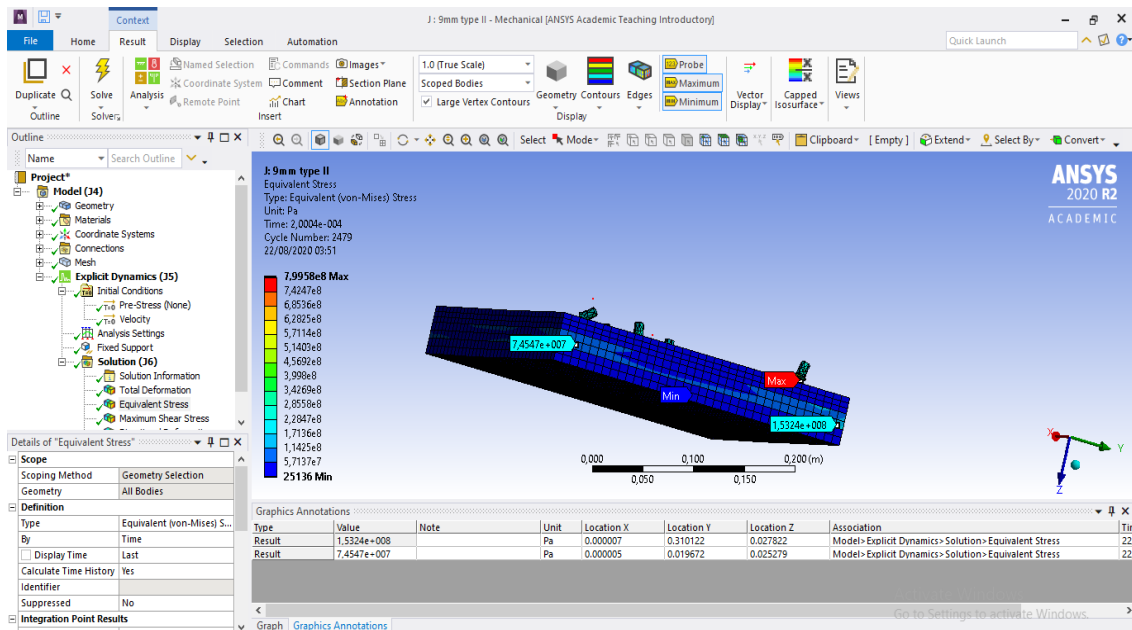


Figure 4.37 Equivalent stress result side view associated with Type II armor conditions of 9 mm projectile

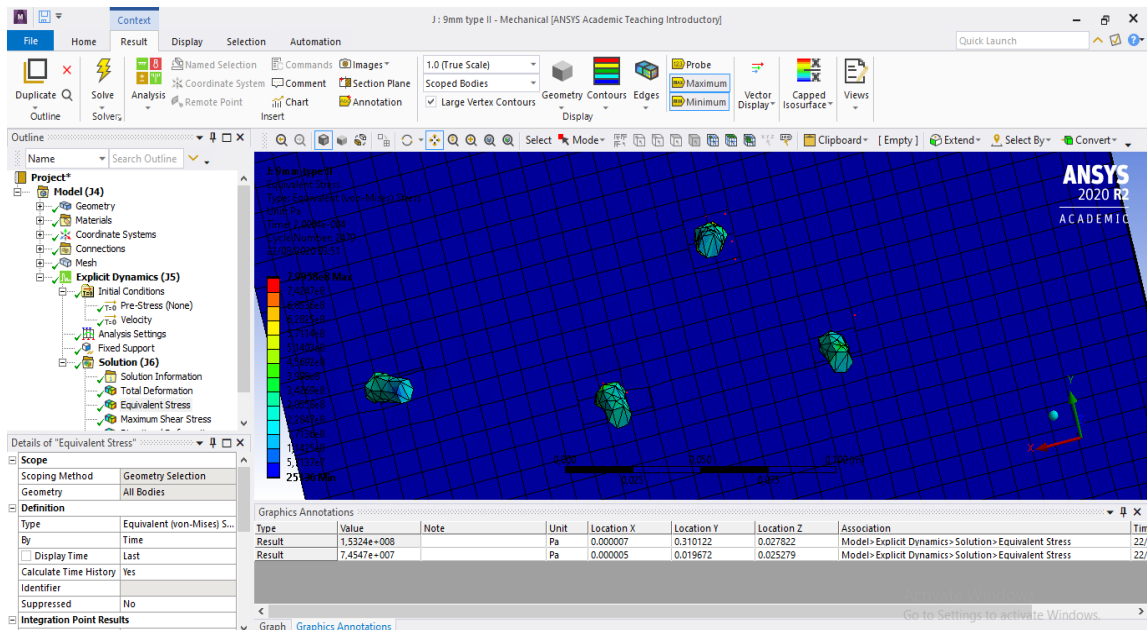


Figure 4.38 Equivalent stress result top view associated with Type II armor conditions of 9 mm projectile

Moreover, Explicit Dynamics provides sufficient data that gives equivalent stress value which could be identified more in detail related with time as provided below. Higher stress point may be noticed in the below Figure 4.39, however at the related time and point on layer (as seen on the ANSYS analysis visual), it is pointed out that the relevant stress value is as given. It is also provided at the last column of the Figure 4.39.

Model (J4) > Explicit Dynamics (J5) > Solution (J6) > Equivalent Stress

Time [s]	Minimum [Pa]	Maximum [Pa]	Average [Pa]
1.1755e-038		0.	0.
1.004e-005	0.	1.2008e+009	8.2647e+006
2.0092e-005		1.1548e+009	1.1956e+007
3.0022e-005	70.775	1.0775e+009	1.7861e+007
4.0055e-005	742.42	1.1711e+009	2.6151e+007
5.0034e-005	1598.1	1.1903e+009	2.9778e+007
6.0023e-005	3211.1	9.6804e+008	2.5484e+007
7.0074e-005	7648.7	9.6083e+008	2.4619e+007
8.0048e-005	17234	8.4308e+008	2.4532e+007
9.0016e-005	18467	1.0665e+009	2.4687e+007
1.0008e-004	33461	7.8281e+008	2.3996e+007
1.1007e-004	26756	8.9392e+008	2.5432e+007
1.2001e-004	26950	7.1132e+008	2.5341e+007
1.3002e-004	24924	7.7654e+008	2.5913e+007
1.4004e-004	22192	7.5484e+008	2.6568e+007
1.5006e-004	21512	7.328e+008	2.6648e+007
1.6001e-004	33742	7.3863e+008	2.6176e+007
1.7004e-004	33748	7.664e+008	2.5918e+007
1.8006e-004	49056	8.0238e+008	2.5366e+007
1.9001e-004	40352	7.2189e+008	2.4341e+007
2.0004e-004	25136	7.9958e+008	2.3901e+007

Figure 4.39 Minimum, maximum and average stress values

In addition, to be able to have a clear comprehension, the graph below is plotted with the values shown, whereas green line representing the equivalent stress, red line representing minimum and the blue line representing the average equivalent stress.

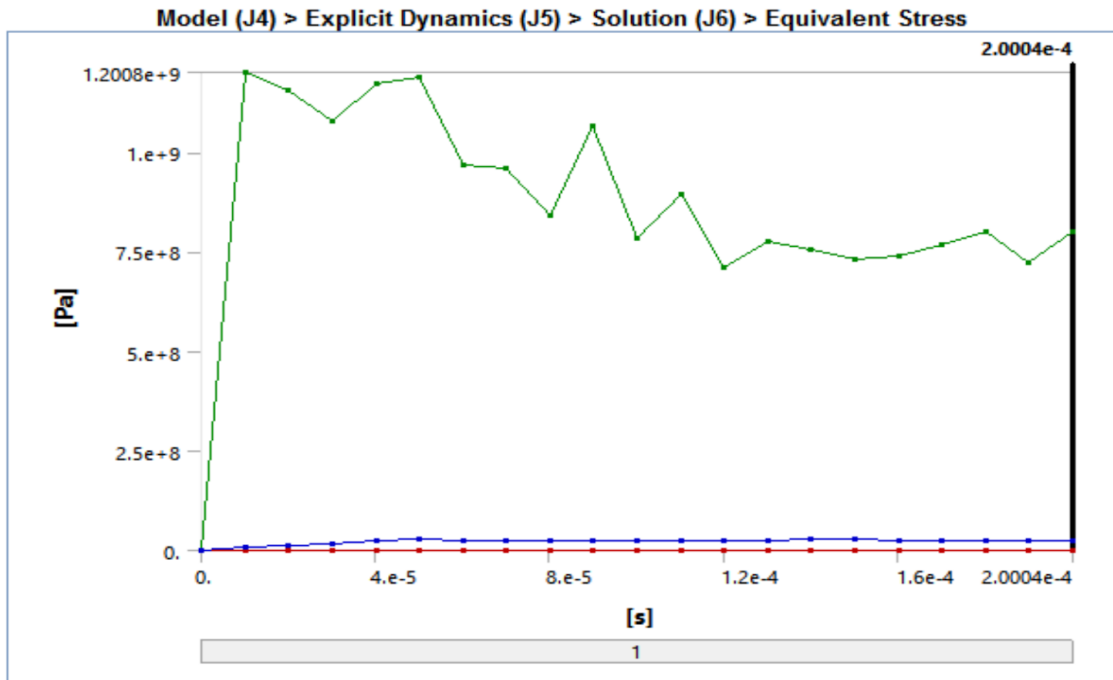


Figure 4.40 Equivalent stress variation in time graph

4.3.3 Shear Stress Results for 9 mm Bullet

The 9 mm bullet of type IIA armor showed a maximum shear stress of $4.6649e^{+8}$ Pa which is more than that of 7.62 mm bullet so it can be evaluated that the bullet with larger diameter has resulted greater maximum shear stress than the one with smaller diameter which was $2.9208e^{+8}$ Pa. Some stress is seen half way through from the side view *approximately 22.5 mm from the top* which is still considerably good because the *Li-Ion layer lies at 30 mm from the top*. Thus, no stress is detected in the bottom layer thus resulting in a successful experiment in terms of maximum equivalent stress also.

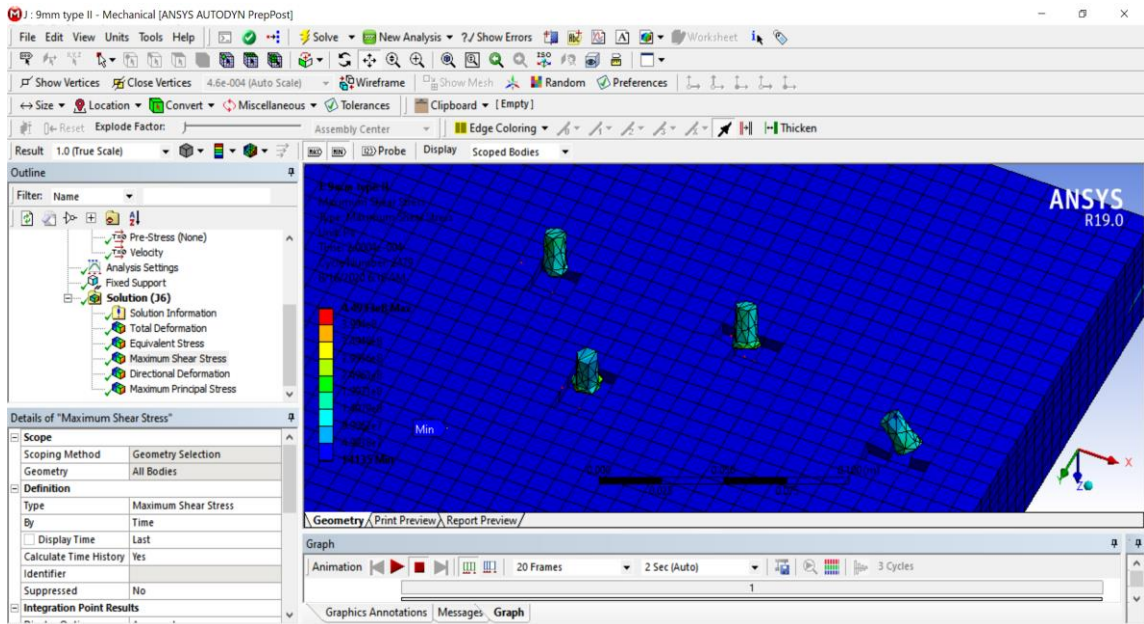


Figure 4.41 Maximum shear stress result top view associated with Type II armor conditions of 9 mm projectile

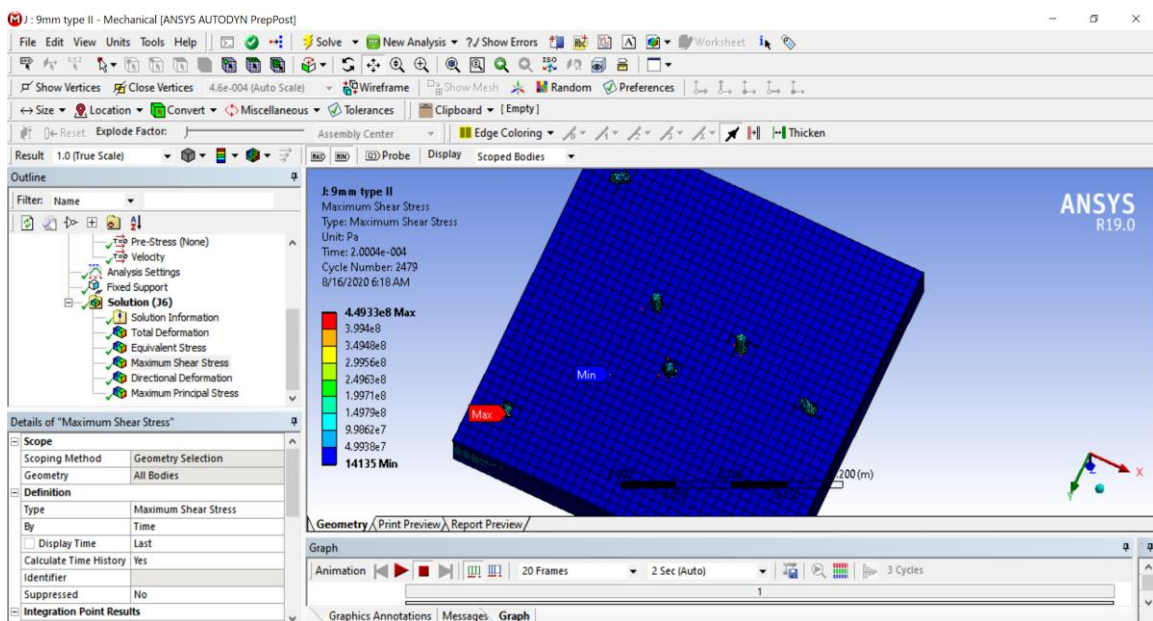


Figure 4.42 Maximum shear stress result front view associated with Type II armor conditions of 9 mm projectile

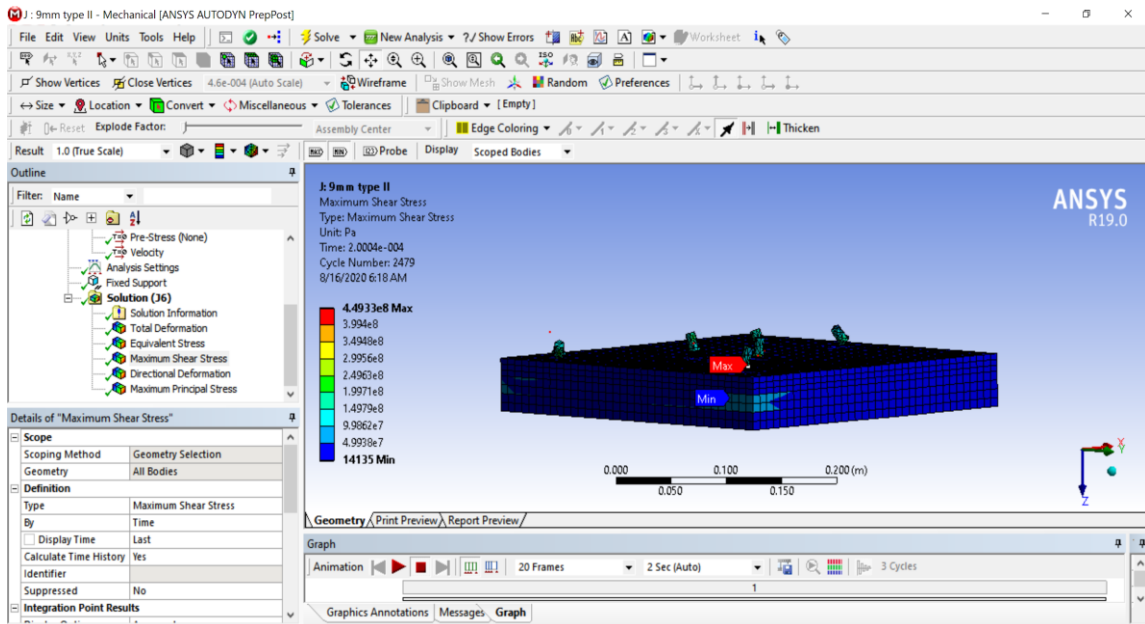


Figure 4.43 Maximum shear stress result side view associated with Type II armor conditions of 9 mm projectile

Consequently, as it could clearly be seen in the Ansys results; not any trace caused by stress is detected on the bottom layer. As seen in the Ansys results, the bullets penetrate few millimeters only through the first layer (SiC) so the penetration depth is within 5 mm and the Li-Ion layer remains in the safe zone.

Moreover, Explicit Dynamics provides sufficient information that gives maximum shear values which could be identified more in detail related with time as provided below. Higher shear stress point may be noticed in the Figure 4.44, however at the related time and point on layer (as seen on the ANSYS analysis visual), it is pointed out that the relevant shear stress value is as given. It is also provided at the last column of the below, Figure 4.44.

Model (J4) > Explicit Dynamics (J5) > Solution (J6) > Maximum Shear Stress

Time [s]	Minimum [Pa]	Maximum [Pa]	Average [Pa]
1.1755e-038		0.	0.
1.004e-005	0.	6.7905e+008	4.4213e+006
2.0092e-005		6.4677e+008	6.4474e+006
3.0022e-005	39.84	6.004e+008	9.7647e+006
4.0055e-005	403.94	6.3367e+008	1.4228e+007
5.0034e-005	917.85	6.3895e+008	1.6354e+007
6.0023e-005	1795.3	4.9079e+008	1.4186e+007
7.0074e-005	4407.4	5.1268e+008	1.3727e+007
8.0048e-005	9750.7	4.7892e+008	1.372e+007
9.0016e-005	10594	5.5424e+008	1.3768e+007
1.0008e-004	17120	4.3644e+008	1.3371e+007
1.1007e-004	14840	4.9374e+008	1.4199e+007
1.2001e-004	15267	4.1008e+008	1.4145e+007
1.3002e-004	14034	4.4499e+008	1.447e+007
1.4004e-004	12389	4.2464e+008	1.4864e+007
1.5006e-004	11749	3.926e+008	1.4944e+007
1.6001e-004	19153	4.2113e+008	1.4644e+007
1.7004e-004	17768	4.4097e+008	1.4503e+007
1.8006e-004	27132	4.5997e+008	1.4188e+007
1.9001e-004	22326	4.1261e+008	1.3618e+007
2.0004e-004	14135	4.4933e+008	1.3292e+007

Figure 4.44 Minimum, maximum and average stress values

In addition to that, for a clear comprehension, the graph below is plotted with the values shown, green line representing the maximum shear stress, red line representing minimum and blue line representing average shear stress.

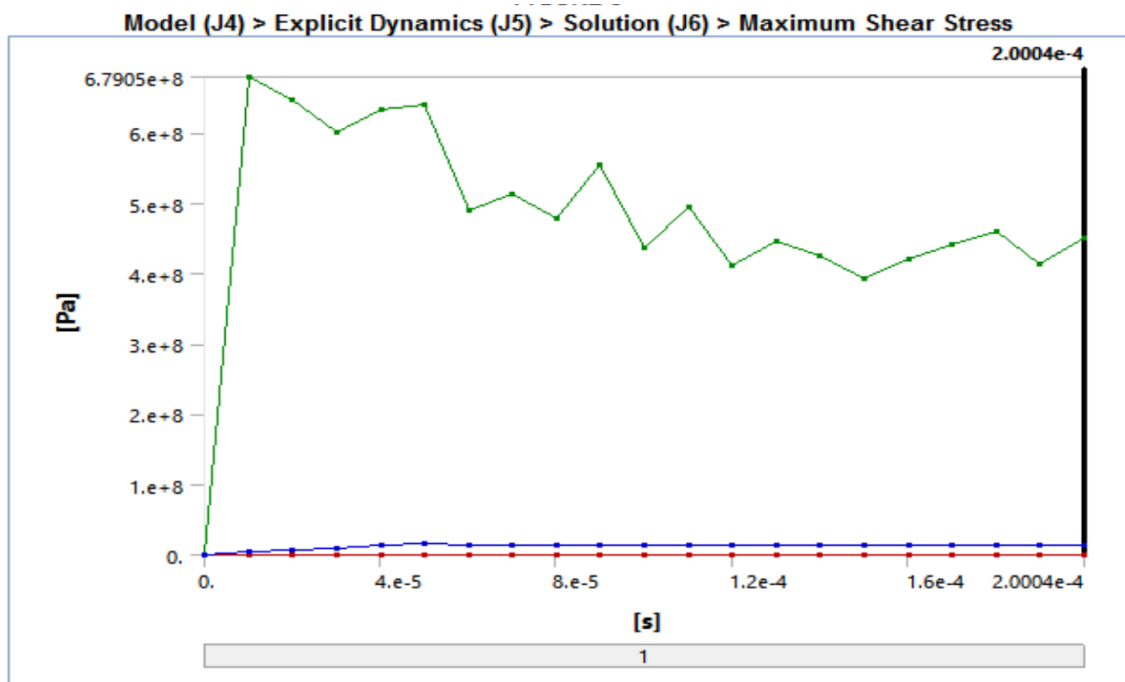


Figure 4.45 Maximum shear stress in time graph

4.3.4 Directional Deformation Results for 9 mm Bullet

The 9 mm bullet of type II armor showed a directional deformation of 0.015738 m which is less than that compared to a 7.62 mm and 9 mm bullet of type IIA vest whose value were around 0.04716 m and 0.017287 m, respectively. Thus, it is noticed that a bullet with greater diameter is less prone to directional deformation than a bullet which has smaller diameter. As seen from the Figure 4.46 below, the lower layer does face some deformation which is around 0.0057542 meters almost equivalent to 5,754 mm, however it still does not exceed the value thus the vest could be considered as safe for usage. Front layer made out of SiC penetration depth is within 5 mm and Li-Ion layer remains in the safe zone, as well as standing within the maximum NIJ 44 mm total perforation limits.

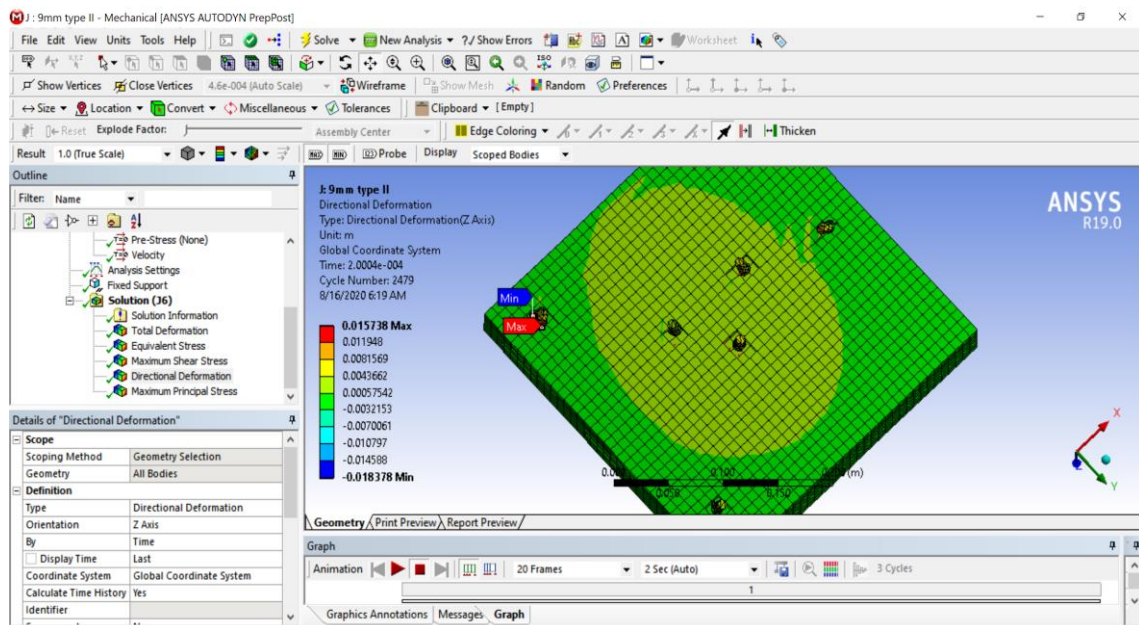


Figure 4.46 Directional deformation result front view associated with Type II armor conditions of 9 mm projectile

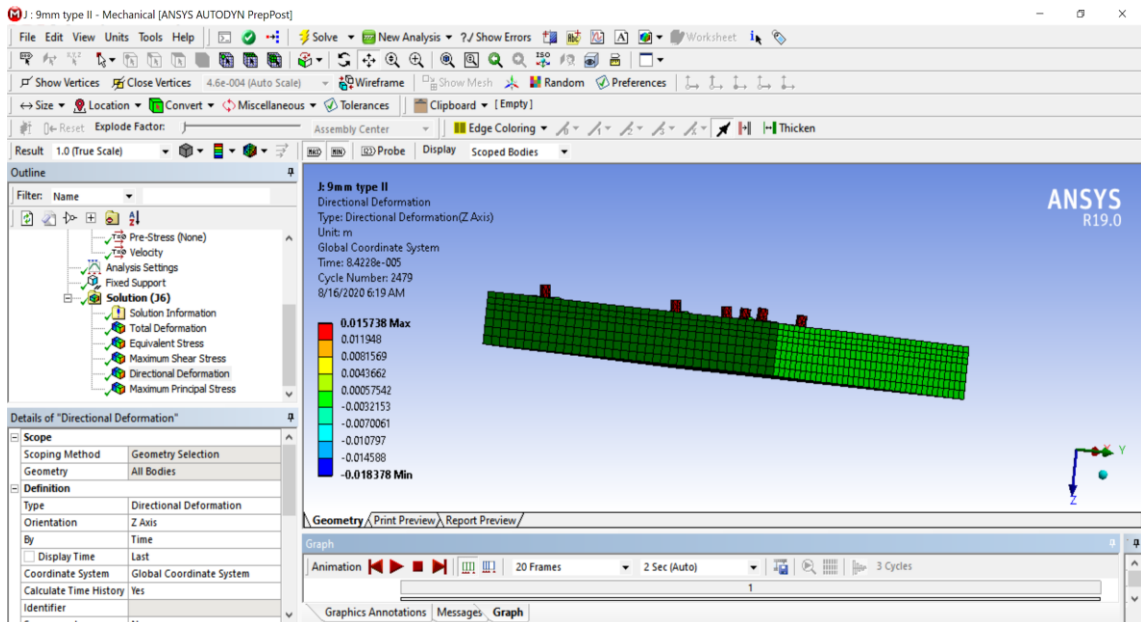


Figure 4.47 Directional deformation result side view associated with Type II armor conditions of 9 mm projectile

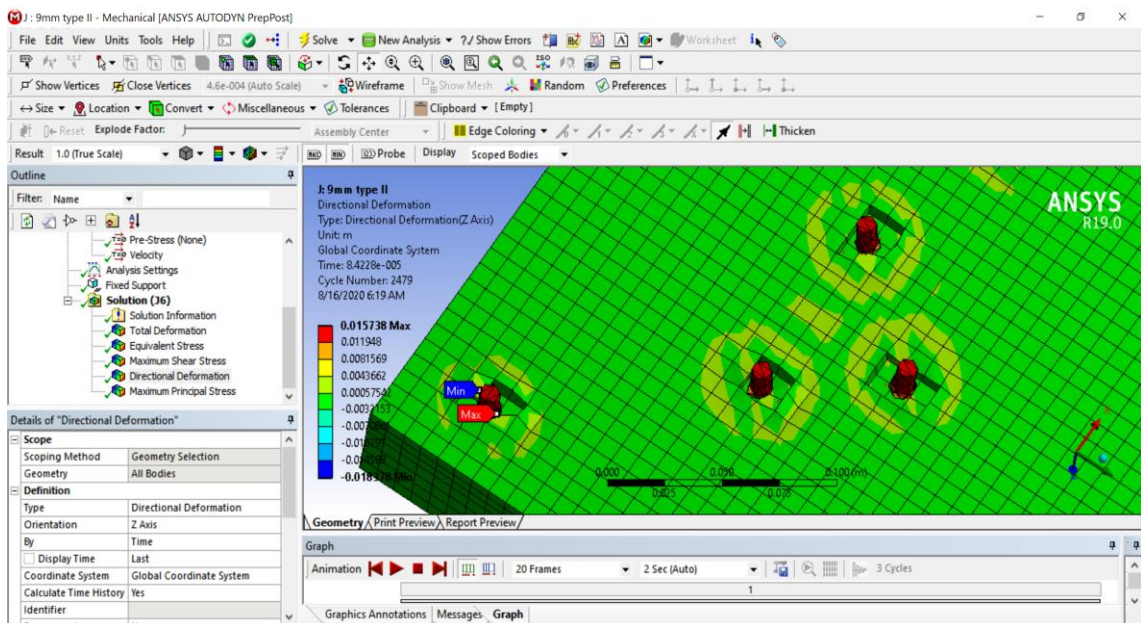


Figure 4.48 Directional deformation result top view associated with Type II armor conditions of 9 mm projectile

Moreover, Explicit Dynamics provides broad data that gives maximum directional deformation which could be identified more in detail related with time as provided below, in Figure 4.49.

Model (J4) > Explicit Dynamics (J5) > Solution (J6) > Directional Deformation

Time [s]	Minimum [m]	Maximum [m]	Average [m]
1.1755e-038	0.	0.	0.
1.004e-005	-4.0957e-006	3.9861e-003	6.3816e-005
2.0092e-005	-1.5594e-004	7.7142e-003	1.2482e-004
3.0022e-005	-7.9812e-004	1.0967e-002	1.8106e-004
4.0055e-005	-1.6866e-003	1.3552e-002	2.2976e-004
5.0034e-005	-2.2525e-003	1.5065e-002	2.7026e-004
6.0023e-005	-2.7927e-003	1.5172e-002	3.0352e-004
7.0074e-005	-2.9401e-003	1.4662e-002	3.2967e-004
8.0048e-005	-2.7722e-003	1.4146e-002	3.5181e-004
9.0016e-005	-2.3306e-003	1.3607e-002	3.7238e-004
1.0008e-004	-1.8371e-003	1.303e-002	3.9316e-004
1.1007e-004	-2.0966e-003	1.245e-002	4.1388e-004
1.2001e-004	-2.9635e-003	1.2159e-002	4.3438e-004
1.3002e-004	-4.8928e-003	1.2396e-002	4.5422e-004
1.4004e-004	-6.8225e-003	1.2775e-002	4.7358e-004
1.5006e-004	-8.7526e-003	1.3177e-002	4.9204e-004
1.6001e-004	-1.0668e-002	1.3633e-002	5.0889e-004
1.7004e-004	-1.2599e-002	1.4129e-002	5.2409e-004
1.8006e-004	-1.453e-002	1.4644e-002	5.3969e-004
1.9001e-004	-1.6447e-002	1.5185e-002	5.5711e-004
2.0004e-004	-1.8378e-002	1.5738e-002	5.7629e-004

Figure 4. 49 Minimum, maximum and average directional deformation values

In addition to that, for a clear comprehension, the graph below is plotted with the values shown, green line representing the directional deformation, red line representing minimum and blue line representing average deformation.

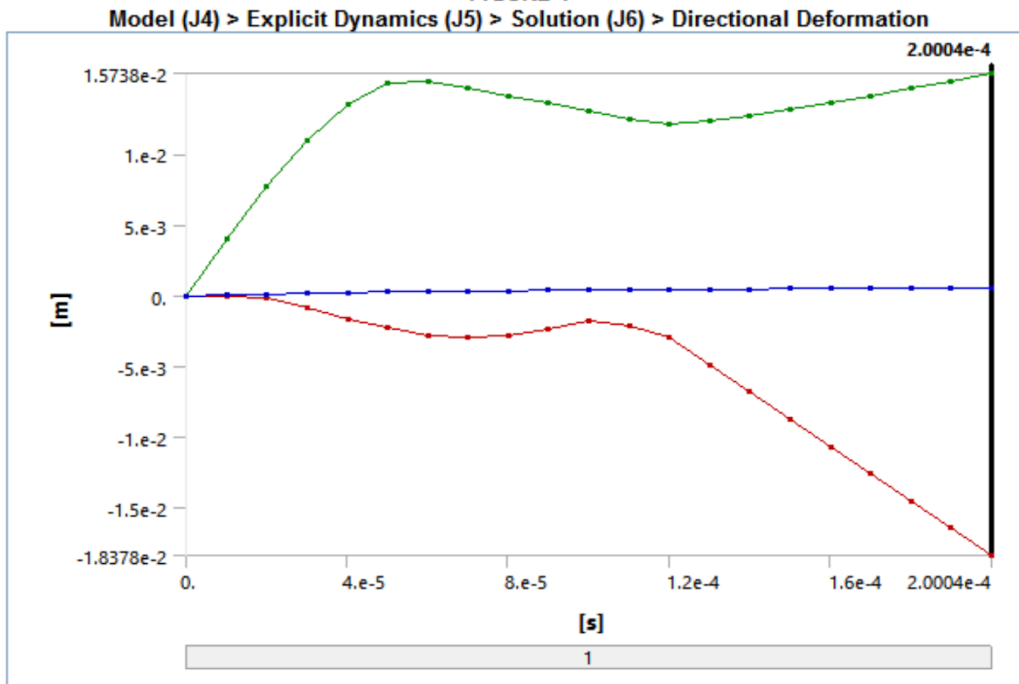


Figure 4.50 Directional deformation variation in time graph

4.4 Ballistic Limit

4.4.1 Fundamental Approach

Ballistic impact is defined and occur usually as a low-mass (projectile/bullet type) but high-velocity impact caused by a propelling source such as a gun-fire [41]. Ballistic Limit (BL) on the other hand, can be defined as is the maximum possible velocity of a bullet at which the complete perforation occurs with precisely zero exit [12] [41] [52] [55]. Two basic methods applied in the literature were used to obtain Ballistic Limit Velocity (BLV) [12] [41] [52] [55]. In the first method, the main criteria is the velocity period history and the latter one is focused on the MIL-STD-662E standard. In the method of history of velocity time, the BLV is determined by the maximum velocity of impact at which a bullet may fully stop. BLV is classified in the second process by finding the average impact speed with three provisional penetration rates and three full penetrations within 38 m/s speed range. To find the ballistic limit of the structures, as to provide a good example, different velocities are applied and solved according to the study by Periyasamy, Sundaresan and Uthirapathy [56]. Simply, the ballistic limit is observed when there is no penetration of any bullet by the projectile.

4.4.2 Ballistic Limit of Bullets under NIJ Protocols

4.4.2.1 Ballistic Limit of 9 mm for Type II

Various velocities are implemented on the projectile and it has been found at a range of velocities of 90-200 m/s. The projectile does not perforate the surface and therefore does not create any kind of hole or significant damage on the surface. Therefore, it was tested that the composite structure's ballistic maximum velocity is safe as up to 90 m/s. It is shown in the following Figure 4.51, below.

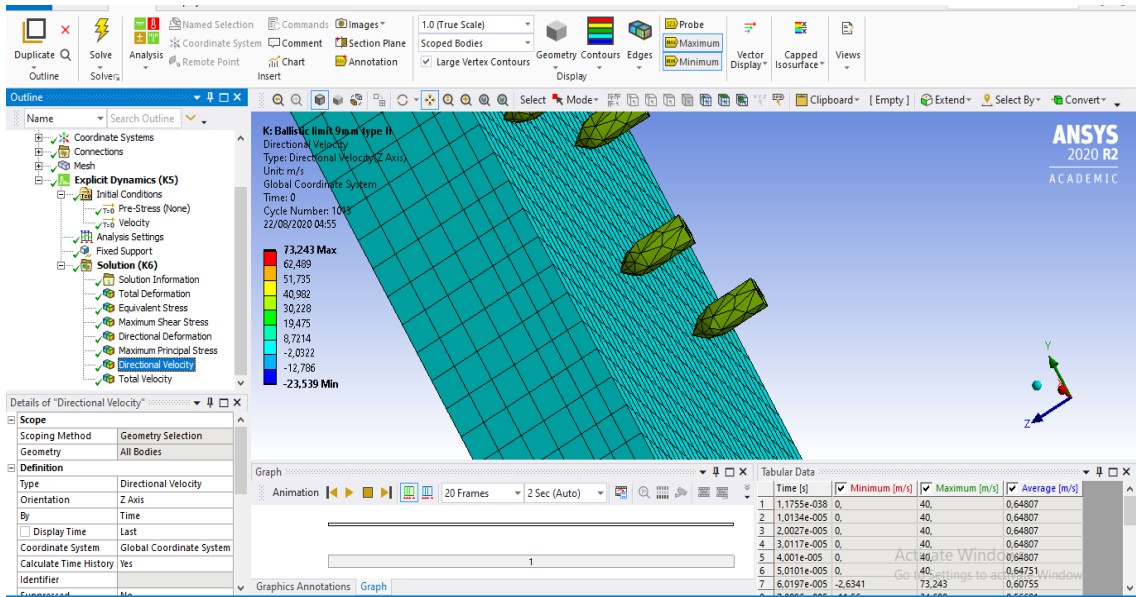


Figure 4.51 FEA directional velocity result for Type II

4.4.2.2 Ballistic Limit of 9 mm for Type IIA

Various velocities are implemented on the projectile and it has been found at a range of velocities of 100-400 m/s. The projectile does not perforate the surface and therefore does not create any kind of hole or significant damage on the surface. Therefore, it was tested that the composite structure's ballistic maximum velocity is safe as up to 100 m/s which is shown in the following Figure 4.52. This value is close to the one obtained for Type II armor because the structure of the composite and the layers remain almost the same.

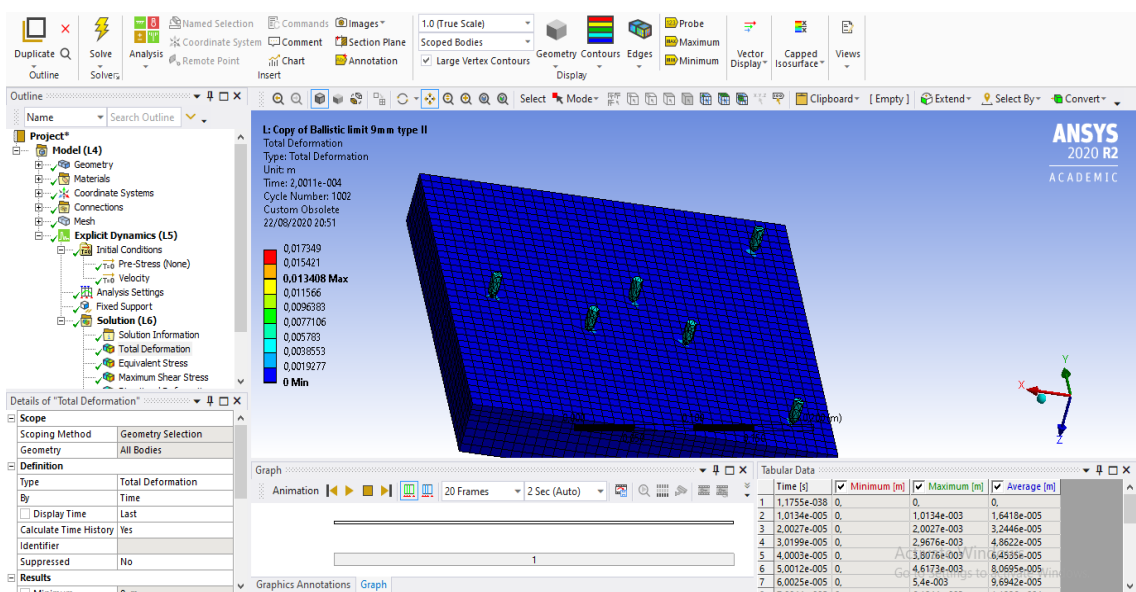


Figure 4.52 FEA directional velocity result for Type IIA

4.4.2.3 Ballistic Limit of 9 mm for Type III

Various velocities are implemented on the projectile and it has been found at a range of velocities of 65-300 m/s. The projectile does not perforate the surface and therefore does not create any kind of hole or significant damage on the surface. Therefore, it was tested that the composite structure's ballistic maximum velocity is safe as up to 65 m/s which is shown in the following Figure 4.53.

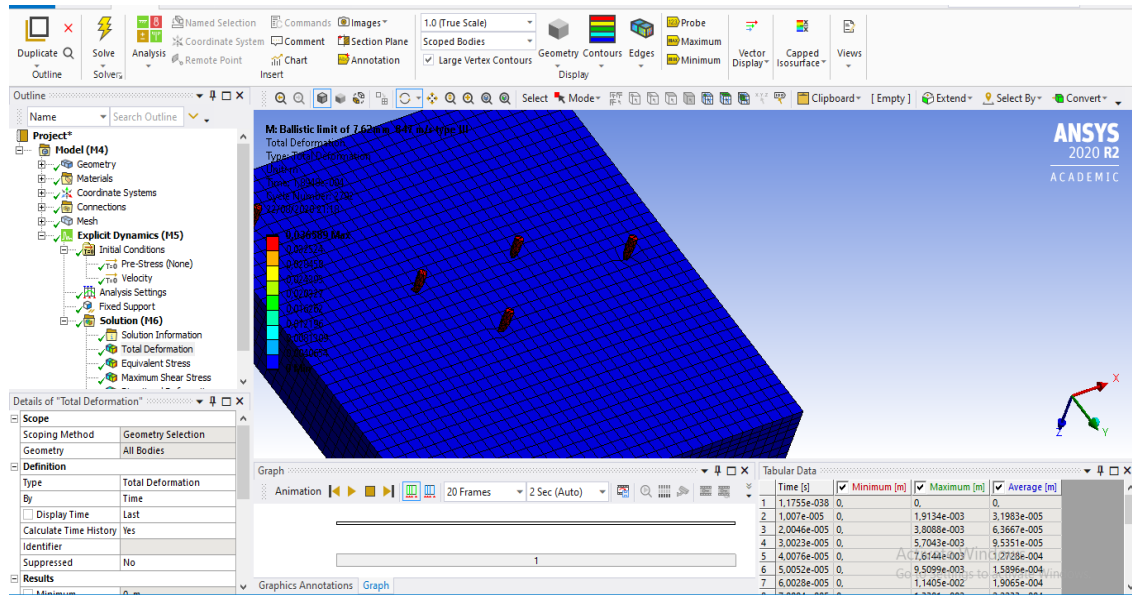


Figure 4.53 FEA directional velocity result for Type III

4.5 Meshing Paradigm

4.5.1 Meshing Determination

Determining the proper meshing style has always been a paradigm, especially in FEA based studies. To be able to determine the proper meshing of the sheets, in this thesis, referenced studies are taken into account [10] [43] [56]. Hence, it was needed to be confirmed that the assumptions of finer meshed part would not create significant deformational difference when compared to coarsely meshed part. To validate the statement and substantiate the matter; on the multilayered structure the meshing type was changed from coarse mesh to a finer mesh to analyze the potential change in deformation value. The aim for this was to make sure whether the change in deformation stays within the range of 5% or not, as it was stated in the theory and referenced in this thesis [10].

Firstly, the face mesh size was changed and decreased from 0.009 m to as low as 0.0007 m, as it could be seen below. This is a finer mesh as each element will thoroughly be covered while running the analysis.



Figure 4.54 Finer mesh front view of the multilayered panel

At first, it was thought to run the analysis with finer mesh on only a single bullet analysis with one sheet but that result would have been incorrect in this regard as our analysis incorporates more than 1 (one) bullet, so it was found to be necessary to check the results with all the bullets and all the sheets with each contact thoroughly be placed. Thus, the analysis was carried out with all the bullets of the same size in this case 7.62 mm with a speed of 847 m/s and the type III bullet.

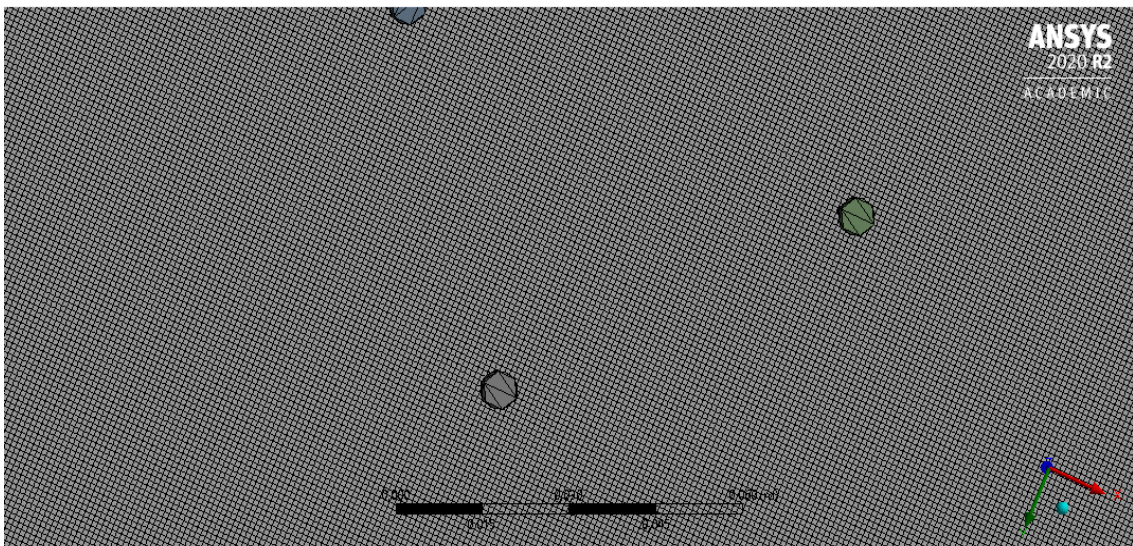


Figure 4.55 Finely meshed panel top view that is fairly hit

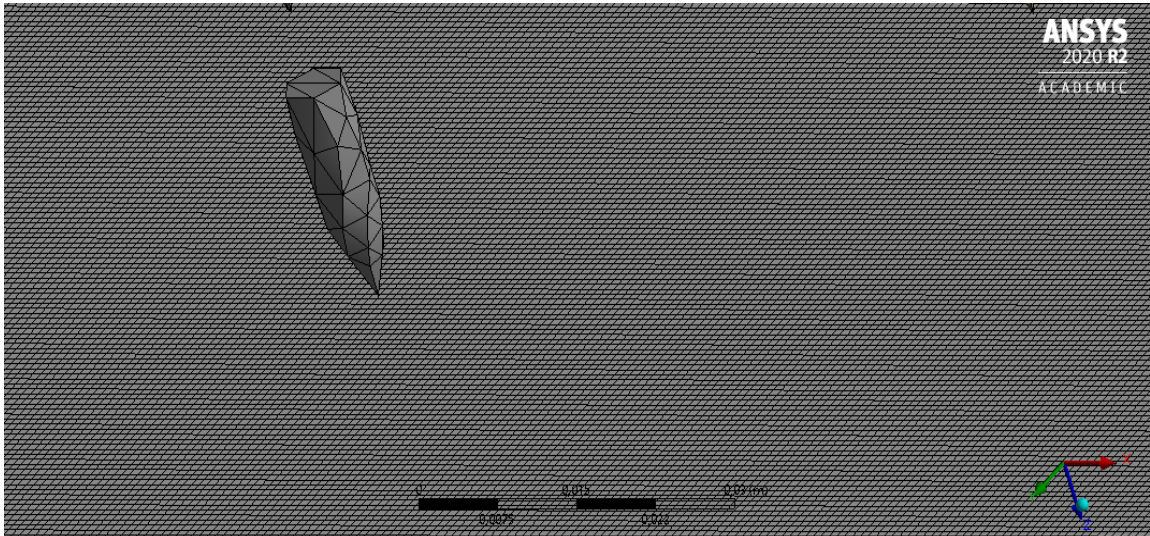


Figure 4.56 The Type III bullet of 7.62 mm with a speed of 847 m/s hitting the multilayered plate visual

The results were run on various tests but the total deformation determination was thought to be the decisive factor, hence it is provided and could be seen below.

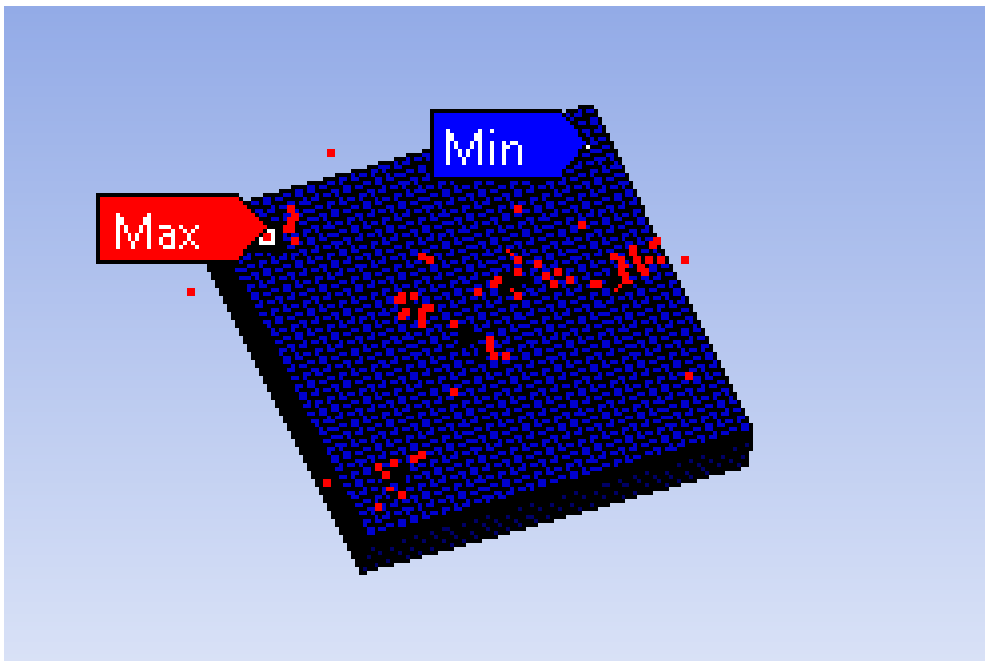


Figure 4.57 The Type III bullet of 7.62 mm with a speed of 847 m/s hitting the multilayered plate visual

Now let's do a comparison of results we obtained previously and of the new analysis with a much finer mesh.

4.5.2 Direct Effects of Meshing on Deformation

Coarse Mesh Results				Fine Mesh Results			
TABLE 21 Model (G4) > Explicit Dynamics (G5) > Solution (G6) > Total Deformation				TABLE 21 Model (G4) > Explicit Dynamics (G5) > Solution (G6) > Total Deformation			
Time [s]	Minimum [m]	Maximum [m]	Average [m]	Time [s]	Minimum [m]	Maximum [m]	Average [m]
1,1755e-038	0,	0,	0,	1,1755e-038	0,	0,	0,
1,007e-005		8,5295e-003	1,4258e-004	1,007e-005		9,1886e-003	1,4979e-004
2,0046e-005		1,6979e-002	2,8382e-004	2,0046e-005		2,8099e-002	2,9322e-004
3,0023e-005		2,5429e-002	4,2506e-004	3,0023e-005		2,8099e-002	4,2996e-004
4,0036e-005		3,3946e-002	5,6447e-004	4,0036e-005		3,6192e-002	5,9427e-004
5,002e-005		4,2056e-002	6,8458e-004	5,002e-005		4,4251e-002	6,9499e-004
6,0003e-005		4,882e-002	7,7995e-004	6,0003e-005		5,2861e-002	7,9895e-004
7,0022e-005		5,2729e-002	8,3999e-004	7,0022e-005		5,2999e-002	8,4814e-004
8,0011e-005		5,3399e-002	8,7264e-004	8,0011e-005		5,3957e-002	8,7879e-004
9,0009e-005		5,2861e-002	8,9293e-004	9,0009e-005		5,9264e-002	9,0793e-004
1,0001e-004	0,	5,8715e-002	9,0406e-004	1,0001e-004	0,	6,6879e-002	9,0826e-004
1,1e-004		6,6192e-002	9,1405e-004	1,1e-004		6,9922e-002	9,2004e-004
1,2004e-004		7,3959e-002	9,2821e-004	1,2004e-004		7,4259e-002	9,2821e-004
1,3004e-004		8,1886e-002	9,4814e-004	1,3004e-004		8,4814e-002	9,3479e-004
1,4003e-004		8,9938e-002	9,6879e-004	1,4003e-004		8,8302e-002	9,7981e-004
1,5003e-004		9,8099e-002	9,8302e-004	1,5003e-004		9,9293e-002	9,8792e-004
1,6002e-004		0,10633	9,928e-004	1,6002e-004		0,10793	9,988e-004
1,7002e-004		0,1139	1,0026e-003	1,7002e-004		0,1105	1,0028e-003
1,8002e-004		0,11585	1,0135e-003	1,8002e-004		0,11782	1,0185e-003
1,9001e-004		0,11604	1,0216e-003	1,9001e-004		0,11881	1,0230e-003
2,0003e-004		0,11661	1,0253e-003	2,0003e-004		0,11978	1,0281e-003

Figure 4.58 Comparison on total deformation value between coarse mesh and fine mesh.

As it can be seen in the comparison of the results above, the values of deformation have increased to some extent but these values are surely stays within the 5 % range which proves that whether meshing is applied coarse or fine, effective results on deformation has not changed at significant levels [10].

The reason of coarse mesh size was used for all previously run analysis for the sake of avoiding excessive analysis times and to run all the tests efficiently. It is widely known and also made sure by this final analysis that using finer size meshing increases the run time of the analysis significantly. This specific analysis took more than 15 hours to be completed including meshing and running stages of software.

In addition, to validate our results on the reliability of directional deformation in Z direction results, the study has been made in 2018 by Soydan et al. can be provided [11]. Even though the standards (EN 1063 vs NIJ), protocols - bullet types and materials used in between these two studies are different, assumptions and final results are found to be similar on directional deformation values. Especially mesh modeler with size multizone method and hex tetra element for the jacket and hex element for the core all with medium relevance center, element size and the coarse span angle shows the meshing methodology

similarity and the relevant approach [10] [11]. Moreover, the directional deformation results found by Soydan et al in the same study was found to be very attractive for validation to our study for 9 mm bullet, whereas their materials properties and their thicknesses were different compared to our study [11]. To compare and contrast, our study showed a directional deformation result in between 0.015738 meters to 0.017287 meters, their study resulted in 0.00013921 meters being minimum to 0.0029322 meters whereas the end time of analysis was 0.0007 seconds and maximum number of cycles equals to $1e^{+7}$. In this regard, by comprehending the lower velocity (400 m/s) being used and tougher materials are elaborated, both studies' approach and findings were highly similar.

4.6 Table of Results

Following tables ve figures are providing overall results and their comparison in between for the finite element analysis studies that has been made in this thesis.

Table 4.1 An overall results' comparison for all FE analysis successfully computed

Results	9 mm type II	9 mm bullet for Type IIA	7.62 mm bullet
Equivalent Stress (Pa)	7.9958e+8	8.3242e+8	5.3304e+8
Maximum shear stress (Pa)	4.4933e+8	4.6649e+8	2.9208e+8
Directional deformation (m)	0.015738	0.017287	0.044716
BLV (m/s)	90	100	65

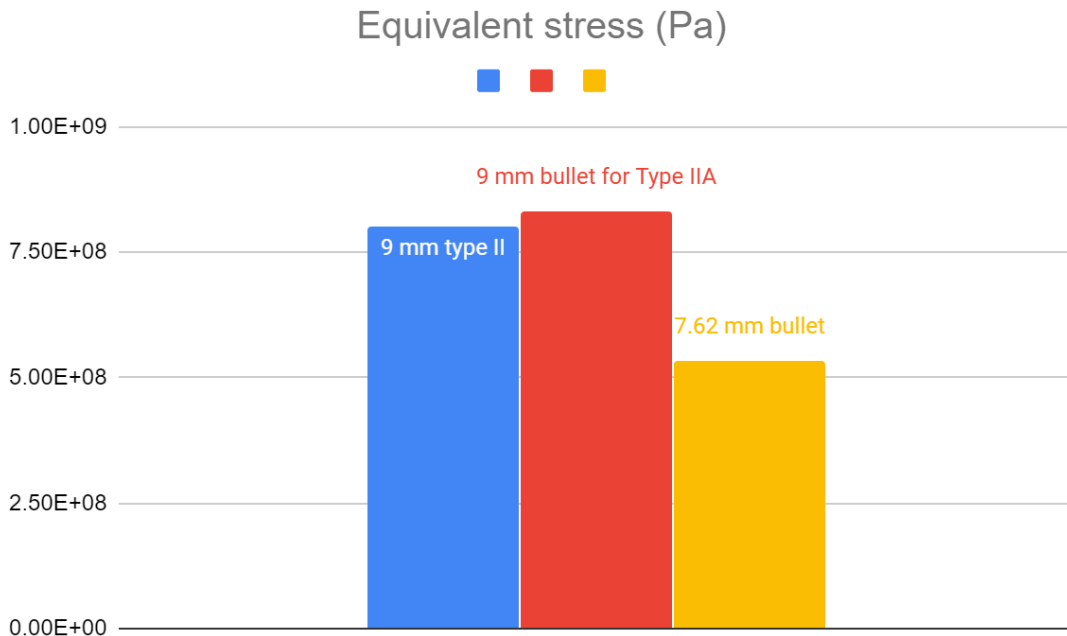


Figure 4.59 Equivalent stress results chart providing a specific comparison for all tested projectiles

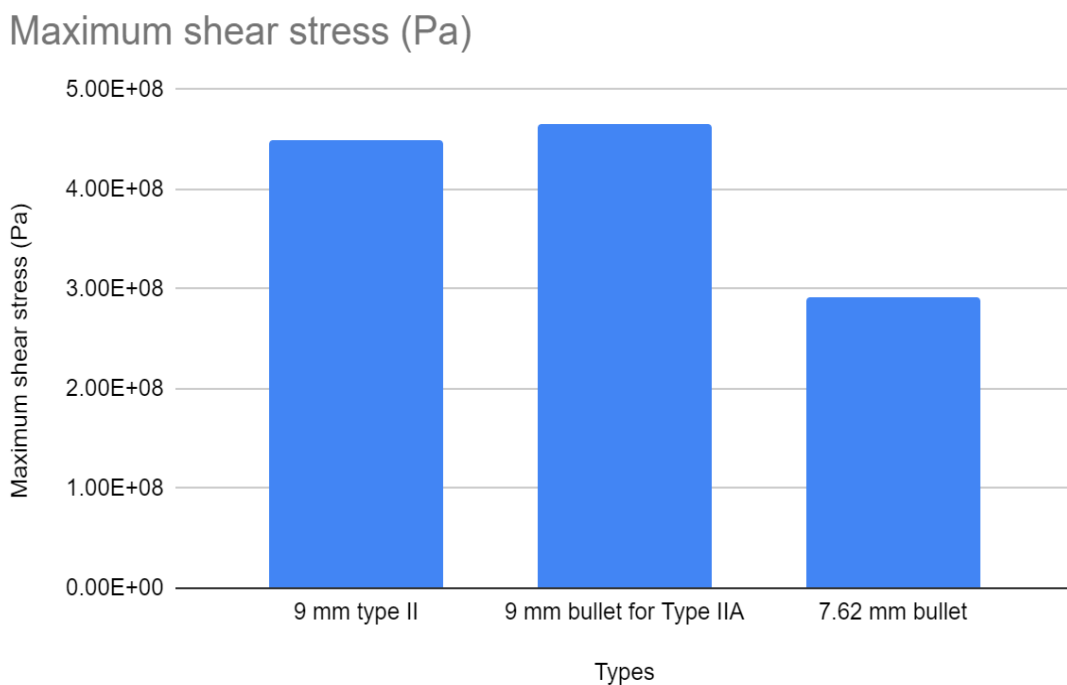


Figure 4.60 Maximum shear stress results chart providing a comparison for all tested projectiles

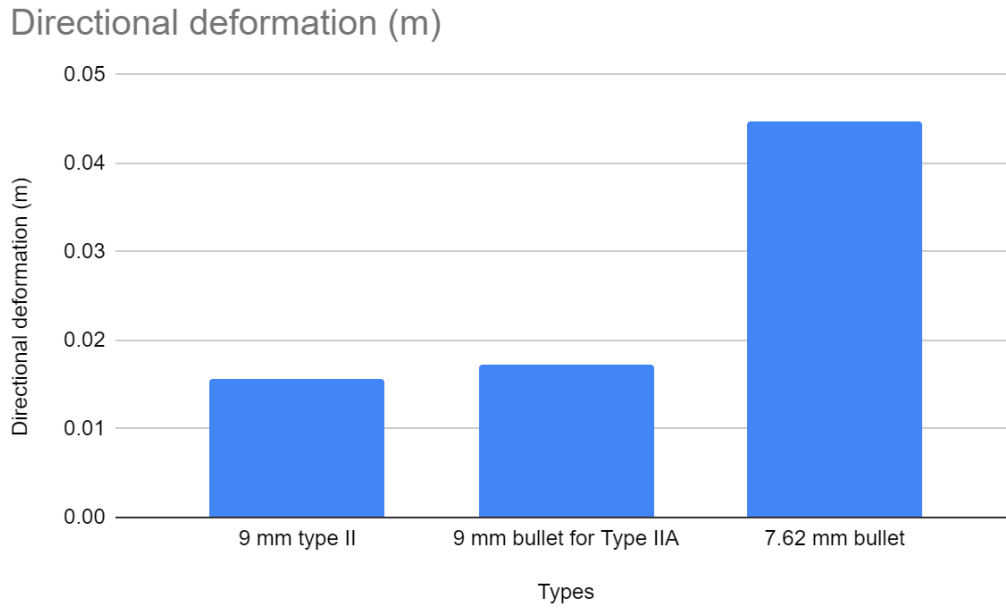


Figure 4.61 Directional deformation results chart providing a comparison for all tested projectiles

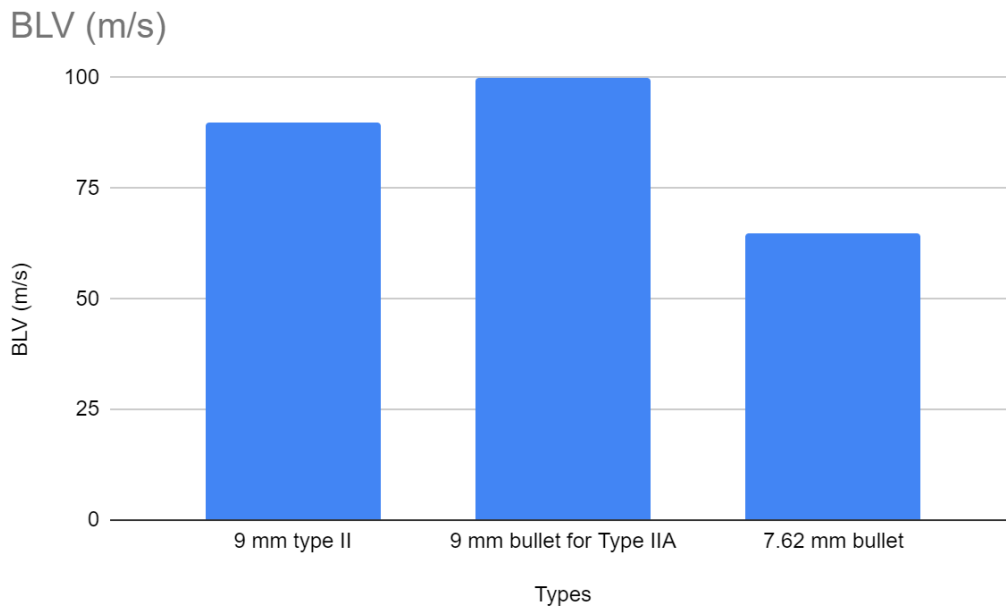


Figure 4.62 Ballistic limit velocity (BLV) results chart providing a comparison for all tested projectiles.

Chapter 5

Conclusions and Future Prospects

5.1 Conclusions

The ballistic jackets used in the military are typically constructed from layers of different materials and then assembled to form a conservative solitary jacket. The examination methodology used in this method was achieved by finite element software. In such a way Ansys was specifically used. The initial postulation section deals with the choice of first / front layer content. As a core, front layer material silicon carbide was picked on the grounds that it demonstrated least deformation and least stress compared to other materials that were tested in Ansys. The fitting development of the layers was subsidized from investigating various articles and it was discovered that a vest of having width of at least 20 mm is adequate to stop a bullet impact. The dimensions of the layers are taken from NIJ standards choosing the smallest size of an armor which was 317.5 x 317.5 mm [30]. The armor, ideally was idealized as a square plate to minimize any functional errors. The testing was done with 6 bullets to exclude any errors and give a better image of the testing. This was done to optimize the hybridization and see actually how several bullets affect the ballistic performance. As shown by above speculative understandings of different ballistic properties in different defensive equipment, the layers were discreetly placed and no spacing was left between them to ensure compact bonding. The thesis examines the protection of ballistic protective vests from serious military injuries during combat and the development of a hybrid solution that will provide the vest with a new function to provide the power needs of the equipment the soldier will need during combat. In this study a novel idea was used in which a lithium-ion battery system was added in addition to conventional ballistic vests and the materials to be used for the vest were tested by finite element analysis, taking into account the NIJ standards. With these computational results, it is aimed to design a protective, lightweight and easy-to-use compact vest that provides energy too.

A three dimensional model of an armor, composed of various materials including an additional layer of a battery pack, has been created in Ansys design modeler and FEA analysis has been applied assuming the hit by a projectile at normal incidence as stated the National Institute of Justice (NIJ) standards.

The structure was made in a composite way which consisted of layers SiC of 5 mm, epoxy resin of 10 mm and of Kevlar of 15 mm. A Li-Ion battery layer was also introduced in design but for Ansys analysis the material that was used was PVC since the bullet must not penetrate past the Kevlar layer so the Li-Ion material is of little use in analysis. The basic function of the ceramic layer is to deflect the projectile and the artificial fibers that are used in the middle layers hold the bullet particles and prevent them from penetrating, the Kevlar or metal layer completely stops the bullet.

9 mm and 7.62 mm round tip samples were tried and tested on the composite layered structure and analyzed with the ballistic performance. The bullets were shot at the front layer which is the silicon carbide layers and the deformation and other analysis were run. The bullets were shot at a distance of 30 mm and shot with the velocity as prescribed in the NIJ standards. From the results it can be evaluated that the total deformation values of both 9mm types are the same but the one with greater speed shows more deformation on the surface as compared to the one with lesser speed. When these deformation values are compared to 7.62 mm projectile the 7.62 mm projectile has greater deformation compared to both thus it can be concluded that the diameter of the bullet has an impact on the deformation rate. For equivalent stress, it can be seen that the 9mm bullet with less speed is less prone to high stress as compared to the 9 mm and 7.62 mm with high speed. The impact of the 7.62 bullet is lesser than the type II bullet. In the case of maximum shear stress, the shear stress caused by 7.62 mm bullet is the least as compared to both the 9 mm one. This shows that the bullet with lesser diameter would have less shear and the bullet greater diameter and greater speed will have the highest shear stress.

Directional deformation is caused the most by the 7.62 mm bullet which shows that the smaller the diameter the greater the deformation is in Z direction. More importantly, directional deformation of 44,716 cm gained by analysis for 7.62 mm indicates that it barely pushes the limits determined by NIJ Standard which is given as maximum of 44 mm. It can be concluded that the ballistic vest design may be considered as pushing the limits to be considered as safe for our design for usage based on NIJ standards.

The Ballistic limit velocity is tested for several velocities for all three bullet type and then the best velocity is found which does not penetrate or create a hole in the surface of the layer.

In all of the Ansys results none of the 9 mm bullets penetrate past the Kevlar/epoxy layer ensuring that our design is safe to use and Li-Ion battery won't be effected in this regard, excluding the 7.62 mm projectile case.

5.2 Societal Impact and Contribution to Global Sustainability

Ballistic vests and the purpose of being protected have always been a serious need for centuries. In addition, the need of mobility and the comfort of the user are essentially the two main parameters when designing a commercial ballistic vest. The additional part of the vest in this thesis examined is different and unique compared to all other manufactured commercial vests in the industry. The lithium, indeed may be one of the most precious metal nowadays since its usage in various industries such as electrical vehicles, space applications including aviation and weaponry systems etc. The usage of lithium batteries (in many forms in cathode active material such as Lithium Manganese Cobalt Oxide so called NMC, Lithium Iron Phosphate so called LFP, Lithium Titanate Oxide so called LTO etc.) in provides more energy per unit volume compared to other available battery chemistries such as Lead-acid, Nickel Metal Hydride and Nickel Cadmium. Hence, its application in use for batteries and as a component for ballistic vests would increase worldwide. Especially the policies and regulations of emerging economies such as China, USA, India and Western European countries forces to use green energy in many industries and applications, the use of lithium batteries would also increase in ballistic vests. Therefore, usage of lighter and greener elements and technology even in ballistic vest industry could be considered as a significant change for a sustainable environment. It would also have positive and important reflections on the manufacturers and suppliers of ballistic vests. Even though the ballistic vests are mainly used for law enforcement and military purposes; many people such as scientists, working-class, academicians etc. work in those industries and have a very high R&D expenses could be noticed. Lately, it could be seen easily that many countries in Western Europe such as England, Italy, Spain etc. are cutting off their military spending due to some

significant macroeconomic situations which cause people to lose their job and R&D budgets for academicians and students. Therefore, by testing and using our design stated in this thesis with the application of Finite Element Method would provide more economical advantages. In addition, a new way of looking in the industry may provide more alternatives for vest and battery designers and manufacturers hence resulting new R&D studies and more jobs for fresh engineers and academicians working within these fields.

5.3 Future Prospects

For future prospects, a thermal simulation can be done to ensure that the vest does not get overheated since lithium batteries are considered as dangerous goods materials. There are very strict regulations worldwide for lithium materials' handling and transportation especially forced by aviation authorities since the lithium element may be highly flammable if not handled with care. In addition, it could be investigated that the soldier does not get too sweaty from too much heat caused by the vest and battery itself, so a cooling mechanism could be considered. Because of the almost impassable aspect of ballistic material, sweat evaporation is curtailed, as airflow is limited in the region bounded by the multi-layered vest, as it is perfectly bonded as well. Traditional single-layer or multiple layer fabric approaches could be used to support an insulated vest's thermal fatigue but these methods are built on the notion of eliminating moisture from the skin. That being said, since sweat cannot be transmitted to the outside, since it is absorbed by the ballistic material; certain textile industries are really only partly equipped to be used underneath bulletproof vests. The enhancement of ventilation under the ballistic reinforcements is more desirable for the clothing comfort of an armored ballistic vest. The installation of three dimensional (3D) structures in between the human skin and the military fabric could be able to accomplish this phenomenon. Some rather designs maintain a separation both between the skin and the outer part, and thus promote air circulation inside the microclimate, allowing sweat convection. Further works on these areas could be very helpful in this regard to achieve an ease and comfort for ballistic vest users.

BIBLIOGRAPHY

- [1] Y. Wang, Y. Miao, D. Swenson, B. A. Cheeseman, C. F. Yen, and B. LaMattina, "Digital element approach for simulating impact and penetration of textiles," *Int. J. Impact Eng.*, vol. 37, no. 5, pp. 552–560, 2010, doi: 10.1016/j.ijimpeng.10.009 (2009).
- [2] R. Nayak et al., "Body armor for stab and spike protection, Part 1: Scientific literature review," *Text. Res. J.*, vol. 88, no. 7, pp. 812–832, doi: 10.1177/0040517517690623 (2018).
- [3] G. Gopinath, J. Q. Zheng, and R. C. Batra, "Effect of matrix on ballistic performance of soft body armor," *Compos. Struct.*, vol. 94, no. 9, pp. 2690–2696, doi: 10.1016/j.compstruct.2012.03.038 (2012).
- [4] B. Larsen, K. Netto, and B. Aisbett, "The Effect of Body Armor on Performance, Thermal Stress, and Exertion: A Critical Review," *Mil. Med.*, vol. 176, no. 11, pp. 1265–1273, doi: 10.7205/milmed-d-10-00470 (2011)
- [5] X. Li et al., "Preparation of body armor material of Kevlar fabric treated with colloidal silica nanocomposite," *Plast. Rubber Compos.*, vol. 37, no. 5–6, pp. 223–226, doi: 10.1179/174328908X309439 (2008).
- [6] E. Medvedovski, "Ballistic performance of armor ceramics: Influence of design and structure. Part 2," *Ceram. Int.*, vol. 36, no. 7, pp. 2117–2127, doi: 10.1016/j.ceramint.2010.05.022 (2010).
- [7] "Ethanol Fuel Market Size Worth \$115.65 Billion By 2025,". [Online]. Available: <https://www.grandviewresearch.com/press-release/global-fuel-ethanol-market> (2019).
- [8] X. Chen, Y. Zhou, and G. Wells, "Numerical and experimental investigations into ballistic performance of hybrid fabric panels," *Compos. Part B Eng.*, vol. 58, pp. 35–42, doi: 10.1016/j.compositesb.2013.10.019 (2014).
- [9] N. C. Armstrong, "Reducing the burden on the dismounted soldier," *J. Sci. Med. Sport*, vol. 20, no. September, p. S148, doi: 10.1016/j.jsams.2017.09.549 (2017).
- [10] T. Aure and A. Ioannides, "Simulation of crack propagation in concrete beams with cohesive elements in ABAQUS," *Transp. Res. Rec.*, vol. 1, no. 2154, pp. 12–21, doi: 10.3141/2154-02 (2010).
- [11] A. M. Soydan, B. Tunaboylu, A. G. Elsabagh, A. K. Sari, and R. Akdeniz, "Simulation and Experimental Tests of Ballistic Impact on Composite Laminate Armor," *Adv. Mater. Sci. Eng.*, vol. 2018, doi: 10.1155/2018/4696143 (2018)
- [12] M. A. G. Silva, C. Cismaşiu, and C. G. Chiorean, "Numerical simulation of ballistic impact on composite laminates," *Int. J. Impact Eng.*, vol. 31, no. 3, pp. 289–306, doi: 10.1016/j.ijimpeng.2004.01.011 (2005)
- [13] P. M. Cunniff, "An Analysis of the System Effects in Woven Fabrics under Ballistic Impact," *Text. Res. J.*, vol. 62, no. 9, pp. 495–509, doi: 10.1177/004051759206200902 (1992).
- [14] A. Banerjee, S. Dhar, S. Acharyya, D. Datta, and N. Nayak, "Numerical Simulation of Ballistic Impact of Armor Steel Plate by Typical Armor Piercing Projectile," *Procedia Eng.*, vol. 173, pp. 347–354, doi: 10.1016/j.proeng.2016.12.028 (2017)
- [15] S. Kant and S. L. Verma, "Paper publish - Copy," vol. 4, no. 3, pp. 71–80, doi: 10.17148/IARJSET (2017).
- [16] C. Y. Tham, V. B. C. Tan, and H. P. Lee, "Ballistic impact of a KEVLAR® helmet: Experiment and simulations," *Int. J. Impact Eng.*, vol. 35, no. 5, pp. 304–318, doi: 10.1016/j.ijimpeng.2007.03.008 (2008)
- [17] D. Cvetkovic, G. Birajdar, S. Kirkup, and B. Leye, "Numerical Modeling and Computer Simulation," *Numer. Model. Comput. Simul.*, no. June, doi:

10.5772/intechopen.77641 (2019).

[18] I. G. Crouch, "Body armor – New materials, new systems," *Def. Technol.*, vol. 15, no. 3, pp. 241–253, doi: 10.1016/j.dt.2019.02.002 (2019).

[19] P. Cunniff, "Dimensionless Parameters for Optimization of Textile-Based Body Armor Systems," *Proceeding 18th Int. Symp. Ballist.*, no. January 1999, pp. 1303–1310, (1999).

[20] U. Mawkhlieng, A. Majumdar, and A. Laha, "A review of fibrous materials for soft body armor applications," *RSC Adv.*, vol. 10, no. 2, pp. 1066–1086, doi: 10.1039/c9ra06447h (2019)

[21] P. Tan, "Numerical simulation of the ballistic protection performance of a laminated armor system with pre-existing debonding/delamination," *Compos. Part B Eng.*, vol. 59, pp. 50–59, 2014, doi: 10.1016/j.compositesb. 10.080 (2013).

[22] V. Alankaya, H. K. Senyilmaz, and M. Türker, "Inspection of failure caused by ballistic impact on body armors composed of laminated dyneemaTM," *Gazi Univ. J. Sci.*, vol. 26, no. 2, pp. 253–259, (2013).

[23] S. Yan, J. Deng, C. Bae, Y. He, A. Asta, and X. Xiao, "In-plane orthotropic property characterization of a polymeric battery separator," *Polym. Test.*, vol. 72, no. October, pp. 46–54, doi: 10.1016/j.polymertesting.2018.10.001 (2018)

[24] E. Medvedovski, "Ballistic performance of armor ceramics: Influence of design and structure. Part 1," *Ceram. Int.*, vol. 36, no. 7, pp. 2103–2115, doi: 10.1016/j.ceramint.2010.05.021 (2010)

[25] B. Heidenreich, M. Gahr, and E. Medvedovski, "Biomorphic reaction bonded silicon carbide ceramics for armor applications," *Ceram. Trans.*, vol. 178, no. January, pp. 45–53, doi: 10.1002/9781118408100.ch4 (2006).

[26] C. Kaufmann, D. Cronin, M. Worswick, G. Pageau, and A. Beth, "Influence of material properties on the ballistic performance of ceramics for personal body armor," *Shock Vib.*, vol. 10, no. 1, pp. 51–58, doi: 10.1155/2003/357637 (2003).

[27] R. L. Woodward and B. J. Baxter, "Ballistic evaluation of ceramics: Influence of test conditions," *Int. J. Impact Eng.*, vol. 15, no. 2, pp. 119–124, doi: 10.1016/S0734-743X(05)80024-7 (1994).

[28] J. Sternberg, "Material properties determining the resistance of ceramics to high velocity penetration," *J. Appl. Phys.*, vol. 65, no. 9, pp. 3417–3424, doi: 10.1063/1.342659 (1989).

[29] Z. Rozenberg and Y. Yeshurun, "The relation between ballastic efficiency and compressive strength of ceramic tiles," *Int. J. Impact Eng.*, vol. 7, no. 3, pp. 357–362, doi: 10.1016/0734-743X(88)90035-8 (1988).

[30] NIJ Standard-0101.06, "Ballistic Resistance of Personal Body Armor," *NIJ Stand.*, p. 89, doi: 10.1017/CBO9781107415324.004 (2008).

[31] J. A. Zukas, "Impact Dynamics: Theory and Experiment," *US Army Armament Res. Dev. Command*, pp. 1–66, doi: ARBRL-TR-02271 (1980).

[32] R. T. Sedgwick, "Best Available Copy for all Pictures," [Online]. Available: <http://www.dtic.mil/dtic/tr/fulltext/u2/p004398.pdf> (1972).

[33] C. J. Hu, P. Y. Lee, and J. S. Chen, "Ballistic performance and microstructure of modified rolled homogeneous armor steel," *J. Chinese Inst. Eng. Trans. Chinese Inst. Eng. Ser. A/Chung-kuo K. Ch'eng Hsuch K'an*, vol. 25, no. 1, pp. 99–107, doi: 10.1080/02533839.2002.9670684 (2002).

[34] T. Deniz, "Ballistic penetration of hardened steel plates," (2010).

[35] G. Moss, "Us army armament research and development command," (1982).

[36] T. Wierzbicki, "Petalling of plates under explosive and impact loading," *Int. J. Impact Eng.*, vol. 22, no. 9, pp. 935–954, doi: 10.1016/S0734-743X(99)00028-7 (1999).

- [37] W. W. Chen, A. M. Rajendran, B. Song, and X. Nie, "Dynamic fracture of ceramics in armor applications," *J. Am. Ceram. Soc.*, vol. 90, no. 4, pp. 1005–1018, doi: 10.1111/j.1551-2916.2007.01515.x (2007).
- [38] M. Yang and P. Qiao, *High energy absorbing materials for blast resistant design*. Woodhead Publishing Limited, (2010).
- [39] R. Yadav, M. Naebe, X. Wang, and B. Kandasubramanian, "Body armor materials: from steel to contemporary biomimetic systems," *RSC Adv.*, vol. 6, no. 116, pp. 115145–115174, doi: 10.1039/c6ra24016j (2016).
- [40] E. P. Carton, B. B. Johnsen, D. B. Rahbek, H. Broos, and A. Snippe, "Round robin using the depth of penetration test method on an armor grade alumina," *Def. Technol.*, vol. 15, no. 6, pp. 829–836, doi: 10.1016/j.dt.2019.07.014 (2019)
- [41] N. K. Naik and P. Shrirao, "Composite structures under ballistic impact," *Compos. Struct.*, vol. 66, no. 1–4, pp. 579–590, doi: 10.1016/j.compstruct.2004.05.006 (2004).
- [42] J. B. Coates and J. C. Beyer, *Wound Ballistics*. Washington, D.C.: Dept. of the Army, (1962).
- [43] M. M. Shokrieh and G. H. Javadpour, "Penetration analysis of a projectile in ceramic composite armor," *Compos. Struct.*, vol. 82, no. 2, pp. 269–276, doi: 10.1016/j.compstruct.2007.01.023 (2008).
- [44] B. G. Kiral, "Effect of the clearance and interference-fit on failure of the pin-loaded composites," *Mater. Des.*, vol. 31, no. 1, pp. 85–93, doi: 10.1016/j.matdes.2009.07.009 (2010).
- [45] F. S. Alkhatib, "Development of Hybrid and Non-Hybrid Composite Body Armor Plate for Ballistic Protection," Qatar University, (2017).
- [46] V. Kulíšek, "Finite element analysis of composite structures," doi: 10.1016/0263-8223(94)90102-3 (1994).
- [47] Z. Zhang et al., "Vibration-based assessment of delaminations in FRP composite plates," *Compos. Part B Eng.*, vol. 144, pp. 254–266, doi: 10.1016/j.compositesb.2018.03.003 (2018).
- [48] K. Dateraksa, K. Sujirote, R. Mccuiston, and D. Atong, "Ballistic Performance of Ceramic/S 2 -Glass Composite Armor," *J. Met. Mater. Miner.*, vol. 22, no. 2, pp. 33–39, (2012).
- [49] A. M. Soydan, B. Tunaboynu, A. G. Elsabagh, A. K. Sari, and R. Akdeniz, "Simulation and Experimental Tests of Ballistic Impact on Composite Laminate Armor," *Adv. Mater. Sci. Eng.*, p. 4696143, doi: 10.1155/2018/4696143 (2018).
- [50] F. Concli, A. Gonzalez-Jimenez, A. Manes, and M. Giglio, "Experimental testing and numerical modelling of a Kevlar woven - Epoxy matrix composite subjected to a punch test," *Procedia Struct. Integr.*, vol. 24, no. 2019, pp. 3–10, doi: 10.1016/j.prostr.2020.02.001 (2019).
- [51] K. Krishnan, S. Sockalingam, S. Bansal, and S. D. Rajan, "Numerical simulation of ceramic composite armor subjected to ballistic impact," *Compos. Part B Eng.*, vol. 41, no. 8, pp. 583–593, Dec. doi: 10.1016/j.compositesb.2010.10.001 (2010).
- [52] A. K. Bandaru, V. V. Chavan, S. Ahmad, R. Alagirusamy, and N. Bhatnagar, "Ballistic impact response of Kevlar® reinforced thermoplastic composite armors," *Int. J. Impact Eng.*, vol. 89, pp. 1–13, doi: 10.1016/j.ijimpeng.2015.10.014 (2016).
- [53] Z. Guoqi, W. Goldsmith, and C. K. H. Dharan, "Penetration of laminated Kevlar by projectiles-I. Experimental investigation," *Int. J. Solids Struct.*, vol. 29, no. 4, pp. 399–420, doi: 10.1016/0020-7683(92)90207-A (1992).
- [54] M. A. Pulungan, S. Sutikno, and M. S. M. Sani, "Analysis of Bulletproof Vest Made from Fiber Carbon Composite and Hollow Glass Microsphere (HGM) in Absorbing Energy due to Projectile Impact," *IOP Conf. Ser. Mater. Sci. Eng.*, vol. 506,

no. 1, doi: 10.1088/1757-899X/506/1/012001 (2019).

[55] A. K. Bandaru and S. Ahmad, "A COMPUTATIONAL ANALYSIS OF THE BALLISTIC IMPACT PERFORMANCE OF A COMPUTATIONAL ANALYSIS OF THE BALLISTIC IMPACT PERFORMANCE OF KEVLAR / POLYPROPYLENE COMPOSITE," no. December, (2015).

[56] S. Periyasamy, R. Sundaresan, and N. Uthirapathy, "Numerical Investigation on Ballistic Limit Velocity of Armor Materials," *Int. J. Curr. Eng. Technol.*, vol. 8, no. 3, pp. 636–645, doi: 10.14741/ijcet/v.8.3.18 (2018).

CURRICULUM VITAE

2006 – 2010	B.Sc., Mechanical and Aerospace Engineering, The University of Texas at Arlington, TX, USA
2010 – 2012	Mechanical Design Engineer / 609 program for Yokes and Blades, Bell Helicopter, Fort Worth, TX, USA
2013 – 2014	Project Engineer, TUBITAK / Project No#M112348, Kayseri, TURKEY
2015 – 2015	Sr. Procurement Manager, SIMFER AS, Kayseri, TURKEY
2016 – Present	Division Manager of Aviation, Naval Systems and Rolling Stock Platforms, ASPILSAN Inc., Kayseri, TURKEY
2018 – Present	M.Sc. in Advanced Materials and Nanotechnology, Abdullah Gul University, Kayseri, TURKEY

SELECTED PUBLICATIONS AND PRESENTATIONS

C1) Temperature and Stress Examinations on Pistons for Damage Prevention and Efficiency Enhancement: Carbon/Carbon Composite Piston vs. Conventional Aluminum Pistons. ASME August 7, 2015 Author: Murat Kaan. ASME 2015 International Design Engineering Technical Conferences in Engineering Volume 10: ASME 2015 Power Transmission and Gearing Conference; 23rd Reliability, Stress Analysis and Failure Prevention Conference, Boston, Massachusetts, USA, August 2–5, 2015